INFORMATION TO USERS

This manuscript has been reproduced from the microfilm master. UMI films the text directly from the original or copy submitted. Thus, some thesis and dissertation copies are in typewriter face, while others may be from any type of computer printer.

The quality of this reproduction is dependent upon the quality of the copy submitted. Broken or indistinct print, colored or poor quality illustrations and photographs, print bleedthrough, substandard margins, and improper alignment can adversely affect reproduction.

In the unlikely event that the author did not send UMI a complete manuscript and there are missing pages, these will be noted. Also, if unauthorized copyright material had to be removed, a note will indicate the deletion.

Oversize materials (e.g., maps, drawings, charts) are reproduced by sectioning the original, beginning at the upper left-hand corner and continuing from left to right in equal sections with small overlaps. Each original is also photographed in one exposure and is included in reduced form at the back of the book.

Photographs included in the original manuscript have been reproduced xerographically in this copy. Higher quality 6" x 9" black and white photographic prints are available for any photographs or illustrations appearing in this copy for an additional charge. Contact UMI directly to order.

UMI

A Bell & Howell Information Company
300 North Zeeb Road, Ann Arbor MI 48106-1346 USA
313/761-4700 800/521-0600

FIELD DYNAMICS, INSTABILITIES AND NOISE SQUEEZING IN THE ONE-PHOTON AND TWO-PHOTON CORRELATED EMISSION LASER AND TWO-PHOTON MICROMASER

by

JIAN ZHANG

A dissertation submitted to the Graduate Faculty in Physics in partial fulfillment of the requirements for the degree of Doctor of Philosophy, The City University of New York

1996 (year degree awarded)

This manuscript has been read and accepted for the Graduate Faculty in Physics in satisfaction of the dissertation requirement for the degree of Doctor of Philosophy

6/27/96
Date

Chair of Examining Committee

8/5/96
Date

Executive Officer

Professor Ying-chih Chen

Professor Leon Cohen

Professor Mark Hillery

Professor Edward A. Whittaker

Supervisory Committee

The City University of New York

Abstract

Field Dynamics, Instabilities And Noise Squeezing In The One-Photon And Two-Photon Correlated Emission Laser And Two-Photon Micromaser

by

Jian Zhang

Adviser: Professor Janos Bergou

The influence of injected atomic coherence on laser operation is discussed by analyzing the equations of motion of this system. Both stationary steady states and time-dependent regimes of operation are investigated. For small cavity-field detuning and large atomic coherence phase locking occurs. Under certain conditions, in the inverted regime the output intensity is an S-shaped function of the atomic coherence leading to the possibility of a bistable behavior. When the detuning is larger than a critical value there is no phase locking. We find that the time-dependent behavior of the laser intensity in this case is oscillatory (quasiperiodic). There is a small parameter region where a stationary steady state and an oscillatory state may coexist. We find that in steady state the intensity noise can be suppressed below the shot - noise limit but the phase fluctuations are not

affected by pump regularity. For nonzero detuning, we find that transient squeezing of the phase fluctuations is possible.

Both stationary and time-dependent regimes of operation, instabilities, and phase squeezing are investigated in the off-resonant two-photon correlated-spontaneous-emission laser (CEL) by numerical calculation. Initial atomic coherence plays an essential role in lasing without population inversion, phase locking and phase noise squeezing in the system. The field evolution and dynamics are studied. Furthermore, phase noise reduction near bistable areas is also investigated. In addition to the lower branch, where it has been known to exist from previous studies, phase squeezing is also found on the upper branch both with and without population inversion, thus generating a bright source of phase noise squeezed light.

A master equation for the two-photon micromaser with the injected atomic coherence is derived. The photon statistics for the fully excited, partially excited and deexcited two-photon micromaser without coherence is studied. The spectrum is investigated by using Green's function to calculate the two-time correlation function of the micromaser field. We show the influence of the thermal mean photon number on the spectrum of the two-photon micromaser.

Acknowledgments

I would especially like to thank my advisor, Professor János Bergou for introducing me to this amazing world of Laser Physics and for his encouragement, guidance and support. I would like to express my gratitude to the Physics Department of Hunter College for the support over the years. I am grateful to my colleagues, Dr. Chang Su and Mr. Donghui Zhao. It has been a pleasure to work with them.

Finally, I would like to thank my family, my parents for their love, support, and understanding. And I would like to dedicate this thesis to my lovely daughter, Sylvia.

Table of Contents

List of Figures

Chapter I

1. Introduction

Since the initial development of the quantum theory of the laser more than 20 years ago,[1-3] much theoretical and experimental effort has been devoted to the problem of quantum-noise reduction in their output field. The noise in the output of a laser field stems from the interactions with the gain and loss reservoirs. The fluctuation in the number of active atoms(pump fluctuations) and spontaneous emission events(random emissions by the active atoms) contribute to the noise originating from the interaction with the gain reservoir. Vacuum fluctuations enter the cavity through the mirrors and contribute to the noise due to the interaction with the loss reservoir. These noise sources have been addressed in various works recently. Pump - noise suppressed laser schemes address the problem of pump fluctuations[4-15], the correlated -spontaneous - emission laser[16-22] targets spontaneous emission noise through the introduction of atomic coherence in the laser. These systems deal with the reduction of noise due to the interaction with the gain reservoir. Laser buildup from squeezed vacuum[23-25], in turn, targets the reduction of output fluctuations that originate from the interaction with the loss reservoir. This second line of investigations is somewhat less practical since in order to reduce output fluctuations one needs a field with reduced fluctuations to begin with.

One of the earliest proposals was the laser with an injected signal.[26,27] In this system the phase is not a freely diffusing quantity any longer due to phase locking to a

value determined by the phase of the external signal. While this results in a reduction of the net phase fluctuation noise it leaves the fundamental sources of noise, spontaneous emission in particular, unchanged. It is not surprising therefore that, although the original idea of a laser with injected signal was directed towards stabilization of the output intensity and phase or mode selection, the system became the prime candidate for the study of instabilities (quite in line with some of the findings of the present paper) and chaos in quantum optical system.[28]

A closely related idea, but one which also targets the microscopic mechanism of the emission of light, assumes preparation of the active atoms in a coherent superposition of all levels participating in the laser operation. Following the original suggestion,[16,17] recently a considerable amount of theoretical work (semiclassical as well as quantum theory) has been directed towards lasers with injected atomic coherence.[18, 29-33] It has been demonstrated that with a proper relation among the initial atomic coherence of randomly injected atoms, it is possible to reduce both the photon-number noise and phase noise in the laser simultaneously.[18] Furthermore, the injected atomic coherence plays the role of an injected signal in achieving phase locking[29,30] and may lead to lasing without inversion (LWI).[31,32] In these latter systems LWI may be accompanied by noise quenching with a proper choice of the initial atomic coherence.[33]

These features prompt us to investigate the laser with coherent initial conditions for the active atoms extensively. In particular, we focus on the role played by the various detunings (cavity - field, atom - field) in the dynamics.

An important difference between an ordinary, incoherently pumped laser and a laser with injected atomic coherence is the effect of phase locking.[18,29,30] In an ordinary laser, the phase of the electromagnetic field is not locked to a particular value but can freely diffuse over the entire angular interval of 2π. Injecting atoms with initial coherence, a phase information is introduced into the system and the laser phase will lock to a preferred value in steady state.

In addition in Ref. [18], the full nonlinear quantum theory of a laser with injected atomic coherence has been developed and the possibility of reducing both the intensity and phase noise has been demonstrated. However, that work has dealt with perfect resonance only, i.e., the cavity frequency, laser frequency, and the atomic transition frequency all coincide. In a closely related work, using semiclassical theory, Carty and Sargent[29] have studied the effect of injected atomic coherence on single-mode frequency locking in a cavity. It has been assumed that the laser frequency coincides with the atomic transition frequency and the discussion has been restricted to cavity-atom detunings small enough to allow phase locking.

We will give a detailed study of the field dynamics of a laser with injected atomic coherence for arbitrary detuning. Also we will consider the full quantum theory including fluctuations. First we will restrict our treatment to what essentially amounts to the semiclassical approximation. We rely on the results of Ref.[18] which employed density operator methods,[34] and derive from them the nonlinear equations of motion for intensity and phase. These equations exhibit the dependence of intensity and phase on the external parameters (population inversion, amplitude of atomic coherence, and detunings). They

also give a simple physical picture of the time-dependent behavior of the system, as well as the steady-state characteristics. In our discussion we will investigate the stability of the assumption, made in Ref. [29], that the laser frequency locks to the atomic transition frequency. When the atoms are injected into the cavity in a coherent superposition, a new feature appears in the coupling of the atoms with the cavity. Even if the laser frequency equals the atomic transition frequency, the coupling strength still depends on the cavity-field detuning. When this detuning is zero, we obtain total cavity resonance which represents the strongest coupling. As the detuning increases, the coupling strength decreases and, after a certain critical value, phase locking cannot be achieved.

Then, we focus on the reduction of noise in the laser with injected atomic coherence and regular pumping. We turn our attention to pump - noise suppressed and CEL schemes. In particular, we are interested in combining these two effects and we will discuss the influence of the pumping statistics and the injected atomic coherence on the fluctuations of the laser radiation. If these two concepts are considered separately, the following results hold:

1) In pump - noise reduced lasers,[4,5] phase fluctuations are independent of the pumping statistics and intensity fluctuations can be significantly reduced, up to 50% below the shot - noise limit if the pumping noise is eliminated.

2) In the one - photon laser with injected atomic coherence[18], the initial atomic coherence plays an important role in phase locking and noise reduction. It has been demonstrated there that with a proper relation among the initial atomic coherence of randomly injected atoms, it is possible to reduce both the intensity noise and phase noise in such a laser

below the noise level of incoherently pumped lasers. However, no squeezing of either phase noise or intensity noise has been found in coherently pumped two - level one - photon laser.

In our analysis we combine the pumping statistics and the injected atomic coherence and develop the nonlinear quantum theory of this laser scheme. The key feature of our results is the coupling of these two factors. We find that the cavity - field detuning plays an important role in this coupling. It should be noted that the theory of a regularly pumped laser with coherent atomic initial conditions has been worked out by Benkert and Scully for the particular case of zero detuning[35,36]. Similar system with an injected resonant signal has been investigated in Ref. [37]. On resonance, of course, the question of stability does not arise. Even more important, there is no coupling between the intensity and phase noise and, thus, pump regularity does not affect the phase noise. Here we show that only the photon - number noise is squeezed in steady state if there is regular pumping. More important, however, we show that in some cases with finite cavity - field detuning there is a transient squeezing of phase noise.

Next, we provide a similar analysis for the two-photon laser with injected atomic coherence. Since the beginning of the theoretical research on squeezing in the laser, the problem of squeezed state generation in two-photon systems has attracted much attention. An early work by Yuen[38] suggested the two-photon laser as a potential candidate for generating squeezed states of the radiation field. Later, it was shown[39,40] that due to the spontaneous - emission noise any possible squeezing at steady state would be destroyed and only transient squeezing becomes possible[41,42]. Recent work, including both

linear[17,25,43,44] and nonlinear[45,46] theory, has extended the investigations to coherent initial conditions in this two-photon system: if the atoms are pumped into an appropriate superposition of the lasing states, quenching of spontaneous-emission noise may occur. In this way, it has been shown that the generation of squeezed light is compatible with gain[17,25] and even with atomic inversion by adding an additional lower level[43] or by choosing a fast decaying intermediate relay level[44], thus providing bright sources of squeezed light.

In Chapter 3, we study the field dynamics, instability, and phase noise fluctuations of the two-photon correlated-emission-laser (CEL) as functions of the various detunings (cavity-field, atom-field) and atomic coherence numerically. We consider the simple off-resonant two-photon CEL scheme[17,25] with the middle level unpopulated. Nonlinear theory is adopted in the calculation. It is shown that, similar to the case of the one-photon CEL, the steady state solution exhibits bistability of intensity against initial atomic coherence, population inversion is no longer necessary to maintain lasing and initial atomic coherence provides phase locking. The essential difference between this system and the one-photon CEL is that there exists a threshold, below which the lower branch of the bistable intensity is always zero. In addition, tristable behavior can be found in the two-photon CEL. We study the field dynamics and instabilities with limit cycle behavior. We then investigate the effect of initial atomic coherence on noise. Besides showing that phase noise can be squeezed on the lower branch, we find that the phase noise squeezing persists on the upper branch for the non-inverted regime and, more importantly, even for the inverted regime. We therefore obtain a bright source of squeezed light in the simple

two-photon CEL scheme without the need of additional lower level or the fast decaying intermediate relay level[47].

The development of a single-atom micromaser[48,49] allows the detailed study of the atom-field interaction. Due to the development of the preparation of highly excited atoms called Rydberg atoms and the construction of high-Q superconducting cavities, it is possible to build a mocromaser which operates at a very low threshold, down to one atom at a time in the cavity. Though the injection rate of atoms is lower enough that at most one atom at a time is present inside the cavity, it is still lager enough that a large number of atoms can be injected before cavity damping becomes important. Therefore, a field is built up inside the cavity. This gives us a very useful tool to test some fundamental problems in quantum optics, and can display a variety of interesting quantum phenomena.

The one-photon micromaser has been the subject of studies in recent years, both theoretically[49,50] and experimentally[48,51]. It has been shown that a micromaser can exhibit many interesting features. In particular, so-called trapping states[52] were found. If the two-level atoms are injected inside the cavity in a coherent superposition of their upper and lower states, the field may evolve to pure states[53] even for mixed-state initial conditions, and a value of 52% of squeezing was found in connection with these trapped states. [54]

Interest in two-photon oscillators has recently been revived by the experimental demonstration of the continuous-wave operation of a two-photon micromaser.[55] The theory of the two-photon micromaser was first introduced by Brune et al.[41] and Davidovich et al.[42] Under certain conditions, the field inside the cavity exhibited sub-Possonian statistics. Later, Ashraf et al.[56] gave a comprehensive study of the photon

statistics of the two-photon micromaser, including long interaction times, and zero and finite detuning of the intermediate level. The linewidth is another important quantum-noise aspect of a field in an oscillator. Davidovich et al.[42] evaluated the decay rate of the off-diagonal density-matrix elements $\rho_{n,\,n+l}$ for the micromaser in the limit of large mean photon number and short interaction time. Scully et al.[57] have calculated the linewidth of the micromaser for long interaction times, and Qamar et. al.[58] have obtained the linewidth in the absence of the cavity losses by evaluating the two-time correlation function. Ning Lu[59] studied the micromaser spectrum for trapped states through the approach of the two-time correlation function. Quang et al.[60] calculated the two-time correlation function of the micromaser field via Green's - function approach and approximate analytical techniques.

In the fourth chapter, we focus on the two-photon micromaser with the injected atomic coherence. We first derive the master equation for this system. We analyze the effect of completely excited, partially excited and deexcited atoms without the injected atomic coherence, on the photon statistics. We show that one can change the photon statistics from sub-Poissonian to super-Poissonian by decreasing the gain. We apply a Green's function approach introduced by Quang et al. to calculate the two-time correlation function of the micromaser field. We then study the spectrum of the two-photon micromaser.

This thesis is organized as follows. In Chapter II, first we present the general equations of motion and discuss the steady-state operation with the injected atomic coherence for the one-photon laser in Sec. 2. We study the stability of the steady state in

Sec. 3 and field dynamics in Sec. 4. In Sec. 5 we derive a general Fokker-Planck equation for the scaled intensity and phase in P representation with pumping terms and express the noise in terms of moments. We present numerical solutions for the noise in steady state as well as time-dependent states. Chapter III is devoted to the two-photon laser with injected atomic coherence. In Sec. 6, we derive a general Fokker-Planck equation for the scaled intensity and phase in Q representation, and discuss the steady-state operation, instabilities. The study of field dynamics is given in Sec. 7. In Sec. 8, we show that a bright source of squeezed light can be obtained in the simple two-photon laser with injected atomic coherence. In Chapter IV, we study the two-photon micromaser with injected atomic coherence. In Sec. 9, we derive the master equation for the reduced field density operator. We investigate the photon statistics for a resonant two-photon micromaser and an off - resonant two-photon micromaser in Sec. 10. In Sec. 11, we numerically calculate the spectrum by using the Green's function approach. Finally, we summarize the results of this thesis in Chapter V.

Chapter II

One Photon Laser With Injected Atomic Coherence

2. Equations of Motion and Steady States

The system under consideration is the same as that of Refs.[18,29-30]: two-level atoms consisting of upper level *a* and lower level *b* and a single cavity mode. The atoms, initially prepared in a proper form of the atomic coherence, are injected into the laser cavity at a rate r and allowed to interact with the laser field in the single mode. The initial density matrix for the j-th atom injected at time t_j is

$$\rho^j(t_j) = \begin{pmatrix} \rho_{aa} & \bar{\rho}_{ab} e^{-i\nu t_j} \\ \bar{\rho}_{ba} e^{i\nu t_j} & \rho_{bb} \end{pmatrix}, \qquad j = 1, 2, \ldots \ . \tag{2.1}$$

Here ν is the laser frequency. ρ_{aa} , ρ_{ab} and $\bar{\rho}_{ab} = \bar{\rho}^*_{ba}$ are the same for all atoms. The Hamiltonian under the electric dipole and rotating wave approximations can be written as[5]

$$H = \hbar H_0 + \hbar V = \hbar \left[\Omega a^+ a + \sum_{j=1}^{\infty} (H_j^{at} + \theta(t - t_j) V_j) \right] , \tag{2.2}$$

with

$$H_j^{at} = \sum_{A=a,b} \omega_A |A^j><A^j| , \tag{2.3}$$

and

$$V_j = g\sigma_j^+ a + g a^+ \sigma_j \quad . \tag{2.4}$$

Here Ω is the frequency of the bare cavity eigenmode, $a(a^+)$ the field annihilation(creation) operator, H_j^{at} the free Hamiltonian of the j-th atom, $\sigma^{\pm}$ the atomic raising and lowering operator. $\theta(t-t_j)$ is the step function. Finally, g is the atom field coupling constant.

The corresponding Fokker-Planck equation has been obtained in Ref.[18] by employing standard techniques of the quantum theory of the laser[34]. First, a master equation for the density operation of the field has been derived and then it has been converted into a FP equation in the P representation. From that Fokker-Planck equation, we can get a set of equations of motion for the mean and variance of the intensity and phase variables. In this section we will focus on the semiclassical features of the system, without the quantum fluctuations (the behavior described by semiclassical theory). In the absence of fluctuation terms, we obtain the following equations of motion for the scaled intensity, I(≡photon number), and phase, Ψ, of the field,

$$\frac{dI}{dt} = d_I \ , \tag{2.5}$$

and

$$\frac{d\psi}{dt} = d_\psi \ , \tag{2.6}$$

Here the driving terms, d_I and d_ψ, are given by the following expressions

$$d_I = I\left\{\frac{\alpha(\rho_{aa}-\rho_{bb})}{1+I(\beta/\alpha)} - \gamma\right\} - \frac{2\sqrt{I}|S\bar{\rho}_{ab}|}{1+I(\beta/\alpha)}\sin(\psi-\theta+\arctan\delta) \ , \tag{2.7}$$

and

$$d_\psi = \nu - \Omega - \frac{\alpha(\rho_{aa} - \rho_{bb})}{1 + I(\beta/\alpha)} \frac{\delta}{2} - \frac{|S\bar{\rho}_{ab}|}{\sqrt{I}(1 + (\beta/\alpha))} \{\cos(\psi - \theta + \arctan\delta)$$

$$+ I(\beta/\alpha)\sqrt{1+\delta^2}\cos(\psi - \theta)\}. \qquad (2.8)$$

In the above expressions we introduced the following notations: gain coefficient, $\alpha = \frac{2rg^2}{\Gamma^2 + \Delta^2}$; saturation parameter, $\beta = \frac{8rg^4}{(\Gamma^2 + \Delta^2)^2}$; field-coherence coupling, $S = \frac{rg}{\Gamma + i\Delta}$; scaled atom-field detuning, $\delta = \frac{\Delta}{\Gamma}$; the cavity loss rate, γ; and finally the phase of the atomic coherence, θ. Everywhere in these expressions $\Delta = \omega_a - \omega_b - \nu = \omega - \nu$ is the atom-field detuning and Γ is the atomic decay constant (for simplicity assumed to be the same for all levels).

In steady state $\frac{d}{dt}$=0, the left-hand side of Eqs. (2.5) and (2.6) is zero. The laser intensity and phase are locked to their respective stationary values, I_0 and ϕ_0. The resulting equations become more transparent if we express them in terms of the scaled quantities: n_0=$I_0(\beta/\alpha)$ (photon number vs. saturation parameter), ϕ_0=Ψ_0 - θ (phase relative to the phase of the injected coherence), D=$(\nu-\Omega)/\gamma$ (cavity-field detuning), G=$\frac{\alpha(\rho_{aa} - \rho_{bb})}{\gamma} - 1$ (gain), C=$\alpha|\rho_{ab}|/\gamma$ (amplitude of atomic coherence). First, we want to study the stability of the states resulting from the assumption of frequency locking, δ=0, which was the crucial point of Ref.10. Under these conditions Eqs. (2.5) and (2.6) yield for the steady state

$$G - n_0 - \frac{2C}{\sqrt{n_0}}\sin\phi_0 = 0\,, \tag{2.9}$$

and

$$D - \frac{C}{\sqrt{n_0}}\cos\phi_0 = 0\,. \tag{2.10}$$

To solve for the steady state intensity n_0, we can eliminate the steady state phase, ϕ_0, from the above equations, giving

$$n_0^3 - 2Gn_0^2 + \{4D^2 + G^2\}n_0 - 4C^2 = 0\,. \tag{2.11}$$

This is a cubic algebraic equation for n_0. Equation (2.11) depends on three external parameters: gain, G, coherence, C, and detuning, D. Depending on the values of the parameters, there can be one or three real solutions. In the following Section we will systematically investigate these solutions from the point of view of their stability, finding those regions in the G, C, D parameter space where a single solution exists, two stable solutions may coexist, instabilities develop, etc.

In the remainder of this Section we present numerical results for the state equations for two typical choices of the parameters. First, we note that in an ordinary incoherently pumped laser population inversion, ρ_{aa} - ρ_{bb} > 0, is necessary for laser operation. However, in a laser with atomic coherence, population inversion is not necessary because the atomic coherence, $|\overline{\rho_{ab}}|$, acts as a driving force for the laser intensity. In Fig.1 we plot the laser intensity, n_0, as a function of the coherence parameter, C, for three typical values of the gain G and D. There is one steady state solution for each value of C. We will find in next section that the system with negative population

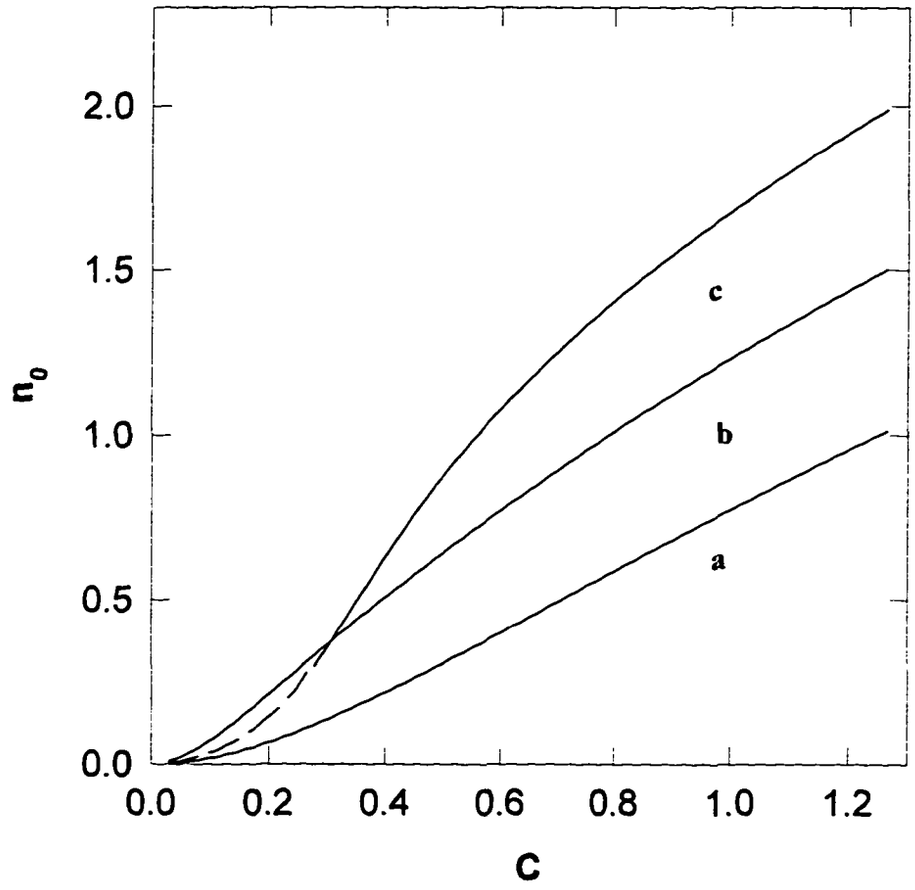

Fig. 1. Steady-state scaled intensity, n_0, vs the amplitude of atomic coherence, C, in the region below threshold and for (a) D=0.2, G=-1.5; (b) D=0.25, G=-0.5; (c) D=0.5, G=0.5. Solid line corresponds to stable steady state, dashed line to unstable steady state.

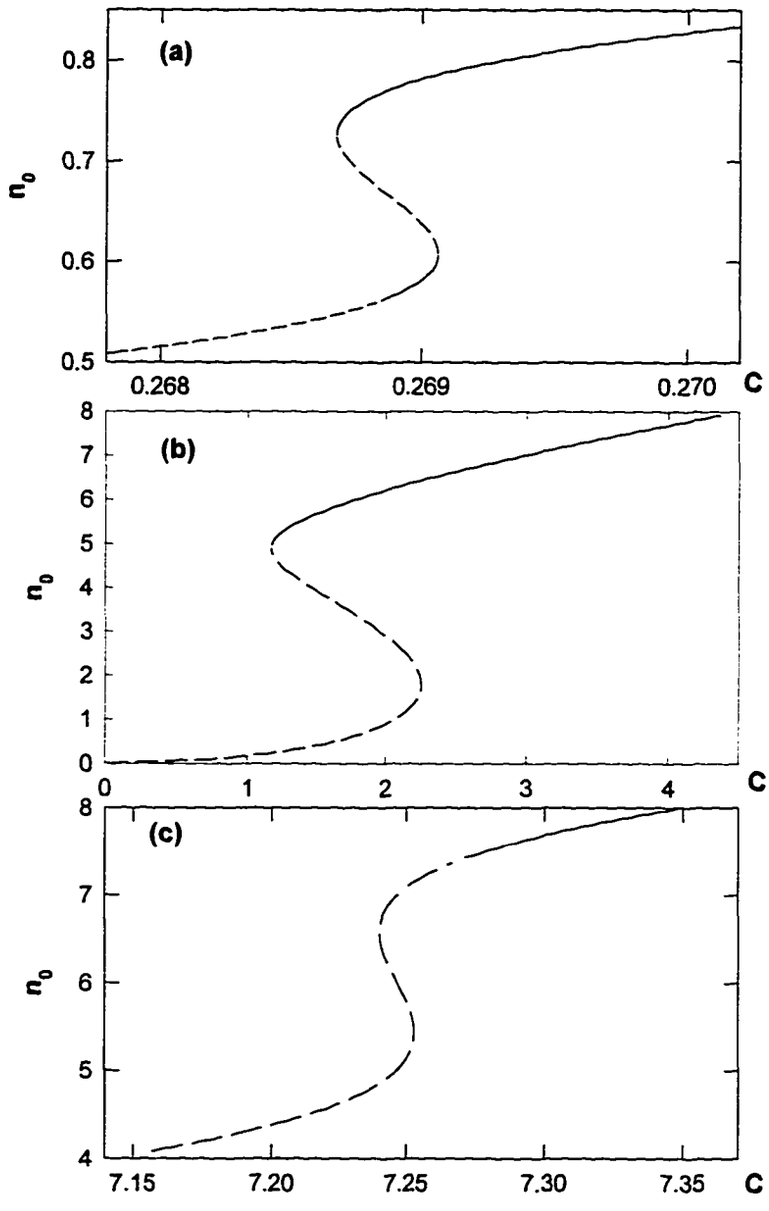

Fig.2. Steady State Scaled intensity, n_0, vs C in the region above threshold with (a) D=0.284, G=1; (b) D=0.525, G=5; (c) D=2.55, G=9. Solid line corresponds to stable steady state, dashed line to unstable steady state.

inversion (G<-1) is always stable. It is also stable in the region -1<G<0 where the inversion is positive but the laser is still below the resonant threshold. In the region $0 < G < \sqrt{12}D$ (gain between the resonant and off-resonant threshold) the dashed part of the curve in Fig.1(c) becomes unstable.

In the region $G>(12)^{1/2}D$ the plot of n_0 as a function of C, obtained from Eq. (2.11), becomes S-shaped, indicating the emergence of a possible bistable behavior in the above threshold regime of operation. As shown in Figs.2, there are three possibilities. Either part of the lower branch and the entire upper branch (Fig.2(a)), or the entire upper branch and none of the lower portions (Fig.2(b)), or just a part of the upper branch (Fig.2(c)) can be stable. Stable portions are denoted by solid line, unstable ones by dashed line. We note that as D increases, the gap between the vertical axis and the turning points of the S-shaped curves also increases. Since it is essentially in this gap region where most of the instabilities occur we can say that with the increase of the detuning the region of unstable behavior also increases. Also we find that the phase has a similar smooth behavior as a function of C.[22]

Figs.1 and 2 illustrate the two basic possibilities: either monotonic dependence on the atomic coherence as in the region below ordinary laser threshold or a multivalued characteristics as in the region above threshold.

3. Stability of the steady state

We study the stability of steady - state by employing the methods of normal mode analysis. In the neighborhood of steady state I_0 and ϕ_0, the intensity I(t) and phase $\phi(t)$ may be written as

$$I(t) = I_0 + \Delta I \; ; \quad \phi(t) = \phi_0 + \Delta\phi \; . \tag{3.1}$$

Substituting (3.1) into the equations of motion (2.5) and (2.6) and expanding d_I and d_ϕ around I_0 and ϕ_0 to first order in ΔI and $\Delta\phi$, neglecting higher order terms in the perturbations, we get the set of linearized equations

$$\frac{\partial \Delta I}{\partial t} = \left(\frac{\partial d_I}{\partial I}\right)_0 \Delta I + \left(\frac{\partial d_I}{\partial \phi}\right)_0 \Delta\phi \; , \tag{3.2}$$

and

$$\frac{\partial \Delta\phi}{\partial t} = \left(\frac{\partial d_\phi}{\partial I}\right)_0 \Delta I + \left(\frac{\partial d_\phi}{\partial \phi}\right)_0 \Delta\phi \; . \tag{3.3}$$

The subscript 0 means that the derivatives have to be evaluated in the steady state. Since this is a system of linear equations we can assume that a simple exponential solution, $\Delta I(t) = \Delta I(0)e^{\lambda t}$ and $\Delta\phi(t) = \Delta\phi(0)e^{\lambda t}$, exists. Substituting this ansatz into the above equations yields the following characteristic equation for λ,

$$\lambda^2 - \lambda\left(\frac{\partial d_I}{\partial I} + \frac{\partial d_\phi}{\partial \phi}\right) + \left(\frac{\partial d_I}{\partial I}\frac{\partial d_\phi}{\partial \phi} - \frac{\partial d_I}{\partial \phi}\frac{\partial d_\phi}{\partial I}\right) = 0 \; . \tag{3.4}$$

For the sake of simplicity we have omitted the subscripts from the derivatives. Solutions are

$$\lambda_{1,2} = \frac{1}{2}\left\{\left(\frac{\partial d_n}{\partial n} + \frac{\partial d_\phi}{\partial \phi}\right) \pm \sqrt{\left(\frac{\partial d_n}{\partial n} - \frac{\partial d_\phi}{\partial \phi}\right)^2 + 4\frac{\partial d_n}{\partial \phi}\frac{\partial d_\phi}{\partial n}}\right\}$$

$$=\frac{2G-4n+nG-n^2}{4(1+n)}\pm\frac{1}{2}\sqrt{\frac{(n^2-2n-nG)^2}{4(1+n)^2}-\frac{4D^2}{1+n}}\ . \tag{3.5}$$

In view of our ansatz for the solution any initial deviation from the steady state will decay exponentially in time if $Re\lambda<0$, where Re stands for the real part. Thus, this is just the condition of stability of the steady states. Applying Hurwitz's criteria, for the negative definiteness of the roots of a quadratic equation, to Eq.(3.4) gives two relations between the coefficients:

$$\frac{\partial d_I}{\partial I}\frac{\partial d_\phi}{\partial \phi}-\frac{\partial d_I}{\partial \phi}\frac{\partial d_\phi}{\partial I}>0\ , \tag{3.6}$$

and

$$\frac{\partial d_I}{\partial I}+\frac{\partial d_\phi}{\partial \phi}<0\ . \tag{3.7}$$

Using the expressions for the drift coefficients, Eqs. (2.7) and (2.8), and the steady state conditions, Eqs. (2.9) and (2.10), we can easily evaluate the left - hand side of Eq. (3.6), yielding

$$4D^2+G^2-4Gn_0+3n_0^2>0\ . \tag{3.8}$$

By comparing this expression to the equation for steady state, Eq.(2.11), we can see that it is equivalent to

$$\frac{\partial n_0}{\partial C}>0\ . \tag{3.9}$$

This is our first condition of stability. The other condition can easily be derived from Eq. (3.7). Again, using the explicit expressions for the drift coefficients and the steady state conditions, we obtain

$$n_0^2 + (4 - G)n_0 - 2G > 0 \,. \tag{3.10}$$

This inequality is satisfied for $n_0<n_{0,1}$ and $n_0>n_{0,2}$ where $n_{0,1}$ and $n_{0,2}$ are the roots of the quadratic expression on the left - hand side, arranged in such a way that $n_{0,1}<n_{0,2}$. The explicit expressions for the roots, from Eq. (3.10), are

$$n_{0,1} = \frac{G - 4 - \sqrt{G^2 + 16}}{2}, \qquad \text{and} \qquad n_{0,2} = \frac{G - 4 + \sqrt{G^2 + 16}}{2} \,. \tag{3.11}$$

From the first of these equations, $n_{0,1}<0$ always, independently of the value of G. Since $n_0>0$, by its definition, $n_{0,1}$ falls in the unphysical region and the inequality $n_0<n_{0,1}$ does not give any new condition for the stability. On the other hand, $n_{0,2}$ may fall in the physical region and the inequality $n_0>n_{0,2}$ may yield a second condition for the stability. As we shall see later, in this case the point $n_{0,2}$ is the critical point at which a Hopf bifurcation occurs. Therefore, with the notation $n_{0,2}=n_c$, the above requirement can be written as

$$n_0 > n_c, \quad \text{where} \quad n_c = \frac{G - 4 + \sqrt{G^2 + 16}}{2} \,. \tag{3.12}$$

This is our second condition of stability. In the following, we shall apply the two conditions, Eq. (3.9) and (3.12), to the investigation of the stability of the single valued steady state (the region below ordinary laser threshold) and multivalued steady state (the region above ordinary laser threshold) separately.

3.1. Stability of the single valued steady states

When we have a single valued steady state the first condition, Eq. (3.9), holds automatically. The slope of the intensity vs. coherence curve is given by Eq. (3.8). From this equation it follows that the steady state is single valued (the slope does not change sign) if $G \leq (12)^{1/2}D$ and multivalued otherwise (see Eq. (3.13) below). We can now distinguish between the regions $G<0$ and $0 \leq G \leq (12)^{1/2}D$. It should be noted at this point that $G_{th,1}=0$ is the threshold for the corresponding incoherently pumped laser without detuning and the expression $G_{th,2}=(12)^{1/2}D$ is the laser threshold for the corresponding incoherently pumped laser with detuning.

(i) In the region $G<0$ (or, equivalently, $G<G_{th,1}$) the critical point, n_c, defined in Eq. (3.12), is negative and the second stability condition, given in the same equation, is satisfied for all $n_0>0$, i.e., in the entire physical region. No part of the curves (a) and (b) in Fig.1 becomes unstable, for any value of the external control parameters.

(ii) In the region $0 \leq G \leq (12)^{1/2}D$ (or, equivalently, $G_{th,1} \leq G \leq G_{th,2}$) the photon number n_0 continues to be a single valued function of the coherence parameter C. In this region, however, $n_c>0$. Applying the second stability condition, Eq. (3.12), to this case gives that the part of the curve (c) in Fig.1, where $0 \leq n_0 < n_c$, is unstable (denoted with dashed line). Here n_c is a Hopf bifurcation point and in the region between the origin and n_c periodic oscillations occur. They branch away continuously from the steady state curve which, thus, is stable above the critical point. The region below the critical point, where the oscillations take place, will be studied in Section 4.

Summarizing the findings of this subsection we can conclude that the steady state is single valued if $G \leq G_{th,2}$. The entire steady state curve is stable if $G \leq G_{th,1}$ and the section between the origin and the critical point is unstable if $G_{th,1} < G \leq G_{th,2}$.

3.2. Stability of the multivalued steady states

When we are dealing with a multivalued steady state, i.e., the plot of the photon number vs. coherence is S-shaped as in Fig.2 then the first stability condition, Eq.(3.9), tells us that the portion with negative slope (the middle section of the S) is unstable. To investigate this case further we note that the two turning points of the S-shapes curve can be calculated from the zeros of the left-hand side of Eq.(3.8) since in these points the slope of the curve changes its sign. The turning points are then given by

$$n_1 = \frac{2G - \sqrt{G^2 - 12D^2}}{3}, \quad \text{and} \quad n_2 = \frac{2G + \sqrt{G^2 - 12D^2}}{3}, \tag{3.13}$$

so that $n_1 < n_2$. Obviously, we need $G > G_{th,2}$ to have two real turning points or a multivalued steady state. Conversely, in the region $G \leq G_{th,2}$ the steady state is single valued, a condition that we used in connection with the stability analysis in Sec. 3.1. It should be noted that, since $G > 0$, n_c is always positive and, thus, a part of the S-shaped function is always unstable. We can now distinguish three different parameter regions: I). $n_c < n_1$, II). $n_1 \leq n_c \leq n_2$, and III). $n_2 < n_c$. In region I the part of the curve with $n_0 < n_c$ on the lower branch in Fig.2(a) is unstable. The rest of the lower branch and the entire upper branch are stable. Between the stable parts of the upper and lower branches steady state

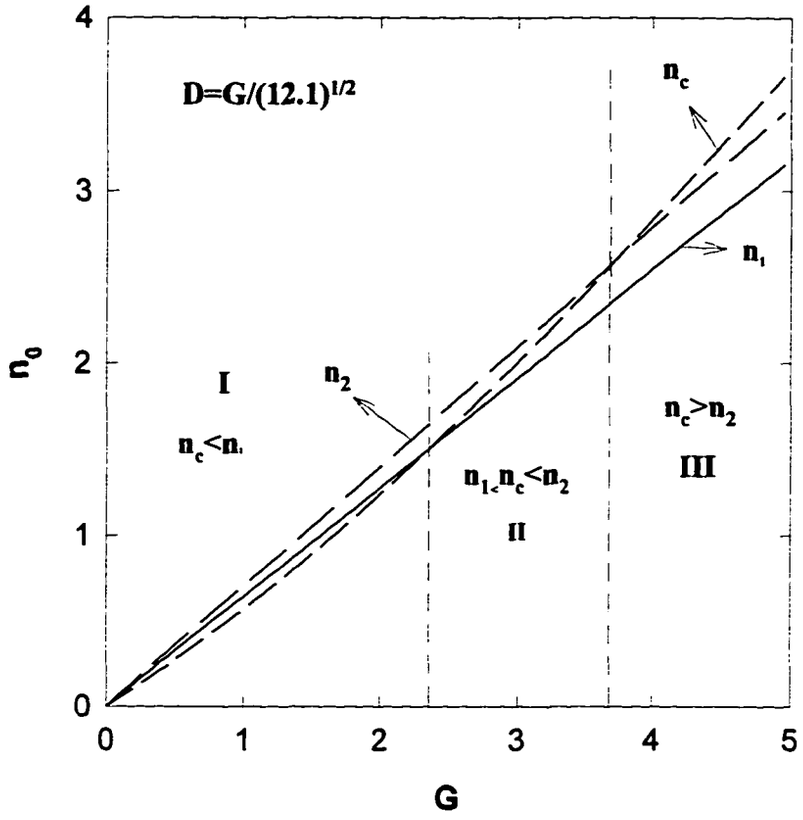

Fig.3. The critical point, n_c, and the lower and upper turning points, n_1 and n_2, vs. G for $D = \frac{G}{\sqrt{12.1}}$.

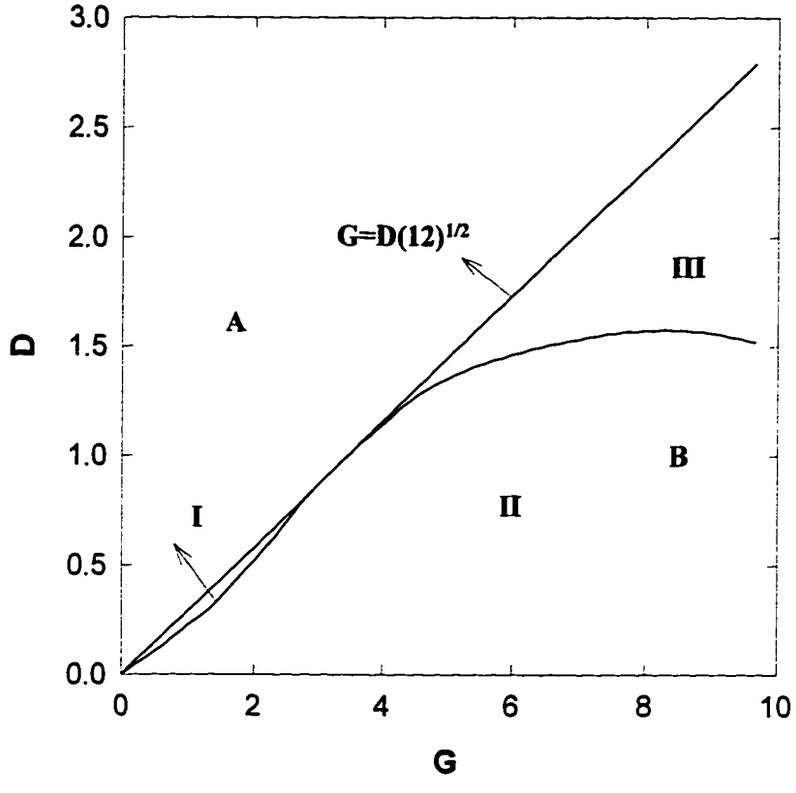

Fig.4. Projection of the D, G, C parameter space onto the D-G plane. The different regions correspond to the different stability regions discussed in the text.

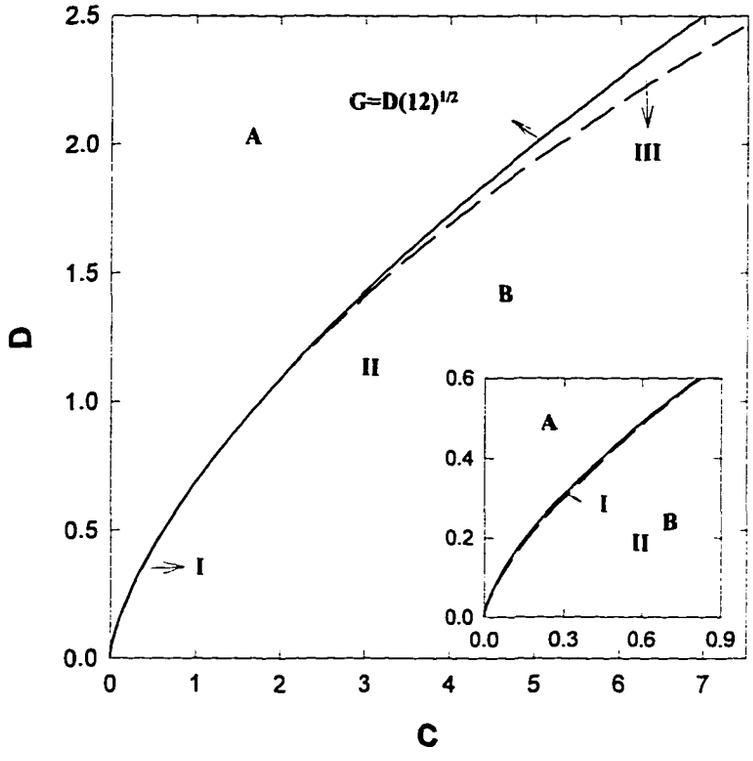

Fig.5. Projection of the D, G, C parameter space onto the C-D plane. The insert shows the lower left corner of the main plot enlarged to exhibit region I more clearly.

bistable behavior is expected. Beyond the Hopf bifurcation point, n_c, located on the lower branch periodic oscillations appear. In region II, n_c falls on the globally unstable middle branch and is never realized. In this case the upper turning point becomes an effective critical point beyond which non-Hopf oscillations appear. The entire upper branch is stable. This situation is depicted in Fig.2(b). Finally in region III the critical point is located on the upper branch. Beyond the critical point stable periodic oscillations evolve. The rest of the upper branch, $n_0>n_c$, is stable. A typical situation is shown in Fig.2(c).

In Figs.3 - 5 we summarize these findings. In Fig.3 the turning points, n_1, n_2, and the critical point, n_c, are depicted as functions of the gain parameter, G, for $D^2=G^2/12.1$. The regions correspond to the regions discussed above. In region I part of the lower branch is unstable, the critical point is a Hopf bifurcation point. In region II the entire upper branch is stable, the upper turning point is the effective non-Hopf bifurcation point. In region III part of the upper branch is stable, the critical point is again a Hopf bifurcation point. In Fig.4 we display the G-D parameter plane. In this plane the equations $G=(12)^{1/2}D$, $n_c=n_1$ and $n_c=n_2$ correspond to lines and play the role of separatrixes. They separate the parameter plane into five regions. Above the line $G=(12)^{1/2}D$ is region A(ii) of the previous subsection, where n_0 is a single valued function of C, as in Fig.1(c), since $0<G^2<12D^2$. The region below this line is region B investigated in this subsection. The other two lines divide region B further. In region I, some part of the lower branch and the entire upper branch are stable. In region II, only the upper branch is stable and the upper turning point is a non-Hopf bifurcation point. Finally, in region III, only part of the upper branch is stable. In Fig.5 we display the D-C parameter plane as for Fig.4. Region I is so

small in this plane that we show the lower left corner of Fig.5, region I, enlarged in the insert in order to make it visible.

4. Dynamical evolution

So far, we have dealt with the steady states of the system by replacing the time derivatives with zero on the left-hand side of Eqs. (2.5) and (2.6). Let us now consider time dependent scenarios by keeping the full time dependence in the equations. In this Section we shall investigate time evolution from a given initial condition. In particular, in Part 4.1 we shall study how the system approaches steady state in those regions of the external control parameters where they exist. In Part 4.2 we shall investigate the states that evolve from a given initial state in the unstable regions.

First, we rewrite Eqs. (2.5) and (2.6) in terms of the scaled external parameters introduced in Eqs. (2.7) and (2.8) and the scaled photon number and phase, n and ϕ, which are obvious generalizations of n_0 and ϕ_0 for the time dependent case, as

$$\frac{dn}{d\bar{t}} = d_n = n\frac{G-n}{1+n} - \frac{2\sqrt{n}C}{1+n}\sin\phi \ , \tag{4.1}$$

and

$$\frac{d\phi}{d\bar{t}} = d_\phi = D - \frac{C}{\sqrt{n}}\cos\phi \ . \tag{4.2}$$

In these equations we introduced the scaled time variable, $\bar{t} = \gamma t$. The nonlinear dynamics of the system is completely determined by Eqs. (4.1) and (4.2).

4.1. Transients around stable steady states

The above equations allow for an approximate separation of the dynamics of the phase and intensity in the vicinity of the critical point, n_c. Eq.(4.1) then determines the intensity and Eq.(4.2), being just the phase locking equation, the phase. Further away from n_c, the dynamics of the phase and intensity become entangled. Instead of separately giving the results of the analytical treatment for the neighborhood of the critical region we just present the numerical results, valid for a broad range of parameters.

We can get some analytical insight into the relaxation dynamics by studying the trajectories in the n-ϕ plane. By transforming equations (4.1) and (4.2) to the form

$$\frac{dn}{d\phi} = \frac{d_n}{d_\phi}, \tag{4.3}$$

we can obtain the governing equation. Since the time $\bar{t}$ does not appear explicitly in this equation, we can exhibit the integral curves in the n-ϕ plane. Each point (n, ϕ) in this plane represents a possible set of initial conditions. A trajectory going through this particular point then determines the time evolution of the system, starting from this initial condition. In Fig.6 we plot the intensity n vs. phase ϕ. The steady state now correspond to attractive singular points. In Fig.6(b), points a and b correspond to stable upper branch and stable lower branch, respectively. In Fig.6(c), corresponding to the situation when the upper turning point is the effective critical point, there are three singularities. Point a (5.6, $-\pi/2$) is an attractive fix point (stable node, all trajectories run towards this point) and the corresponding steady-state is realized. This point corresponds to the stable steady state on

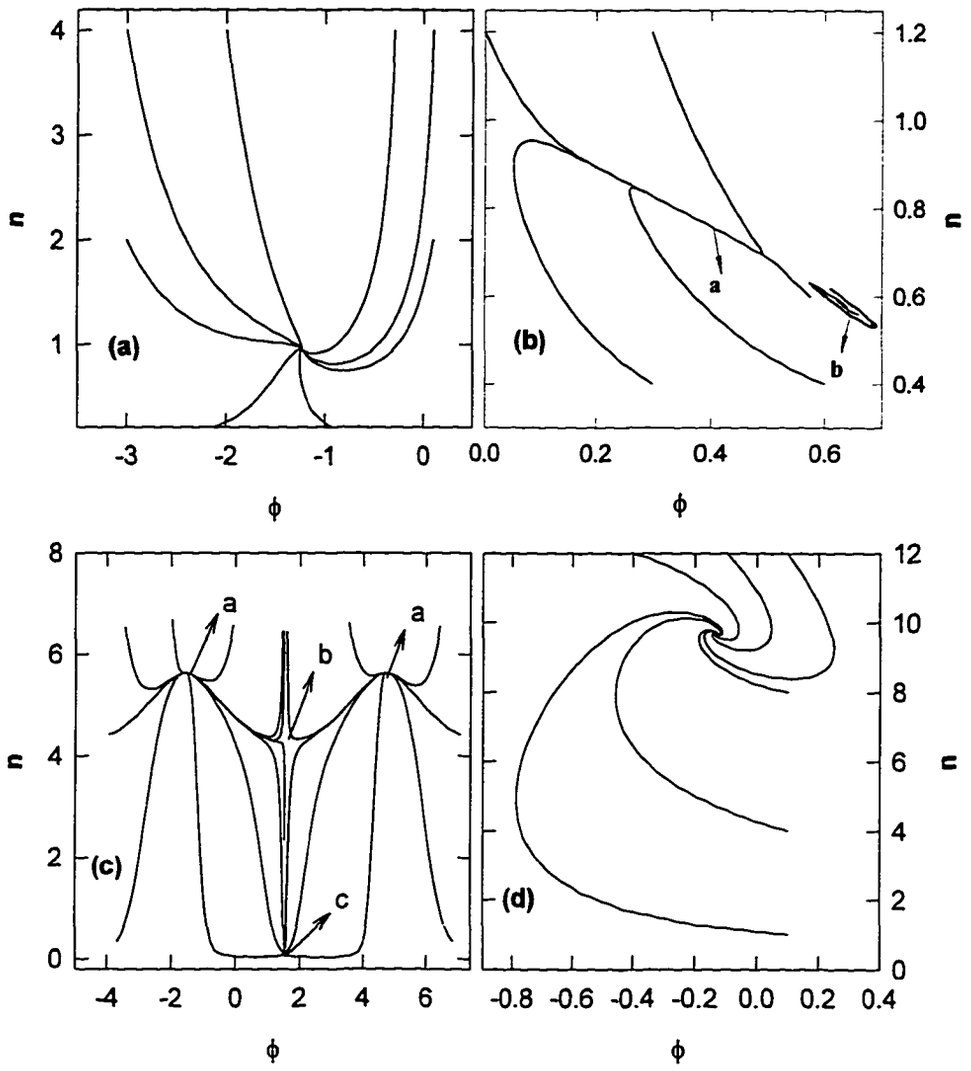

Fig. 6. n-ϕ Trajectories for (a) C=0.75, D=0.25, G=-0.5 [cf. line (b) in Fig.1]; (b) C=0.269, D=0.284, G=1 [cf. Fig.2 (a)]; (c) C=1.40, D=0.525, G=5 [cf. Fig.2 (b)]; (d) C=8, D=2.55, G=9 [cf. Fig.2 (c)].

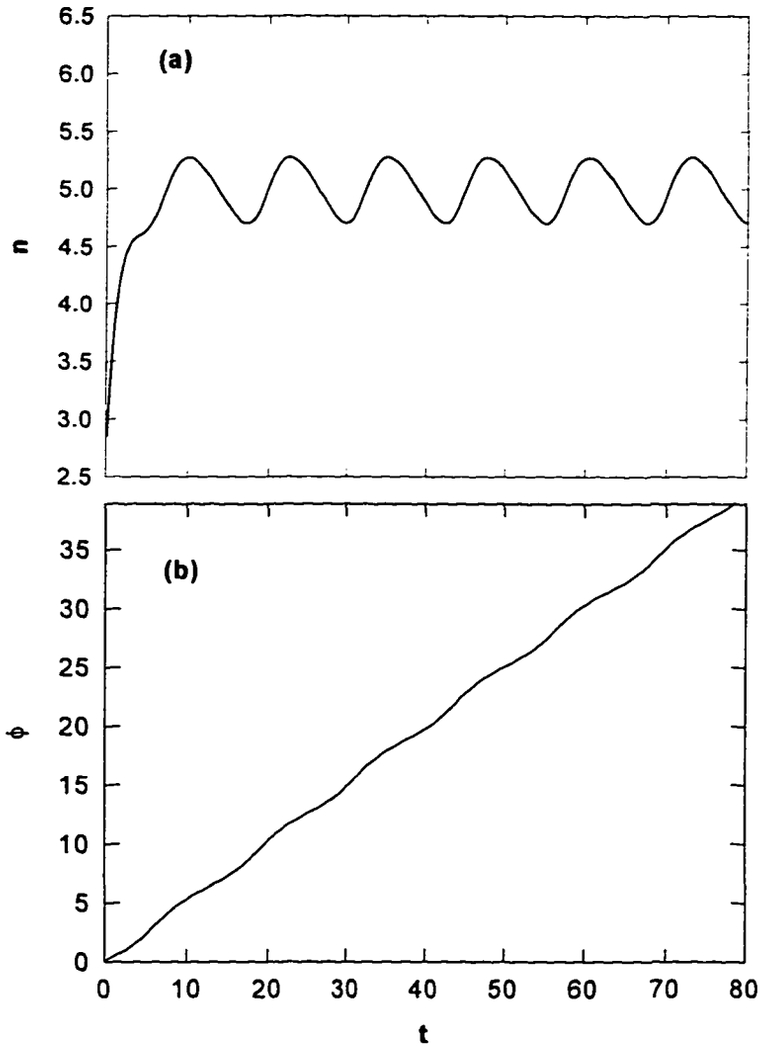

Fig. 7. Time evolution of the intensity n (a) and phase ϕ (b) with D=0.525, G=5, C=0.75.

the upper branch in Fig.2(b). Point b (4.1, $\pi/2$) is a repulsive fix point, all trajectories run away from this point. It corresponds to the unstable steady state on the middle branch. Finally, point c (0.34, $\pi/2$) is a metastable fix point with some trajectories running into others originating from it. It corresponds to the unstable steady state on the lower branch. Any slight deviation from point b or point c will result in passage to the stable point a. In the n-ϕ plane, the point ($n(\bar{t})$, $\phi(\bar{t})$) moves, with the increase of the time $\bar{t}$, along the integral curve and converges ultimately to the stable point a. Thus the time - varying solutions are correlated with the trajectories of (4.3) and the steady - state with the singular points, a, b, and c, in the n-ϕ plane.

4.2. Time evolution in the unstable regions

In this subsection we shall discuss time evolution from a given initial condition in those regions of the external control parameters where the steady state become unstable, i.e., beyond the critical point. This corresponds to a choice of the initial condition such that $n(0)<n_c$. We find that $n(\bar{t})$ oscillates around a value which is very close to the critical intensity, n_c, after the initial transients have decayed. The period of oscillations, T, can be found from

$$T=\int_0^{2\pi}\frac{d\phi}{D-\frac{C}{\sqrt{n_c}}\cos\phi}=\frac{2\pi}{\sqrt{D^2-\frac{C^2}{n_c}}}\,. \tag{4.4}$$

The intensity $n(\bar{t})$ and phase $\phi(\bar{t})$ vs. $\bar{t}$ is depicted in Fig.7(a) and (b), respectively, with D=0.525, G=5, and C=0.75. The phase time dependence has two

ingredients. First, there is a constant shift of the operating frequency which results in a steady increase of the phase, strictly proportional with time. This is represented by the average slope of the phase vs. time curve. Second, superimposed on this straight line development, there is a small oscillation very similar to the oscillation of the average intensity. In particular, the frequency of these phase oscillations is the same as that of the intensity oscillations, given by Eq.(4.4).

Next, we present a more detailed numerical analysis around the Hopf-bifurcation point. We study two typical cases. In the first case, a portion of the lower branch and the entire upper branch are stable(Fig.2(a)), while in the second case only a portion of the upper branch is stable(Fig.2(c)). We display our numerical results for the intensity vs. coherence for the first case in Fig.8(a) and (b). The dashed line corresponds to the unstable steady state, the solid line to stable steady state, and the triangle to the average value of the stable periodic solution. These two figures show the same behavior for the stable steady state and two different possibilities for the stable periodic solution. For the smaller gain G=1.0 and detuning D=0.284, when approaching the Hopf-bifurcation point, the average value of the periodic solutions decreases continuously from around the upper turning point value to the lower stable branch. For the larger gain G=2.1, and detuning D=0.604, there are two branches for the average value of the periodic solutions. One is around the upper turning point, the other is between the lower stable branch and the middle unstable branch. From these two figures, we can find that in some regime there are two stable steady states and in some regime there are a stable steady state and a stable periodic solution.

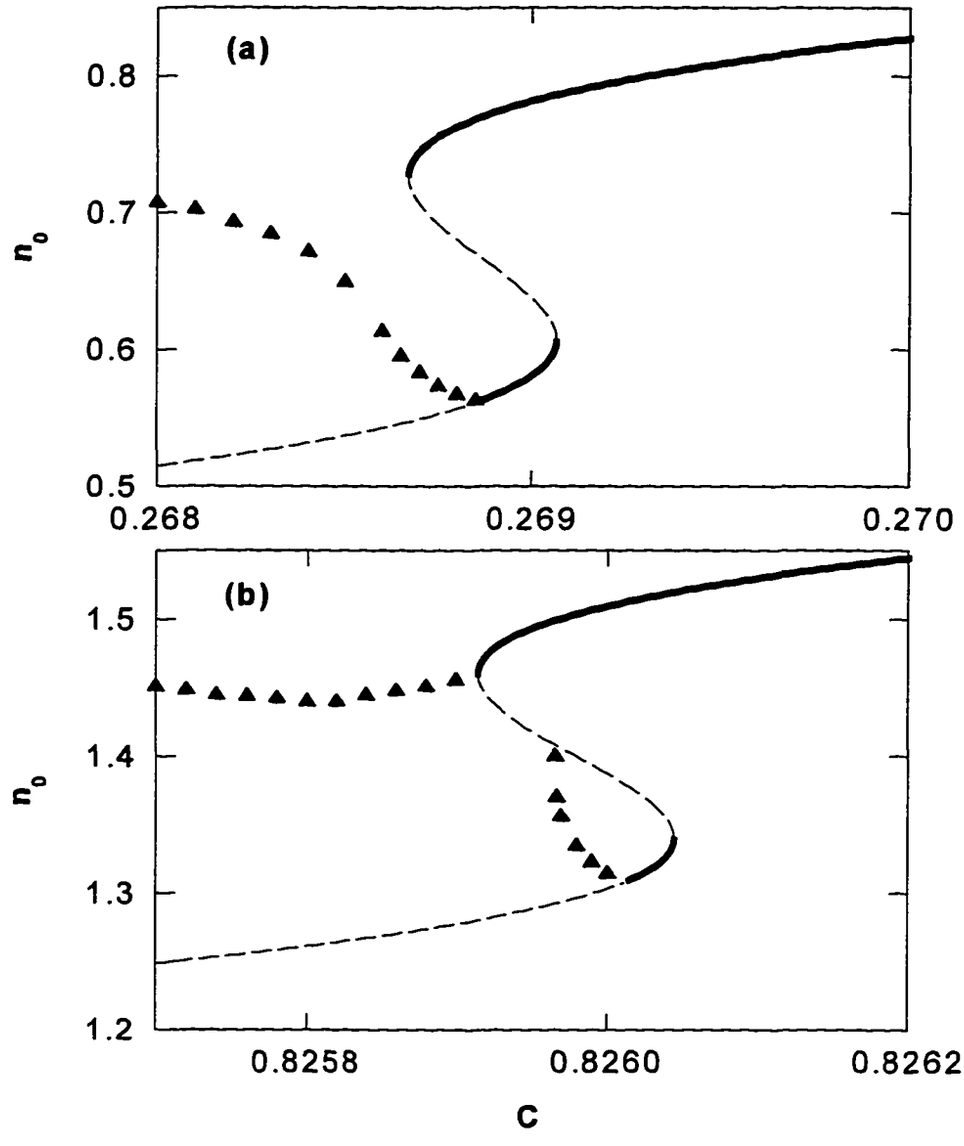

Fig.8. Intensity n_0 vs atomic coherence C with (a) D=0.284 and G=1.0; (b) D=0.604 and G=2.1. Solid line corresponds to the stable steady state, dashed line to unstable state, triangle to the average value of the periodic solution.

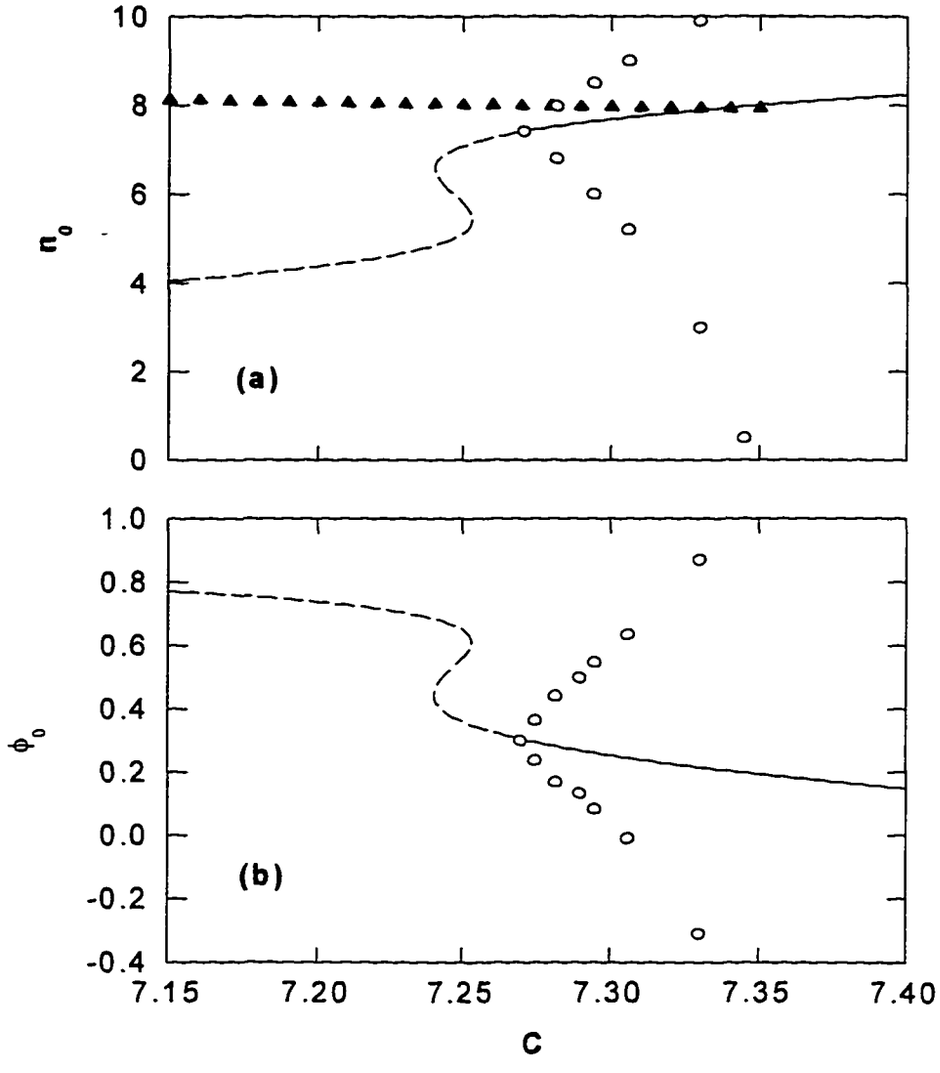

Fig.9. Intensity n_0 (a) and Phase ϕ_0 (b) vs atomic coherence C with D=2.55 and G=9.0. Solid line corresponds to stable steady state, dashed line to unstable steady state, triangle to the average value of the periodic solution, and circles show the boundary between region of the initial values leading to stable steady state and oscillatory behavior, respectively.

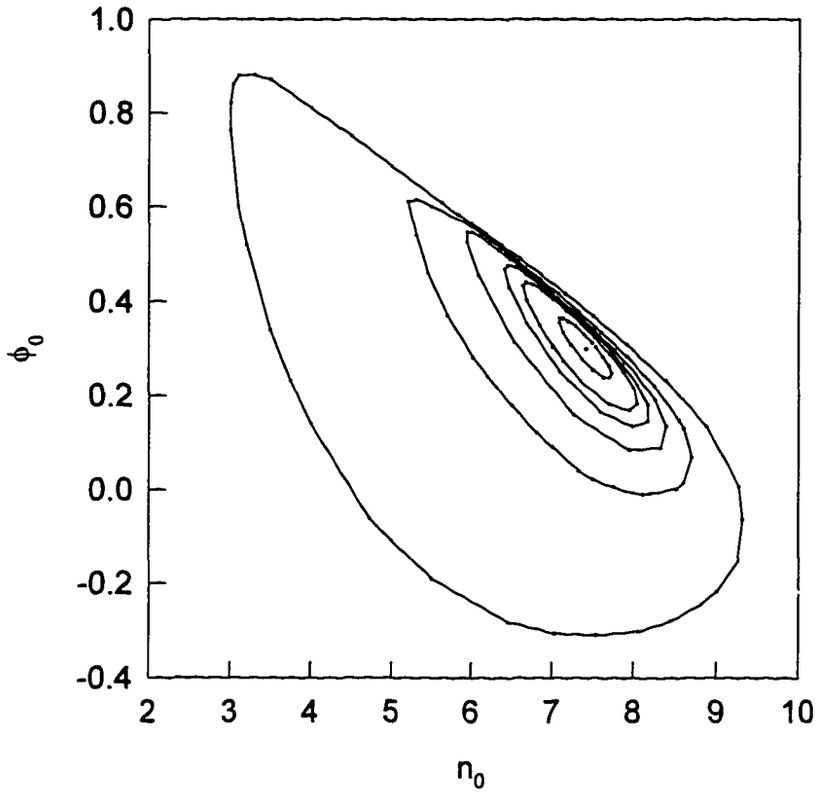

Fig.10. The initial value n_0-ϕ_0 contour with D=2.55 and G=9.0. The C value, starting from center point, is 7.270, 7.275, 7.282, 7.290, 7.295, 7.036, 7.330, respectively.

We plot the stable intensity(solid line), the unstable intensity(dashed line) and the stable periodic solutions in Fig.9(a) for the second case with G=9, D=2.55. The circles show the boundary of the stable range. The intensity with initial value n(0), which is inside the range between the circles, will reach the stable steady state. The intensity with initial value n(0), which is outside the range, will oscillate around the value given by the triangle. We show the corresponding plot for the phase with same gain and detuning in Fig.9(b). There is no stable periodic solution for phase(Fig.7(b)). Since the final state depends on initial values, n(0) and $\phi(0)$, we show the n(0)-$\phi(0)$ contour in Fig.10. Starting from the center point, the values of coherence, C, are 7.270, 7.275, 7.282, 7.290, 7.295, 7.036, 7.330, respectively. For a specific C value, if n(0) and $\phi(0)$ are inside the corresponding contour, the final state is stable steady state. Otherwise, the final state is stable periodic solution.

Before we develop an analytical theory of the frequency shift (the slope of the curves in Fig.7(b)) we display this oscillatory behavior from another point of view. Namely, we again discuss the integral curves, resulting from Eq. (4.3). This time, however, instead of displaying the trajectories in the n-ϕ plane, we will plot them in the X-Y phase plane of quadratures,[61] where $X = \sqrt{n_0}\cos\phi_0$ and $Y = \sqrt{n_0}\sin\phi_0$ are the usual quadratures component variables. Fig.11 shows the trajectories in the X-Y plane with C=0.75 and G=5 and D=0.525. Each trajectory approaches a stable limit cycle. The point $(X(\bar{t}), Y(\bar{t}))$, starting from any initial condition, after the initial transients, i.e., after the approach to the limit cycle, moves along the limit cycle as $\bar{t}$ increases. The period required for the point to complete one cycle is given by (4.4).

Finally, we turn our attention to the study of the operating frequency of the laser. In our assumption, the atom-field detuning is much smaller than the cavity-field detuning, i.e., $\omega - \nu << \Omega - \nu$. In fact, for the case of stable frequency locking, the atom-field detuning vanishes. For the general case, we can write the field as[6]

$$E \propto e^{i\nu t} \propto e^{i\omega t - \phi} . \tag{4.5}$$

Clearly, for frequency locking $\nu=\omega$ and ϕ=constant. In the unstable regimes the phase ϕ of the electric field, in accordance with Fig.7(b), can be represented as $\phi = \Delta\nu t + \Delta\phi(0)\cos(2\pi t/T)$. The deviation from the atomic frequency is given by $\Delta\nu$= $<d\phi/dt>$, where $< >$ stands for time average (it should be noted that frequencies are measured in units of γ and time in units of γ^{-1} throughout this Section). We can now expand the general phase equation (2.6) to lowest order in γ/Γ, keeping the atomic detuning δ in it as in Eq.(2.8), around the mean values of the oscillations, n_{av} and $\Delta\nu t$, to obtain

$$\frac{d\phi}{d\bar{t}} = \frac{D - \dfrac{C}{\sqrt{n_{av}}}\cos\phi}{1 + \dfrac{G+1}{n_{av}+1}\dfrac{\gamma}{2\Gamma} - \dfrac{C}{\sqrt{n_{av}}}\dfrac{\gamma}{\Gamma}\sin\phi} . \tag{4.6}$$

The above expression has some interesting consequences:

(1) For C=0 we have $\dfrac{d\phi}{d\bar{t}} = \Delta\nu = \dfrac{D}{1 + \dfrac{G+1}{n_{av}+1}\dfrac{\gamma}{2\Gamma}}$, giving $\nu = \omega - \Delta\nu = \dfrac{2\Gamma\Omega + \gamma\omega}{2\Gamma + \gamma}$, which is just the operating frequency of a usual incoherently pumped laser as given by the frequency pulling expression.[15]

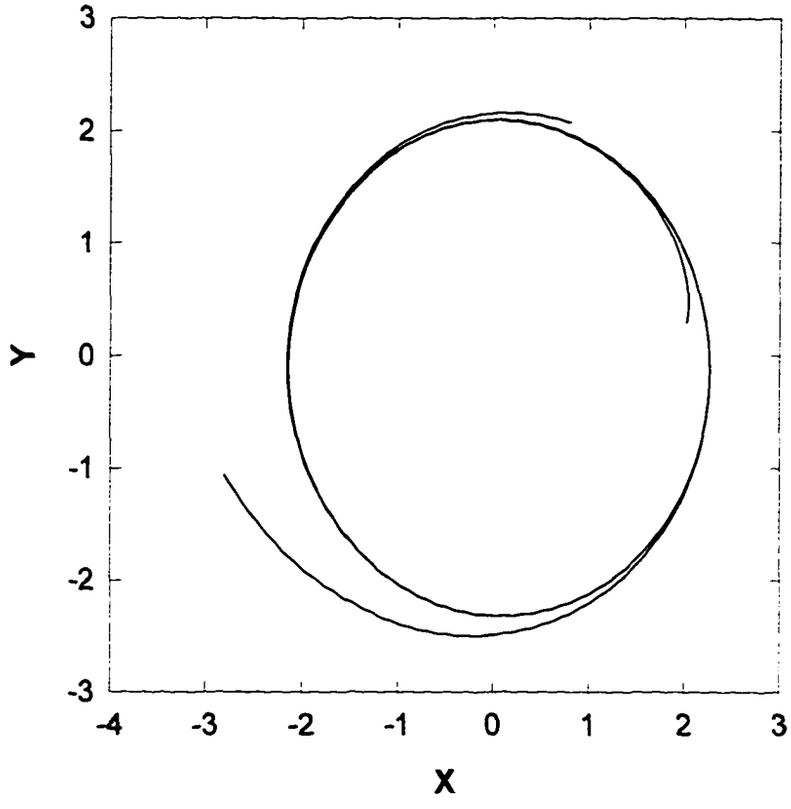

Fig.11. Integral curves in the phase plane of quadratures, X and Y, with D=0.525, C=0.75, G=5.

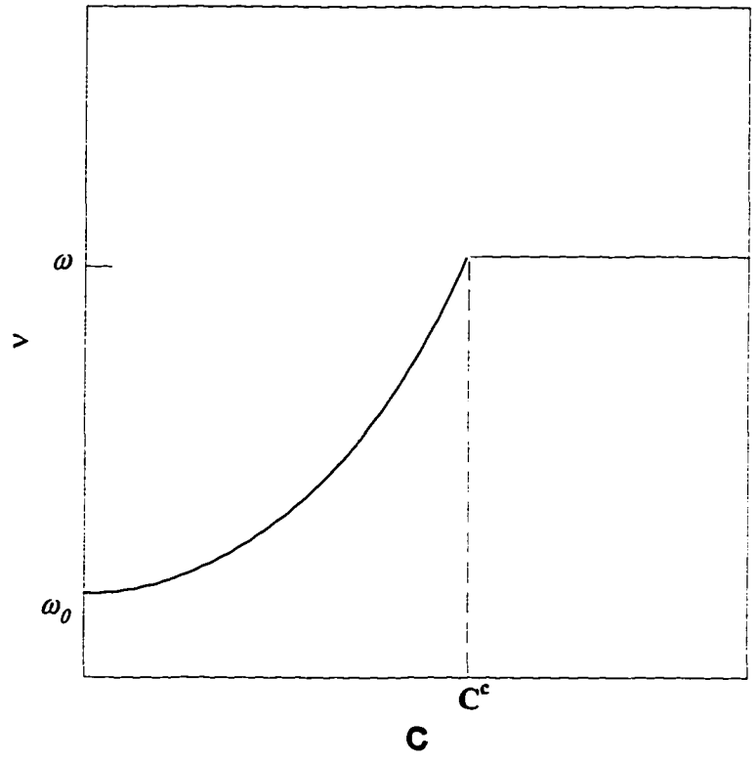

Fig.12. Average operating frequency of the laser in the unstable region of operation. Corresponds to the average slope of the curve in Fig.7.

(2) If $C>C_c$ ($D<D_c$) the phase is locked, $d\phi/dt=0$. This also involves that the laser frequency is locked to the atomic frequency, $\nu=\omega$. (Here C_c and D_c are the values of the coherence and detuning, respectively, in the critical point.)

(3) For the intermediate case, when $C<C_c$ and $D>D_c$, there is no stable frequency locking. As it has already been discussed in connection with Fig.7(b) the frequency is shifted from the atomic frequency and superimposed on this shift, there is also a small oscillatory part of the phase. The frequency shift is a function of the external control parameters and can be obtained in analytical form by taking the average of Eq. (4.6), yielding

$$\Delta\nu = < \frac{d\phi}{dt} > = \frac{\sqrt{D^2 - \frac{C^2}{n_{av}}}}{1 + \frac{G+1}{1+n_{av}} \frac{\gamma}{2\Gamma}} . \qquad (4.7)$$

As the amplitude of atomic coherence C increases, the average deviation decreases. When C is larger than a critical value, the average deviation is zero, i.e., frequency locking occurs. The mean operating frequency, ν, vs. the coherence parameter, C, is plotted in Fig.12 for the unstable region of operation. The result of this calculation is in excellent agreement with the average slope of the various $\phi(t)$ plots in Fig.7(b).

5. Noise dynamics

In order to consider the effect of both atomic coherence and pumping statistics on the quantum noise of the laser we adopt the following model. We assume that a beam of three - level atoms first passes through a preparation region then enters the laser cavity. In

the preparation region, each atom is excited from a distant ground level *c* to the upper level *a* of the lasing transition with a probability p, and then interacts with a preparation field producing the initial atomic coherence between the upper level *a* and lower level *b* of the transition. When the atoms leave the preparation region, they have a proper form of the initial atomic coherence and pumping statistics distribution, which, in some cases, can be adequately described by the Bernoulli's distribution.

Inside the cavity, the system we are going to consider is the same as in the previous Sections, except for the inclusion of pumping statistics of the atoms: two - level active atoms consisting of an upper level *a* and a lower level *b*. These active atoms are injected into the laser cavity at a rate r to interact with the laser field, and the initial density matrix is given by Eq.(2.1).

If we assume that the interaction time of each atom with the field inside the cavity is much smaller than the cavity damping time, the dissipation during the interaction can be neglected. Let the *j*th atom enter the cavity at the time t_j and spend a time τ inside the cavity. We can write

$$\rho(t_j + \tau) = M(\tau)\rho(t_j) \ . \tag{5.1}$$

Here the operator $M(\tau)$ describes the change of $\rho(t_j)$ due to the interaction with a single atom and its explicit form will depend on the particular model under consideration.

If n atoms cross the cavity from initial time 0 to the time t, the density matrix of the field at time t is

$$\rho^{(n)}(t) = M^n\rho(0) \ . \tag{5.2}$$

We have taken into account the fact that each atom finds the field in the state prepared by the preceding atom.

Because the atoms have a pumping statistics distribution we must average Eq.(2.3) with the distribution. Finally, we have[4]

$$\frac{d}{dt}\rho(t) = \frac{r}{p}\ln[1+p(M-1)]\rho(t) \ . \tag{5.3}$$

If M-1 is small, we consider p an expansion parameter, and expand Eq.(5.3)

$$\frac{d}{dt}\rho(t) = r[(M-1)-\frac{p}{2}(M-1)^2+...]\rho(t) \ . \tag{5.4}$$

In Ref[62], Eq.(5.4) remains valid in the sense of an asymptotic expansion to adequately describe the time rate of change of the density operator due to interactions with the gain reservoir even after including the loss into the master equation.

In our model, we will consider a laser with the initial atomic coherence and pumping statistics, so M is the operator with the initial atomic coherence[18]. Using P representation, Eq.(5.3) can be transformed into a Fokker - Planck equation. In this paper we want to discuss the properties of the intensity and phase of laser field. So we will express the Fokker - Planck equation in terms of intensity I and phase ψ. Introducing $n = (\beta/\alpha)I$ and $\phi = \psi - \theta$, where θ is the phase of ρ_{ab}. we have

$$\frac{\partial P}{\partial t} = \{-\frac{\partial}{\partial n}d_n - \frac{\partial}{\partial \phi}d_\phi + \varepsilon\frac{\partial^2}{\partial n^2}D_{nn} + \varepsilon\frac{\partial^2}{\partial \phi^2}D_{\phi\phi} + 2\varepsilon\frac{\partial^2}{\partial n\partial \phi}D_{n\phi}\}P \ , \tag{5.5}$$

$$d_n = \frac{(G-n)n}{1+n} - \frac{2\sqrt{nC}}{1+n}\sin\phi \ , \tag{5.6}$$

$$d_\phi = D - \frac{C}{\sqrt{n}}\cos\phi\,, \tag{5.7}$$

$$D_{nn} = \frac{n}{(1+n)^2}\left(\frac{A+G+1}{2} + \frac{(A-G-1)n}{2} + 2C\sqrt{n}\sin\phi\right) - \frac{p}{2}n\left[\frac{n(1+G)^2}{2(1+n)^2}\right.$$

$$\left. + \frac{2C^2\sin^2\phi}{(1+n)^2} - \frac{2(G+1)C\sin\phi\sqrt{n}}{(1+n)^2}\right], \tag{5.8}$$

$$D_{\phi\phi} = \frac{1}{4n(1+n)}\left(\frac{A+G+1}{2} + \frac{An}{2} + C\sqrt{n}\sin\phi\right) -$$

$$\frac{p}{2}\left(\frac{D^2}{2} + \frac{C^2\cos^2\phi}{2n} - \frac{D\sqrt{n}C\cos\phi}{n}\right), \tag{5.9}$$

$$D_{n\phi} = \frac{\sqrt{n}C\cos\phi}{4(1+n)} - \frac{p}{8(1+n)}[Dn(G+1) - 2D\sqrt{n}C\sin\phi$$

$$-\sqrt{n}(G+1)C\cos\phi + C^2\sin 2\phi]\,. \tag{5.10}$$

where $\varepsilon=\beta/\alpha$ and $A=\alpha/\gamma$. Here we assume the atom - field detuning to be zero.

From the Fokker - Planck equation, we can get an infinite set of ordinary differential equations for moments. If we assume the noise to be very weak, $\varepsilon << 1$, we can truncate these equations into a finite set of nonlinear equations. Here we assume that only the first and second - order moments are non zero. These non zero moments obey the following equations:

$$\frac{d}{dt}<n>=<d_n>\,, \tag{5.11}$$

$$\frac{d}{dt}<\phi>=<d_\phi>\,, \tag{5.12}$$

$$\frac{d}{dt}<(\delta n)^2>=2<d_n\delta n>+2\varepsilon<D_{nn}>, \tag{5.13}$$

$$\frac{d}{dt}<(\delta\phi)^2>=2<d_\phi\delta\phi>+2\varepsilon<D_{\phi\phi}>, \tag{5.14}$$

$$\frac{d}{dt}<(\delta n)(\delta\phi)>=<d_n\delta\phi>+<d_\phi\delta n>+2\varepsilon<D_{n\phi}>. \tag{5.15}$$

Here we introduced the notations $\delta n=n-<n>$, $\delta\phi=\phi-<\phi>$. In this section we will use these equations to discuss the steady - state noise and the dynamical noise.

5.1. Steady State

First we pay attention to the steady - state diffusion coefficients. In steady state (n_0, ϕ_0), for the stable values, the value of $\sin\phi_0$ is less than zero. So both the atomic coherence ρ_{ab} and pumping statistics p can reduce the intensity diffusion coefficient D_{nn}, but only the atomic coherence C can reduce the phase diffusion coefficient $D_{\phi\phi}$. In steady state the diffusion coefficients are

$$D_{nn}^0=\frac{n_0}{(1+n_0)^2}\left(\frac{A+G+1}{2}+\frac{A-G-1}{2}n_0+2C\sqrt{n_0}\sin\phi_0\right)-\frac{p}{2}n_0\left[\frac{n_0(1+G)^2}{2(1+n_0)^2}\right.$$

$$\left.+\frac{2C^2\sin^2\phi_0}{(1+n_0)^2}-\frac{2(G+1)C\sin\phi_0\sqrt{n_0}}{(1+n_0)^2}\right], \tag{5.16}$$

$$D_{\phi\phi}^0=\frac{1}{4n_0(1+n_0)}\left(\frac{A+G+1}{2}+\frac{An_0}{2}+C\sqrt{n_0}\sin\phi_0\right), \tag{5.17}$$

$$D_{n\phi}^0=\frac{Dn_0}{4(1+n_0)}. \tag{5.18}$$

In the following we discuss the steady - state variances of the intensity and phase. In the P representation, the intensity variance is[61]

$$<(\Delta I)^2>=<(\delta I)^2>+<I>, \tag{5.19}$$

and the phase variance is

$$<(\Delta\phi)^2>=<(\delta\phi)^2>+\frac{1}{4<I>}, \tag{5.20}$$

where (δ...) corresponds to the normal ordered part of (Δ...).

Expanding d_n, d_ϕ, D_{nn}, $D_{n\phi}$, and $D_{\phi\phi}$ around steady state n_0, ϕ_0 up to the first order in δn and δϕ, we get

$$\frac{d}{dt}<(\delta n)^2>=2\left(\frac{d}{dn}d_n\right)_0<(\delta n)^2>+2\left(\frac{d}{d\phi}d_n\right)_0<(\delta n\delta\phi)>+2\varepsilon(D_{nn})_0, \tag{5.21}$$

$$\frac{d}{dt}<(\delta\phi)^2>=2\left(\frac{d}{d\phi}d_\phi\right)_0<(\delta\phi)^2>+2\left(\frac{d}{dn}d_\phi\right)_0<(\delta n\delta\phi)>+2\varepsilon(D_{\phi\phi})_0, \tag{5.22}$$

$$\frac{d}{dt}<(\delta n\delta\phi)>=\left(\frac{d}{dn}d_\phi\right)_0<(\delta n)^2>+\left(\frac{d}{d\phi}d_n\right)_0<(\delta\phi)^2>$$

$$+\left[\left(\frac{d}{dn}d_n\right)_0+\left(\frac{d}{d\phi}d_\phi\right)_0\right]<(\delta n\delta\phi)>+2\varepsilon(D_{n\phi})_0. \tag{5.23}$$

By setting d/dt=0 in equations (5.21), (5.22), (5.23) and solving for $(\delta n)^2$ and $(\delta\phi)^2$, then inserting these into (5.19) and (5.20), we can get

$$\frac{<(\Delta I)^2>}{I}=1+\frac{D_2(D_2D_{22}-D_4D_{11}n^2-2D_3D_{12}n)+D_3n^2(D_1+D_3)D_{11}}{n^2(D_1+D_3)(D_2D_4-D_1D_3)}, \tag{5.24}$$

and

$$<(\Delta\phi)^2>I=\frac{1}{4}+\frac{D_4(D_4D_{11}n^2-D_2D_{22}-2D_1D_{12}n)+D_1(D_1+D_3)D_{22}}{(D_1+D_3)(D_2D_4-D_1D_3)}. \qquad (5.25)$$

Here we introduced the notation $D_1=\frac{\partial d_n}{\partial n}$, $D_2=\frac{\partial d_n}{\partial \phi}$, $D_3=\frac{\partial d_\phi}{\partial \phi}$, $D_4=\frac{\partial d_\phi}{\partial n}$. and $D_{11}=(D_{nn})_0$, $D_{12}=(D_{n\phi})_0$, $D_{22}=(D_{\phi\phi})_0$.

Using equations (5.24) and (5.25) , we can plot the values of $<(\Delta I)^2>/I$ and $<(\Delta\phi)^2>I$ as a function of the injected atomic coherence C for several sets of parameters. Intensity noise as a function of C, for zero detuning, is plotted in Fig.13(a). Dashed line is for random pumping(p=0), solid line for regular pumping(p=1). The parameters are: D=0, G=5 and A=7.5. Phase noise is shown in Fig.13(b). We find that injected atomic coherence can reduce both the intensity and phase noise and the larger the injected atomic coherence, the lower the noise. Also we find that pump regularity is a very important factor for intensity noise squeezing but has no effect on the phase noise under the condition of zero detuning. In Fig.13(a) there is almost 75% squeezing in the laser intensity for C=2.25. We notice that the range of ρ_{ab} depends on ρ_{aa} and ρ_{bb}, that is $0 \le \rho_{ab} \le (\rho_{aa}-\rho_{bb})^{1/2}$. For our parameters, the range of ρ_{ab} is: $0 \le \rho_{ab} \le 0.3$, so the range of C is $0 \le C \le 2.25$.

In Figs.14(a) and 14(b) we plot the intensity noise and phase noise, respectively, as a function of detuning D, with A=2.5, G=-1, and C=1.25.

Though the noise with detuning is still larger than the noise without detuning for the same initial atomic coherence C, the coupling of initial atomic coherence C and

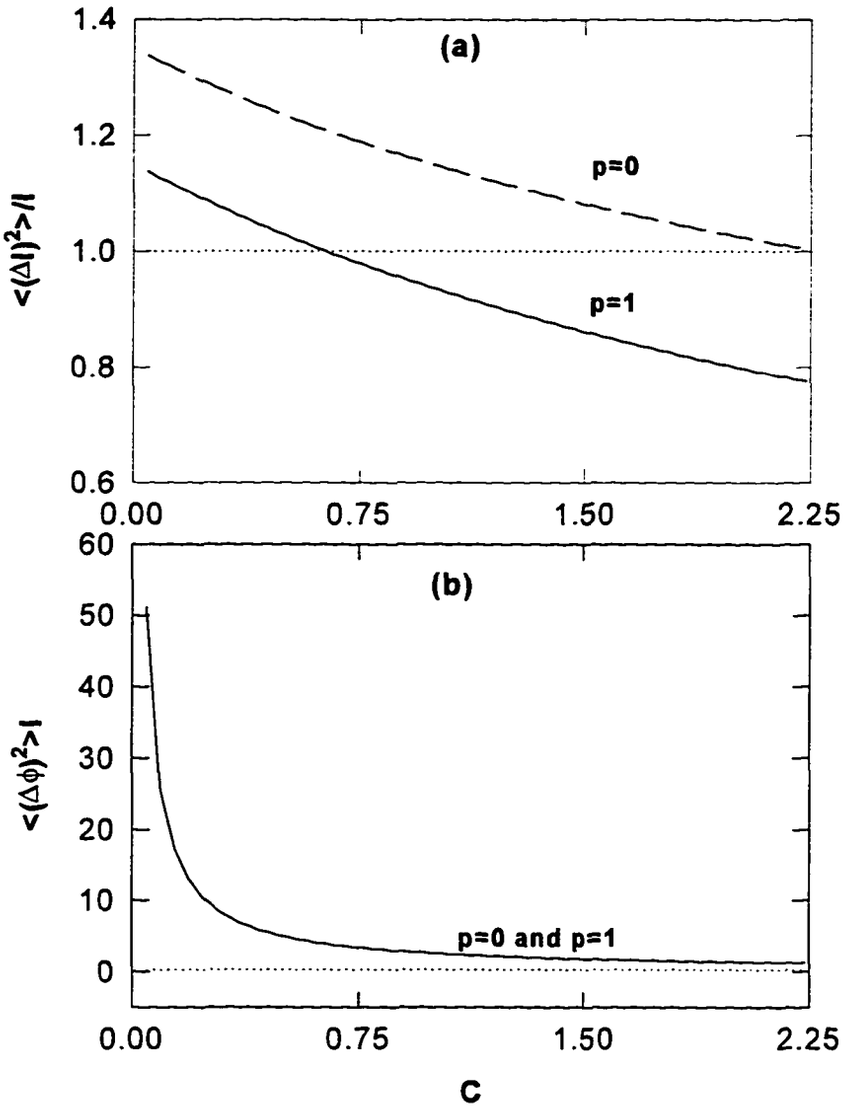

Fig. 13. Intensity noise (a) and Phase noise (b) as a function of the amplitude of atomic coherence C with A=7.5, D=0, and G=5. The dotted line corresponds to the vacuum noise level.

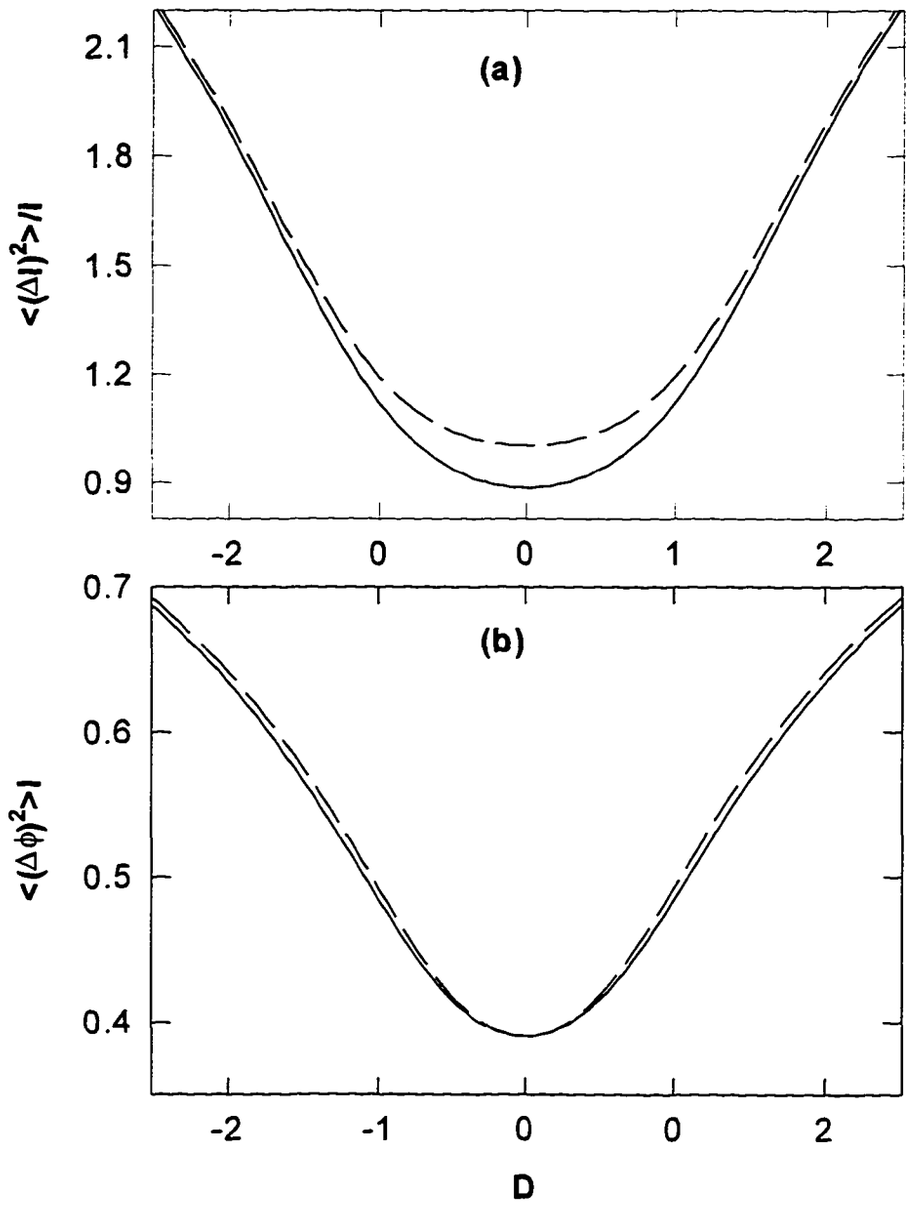

Fig. 14. Intensity noise (a) and phase noise (b) as a function of detuning D with A=2.5, G=-1 and C=1.25 for p=0 (dashed line) and p=1 (solid line).

pumping statistics p suggests a way to reduce or even squeeze the noise of the laser field. We will discuss this aspect later.

5.2. Time Dependent Behavior

In the previous sections we investigated both steady state and time - dependent regimes of operation. Here we will study the transient behavior of the noise around both stationary steady states and time - dependent mean values.

Expanding the coefficients d_n, d_ϕ, D_{nn}, $D_{\phi\phi}$ and $D_{n\phi}$ around mean values $\langle n \rangle(t)$ and $\langle \phi \rangle(t)$, we have the same equations as (5.18), (5.19) and (5.20), except now $\delta n = n - n_0$ is changed to $\delta n = n - \langle n \rangle(t)$ and $\delta\phi = \phi - \phi_0$ to $\delta\phi = \phi - \langle\phi\rangle(t)$.

First we show in Fig.15(a) the intensity as a function of time for different initial conditions. Three trajectories starting at n(0)=0.1, n(0)=2, and n(0)=4, respectively, lead to the same stationary values. Obviously they have different transient behavior.

As discussed earlier, there is no squeezing of phase noise in steady state. The reason is the vanishing of the pumping statistics term in the phase diffusion coefficient $D_{\phi\phi}$ in steady state. In the transient regime, we can have a nonzero pumping statistics term. This nonzero pumping statistics term leads to the transient squeezing of phase noise. This can easily be seen from Eq.(5.9). For nonzero detuning D and sufficiently large initial intensity n(0), the term D^2 becomes the leading one in the phase diffusion coefficient. Under these conditions, the value of $D_{\phi\phi}$ is negative and, thus, the squeezing

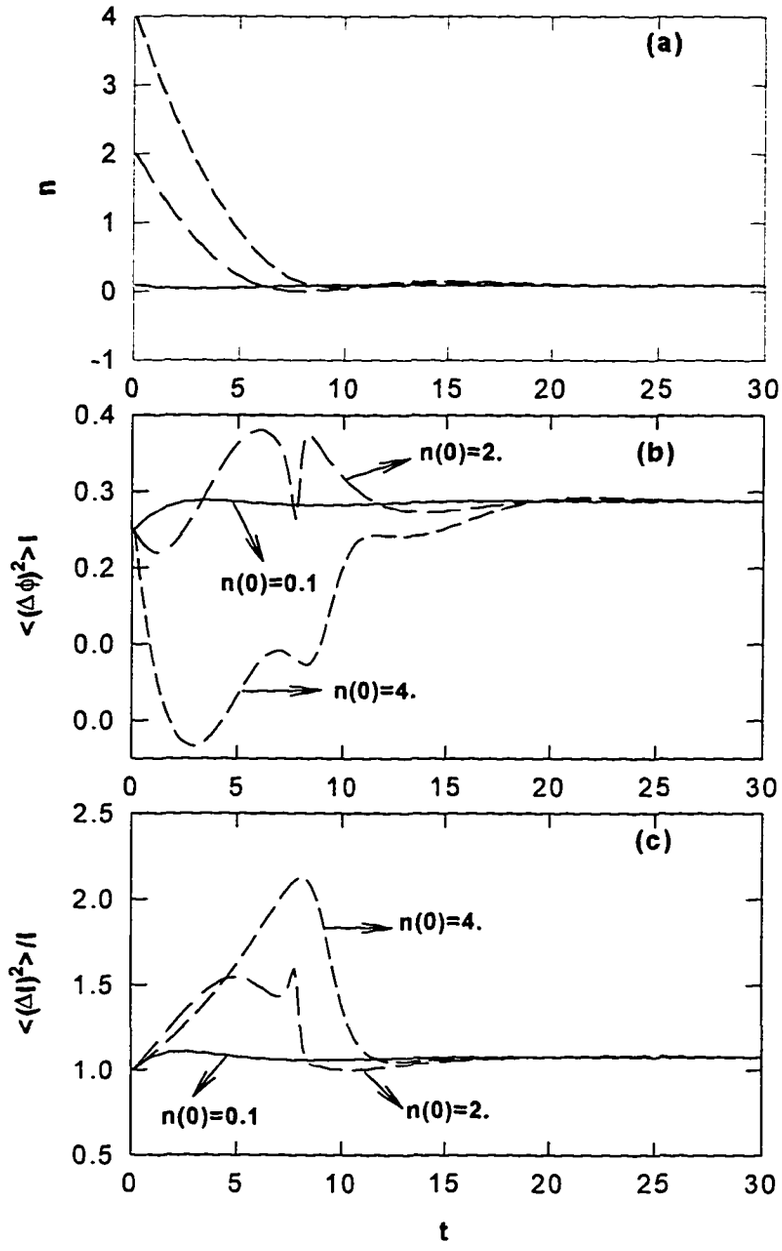

Fig.15. Typical intensity transients (a), typical phase noise transients (b), and typical intensity noise transients (c) for different initial conditions n(0)=4, n(0)=2, and n(0)=0.1, respectively, with p=1. The parameters are A=2.5, D=2.0, G=-3.0, and C=0.5.

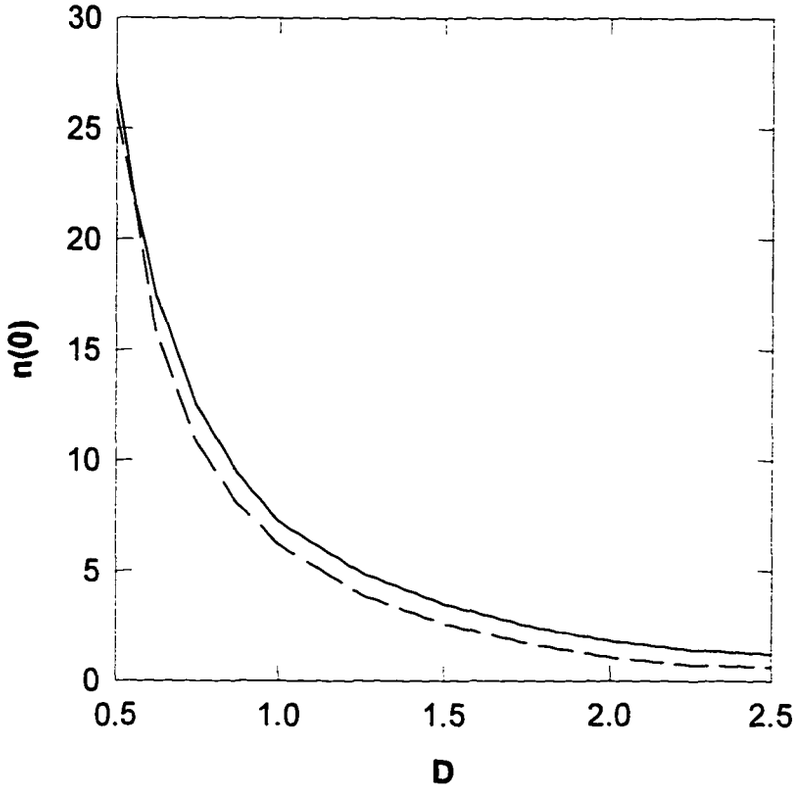

Fig.16. Squeezing boundaries: for a given detuning transient phase noise squeezing occurs if the initial intensity is between the dashed line and solid line. Parameters are same as in Fig.15.

of phase noise occurs. We show this transient phase noise $<(\Delta\phi)^2>I$ in Fig.15(b) with D=2, A=2.5, G=-3, C=0.75 for three initial intensities, n(0)=0.1, n(0)=2, and n(0)=4, respectively. The curve starting at n(0)=0.1 is larger than the squeezing limit 0.25, everywhere. A transient squeezing of phase noise occurs for the curve with n(0)=2. The inverted peak corresponds to the minimum of the curve depicted in Fig.15(a). But there is an unphysical transient behavior for the curve with n(0)=4. This means that there are some limitations on the permissible initial intensities and other parameters where we are allowed to employ a linearized treatment. Using $<(\Delta I)^2><(\Delta\phi)^2>=0.25$, we can find the conditions under which the uncertainty principle is satisfied. The results are displayed in Fig.16. Other parameters are the same as in Fig.15. The region under the solid line is compatible with the uncertainty principle. Of course, this does not mean that the uncertainty principle is violated outside this region. It simply means that our quasilinearized treatment breaks down for initial conditions that are too far off the stationary solutions. Above the dashed line squeezing of the phase noise occurs. We plot the intensity noise as a function of time in Fig.15(c). The parameters are the same as in Fig.15(a) and (b).

Chapter III

Two Photon Laser with Injected Atomic Coherence

6. Fokker-Planck Equation and Steady States

We consider a system of three-level atoms, as shown in Fig.17, interacting with a single - mode field of frequency ν. The Hamiltonian for the system, in the rotating wave approximation, is given by

$$H = H_{at} + H_F + H_{int} , \tag{6.1}$$

where H_{at}, H_F, and H_{int} are, respectively, the atom, field, and interaction terms with

$$H_{at} = \sum_{j=a,b,c} \hbar\omega_j |j><j| , \tag{6.2}$$

$$H_F = \hbar\Omega(a^+a + \tfrac{1}{2}) , \tag{6.3}$$

$$H_{int} = \hbar g_{ab}(a|a><b| + a^+|b><a|) + \hbar g_{bc}(a|b><c| + a^+|c><b|) . \tag{6.4}$$

Here a and a^+ are the field annihilation and creation operators, respectively; Ω is the cavity-mode frequency; $\hbar\omega$ is the energy of level i and |i> are the atomic states(i=a,b,c); g_{ab} and g_{bc} are the coupling constants for the transitions |a>→|b>, and |b>→|c>, respectively (for simplicity from now on we consider g_{ab}=g_{bc}=g). We have assumed that only the |a>→|b>, and |b>→|c> transitions are allowed. We consider the case that the atoms are injected into the laser cavity with initial populations $\rho^j_{aa}(t_j) = \rho_{aa}$ and $\rho^j_{cc}(t_j) = \rho_{cc}$ (=1-ρ_{aa}) and initial coherence between the top and bottom levels

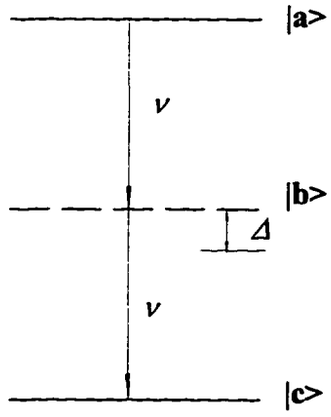

Fig.17. Atomic levels relevant to the two-photon CEL. Atoms are injected in a coherent superposition of levels |a> and |c>, with no initial popution in level |b>.

$\rho_{ac}^{j}(t_j) = \rho_{ca}^{j}(t_j)^* = \bar{\rho}_{ac}\exp(-2ivt_j)$. The middle level b is unpopulated. The atomic injection rate is r_a.

In Q representation this system can be described by a Fokker-Planck equation (Ref.[46]). If we introduce the scaled intensity and phase variables, n and ϕ, the Fokker-Planck equation becomes

$$\frac{\partial Q(n,\phi)}{\partial \bar{t}} = \left(-\frac{\partial}{\partial n}d_n - \frac{\partial}{\partial \phi}d_\phi + \eta\frac{\partial^2}{\partial n^2}D_{nn} + \eta\frac{\partial^2}{\partial \phi^2}D_{\phi\phi} + 2\eta\frac{\partial^2}{\partial n\partial \phi}D_{n\phi}\right)Q(n,\phi)\ , \qquad (6.5)$$

with

$$d_n = \frac{n[G(1+n) - 2\delta C\sin 2\phi]}{(1+n)^2 + \delta^2} - n, \qquad (6.6)$$

$$d_\phi = D - \frac{\delta[\tilde{\alpha} + 2C\cos 2\phi]}{2(1+4n+\delta^2)}\ , \qquad (6.7)$$

$$D_{nn} = n\left[\frac{(1+n)(2\tilde{\alpha} - G) + 2\delta C\sin 2\phi}{2[(1+n)^2+\delta^2]} - \frac{\tilde{\alpha} + 2C\cos 2\phi}{2[1+4n+\delta^2]}\right.$$

$$\left. + \frac{nG[(1+n)^2 - \delta^2] - 4n\delta(1+n)C\sin 2\phi}{[(1+n)^2+\delta^2]^2}\right] + n\ , \qquad (6.8)$$

$$D_{\phi\phi} = \left[\frac{-(1+n)G + 2\delta C\sin 2\phi}{8[(1+n)^2+\delta^2]} + \frac{(2C\cos 2\phi + \tilde{\alpha})(1+4n) - 4\delta C\sin 2\phi}{8[1+4n+\delta^2]}\right] + \frac{1}{4n}, \qquad (6.9)$$

$$D_{n\phi} = \frac{1}{4}\left[\frac{\delta G + 2\delta C\cos 2\phi + 2C\sin 2\phi}{(1+n)^2+\delta^2} - \frac{4\delta n(\tilde{\alpha} + 2C\cos 2\phi)}{[1+4n+\delta^2]^2}\right.$$

$$\left. - \frac{2\delta(1+n)nG + 4n\delta^2 C\sin 2\phi}{[(1+n)^2+\delta^2]^2} - \frac{\delta G}{1+4n+\delta^2}\right], \qquad (6.10)$$

where $G = \frac{\alpha(\rho_{aa} - \rho_{cc})}{\gamma}$, $n = \frac{\beta I}{2\alpha}$, $C = \frac{\alpha|\bar{\rho}_{ac}|}{\gamma}$, $D = \frac{\nu - \Omega}{\gamma}$, $\delta = \frac{\Delta}{\Gamma}$, $\eta = \frac{\beta}{2\alpha}$ and $\bar{t} = t\gamma$,

$\tilde{\alpha} = \frac{\alpha}{\gamma}$ (with I, photon number). Here $\alpha = \frac{2r_a g^2}{\Gamma^2}$ is a linear-gain coefficient, $\beta = \frac{8r_a g^4}{\Gamma^4}$ saturation parameter, Γ atomic decay rate (for simplicity assumed to be the same for all levels, Γ_a=Γ_b=Γ_c=Γ), γ the cavity-loss rate. We have introduced $\phi = \varphi - \frac{1}{2}\theta_{ac}$, where φ is the phase of the laser field and θ_{ac} is the phase of atomic coherence. Furthermore, D is the cavity-field detuning, δ is the atom-field detuning ($\Delta = \omega_{ab} - \nu = -(\omega_{bc} - \nu)$, i.e., overall two-photon resonance is assumed).

In steady state we obtain the following set of coupled nonlinear equations for the intensity, n_0, and phase, φ_0,

$$d_n = \frac{n_0[G(1+n_0) - 2\delta C \sin 2\phi_0]}{(1+n_0)^2 + \delta^2} - n_0 = 0 , \tag{6.11}$$

$$d_\varphi = D - \frac{\delta[\tilde{\alpha} + 2C\cos 2\phi_0]}{2(1+4n_0+\delta^2)} = 0 . \tag{6.12}$$

After eliminating the phase, ϕ_0, we can find a fifth order equation for n_0

$$n_0\{n_0^4 + (4-2G)n_0^3 + [64D^2 + 2\delta^2 + G^2 - 6G + 6]n_0^2 + [(4-2G)(1+\delta^2 - G)$$
$$-16D(\delta\tilde{\alpha} - 2D - 2D\delta^2)]n_0 + [(1+\delta^2 - G)^2 + (\delta\tilde{\alpha} - 2D - 2D\delta^2)^2 - 4\delta^2 C^2]\} = 0, \tag{6.13a}$$

where one solution is always

$$n_0 = 0. \tag{6.13b}$$

From Eqs.(6.13), the steady state curve of intensity n_0 as a function of the atomic coherence C is multivalued for some set of parameters. This multistable behavior is different from that of the one-photon correlated-spontaneous-emission laser. One of the obvious differences is that the lower branch is always n_0 = 0. Another significant difference is that the first derivative at the threshold point C_{th} is not continuous.

6.1. Multivalued Steady States

From Eq.(6.13), we can find that the upper turning point of the multivalued steady state satisfies

$$2n_0^3 + 3(2-G)n_0^2 + (64D^2 + 2\delta^2 + G^2 - 6G + 6)n_0 +$$

$$(2-G)(1+\delta^2 - G) - 8D(\delta\tilde{\alpha} - 2D - 2D\delta^2)] = 0. \qquad (6.14)$$

This equation can be rewritten as

$$(n - n_1)(n - n_2)(n - n_3) = 0, \qquad (6.15)$$

where n_1, n_2, and n_3 are the roots of Eq.(6.14). There are four cases for this system.

Case 1. All three roots are positive, i.e., $n_1 > 0$, $n_2 > 0$, and $n_3 > 0$. We also have $n_1 \neq n_2$, $n_1 \neq n_3$, and $n_3 \neq n_2$ .We have four positive solutions for steady state intensity(Fig.18 (a)).

Case 2. Two roots are positive and one is negative, i.e., $n_1 > 0$, $n_2 > 0$, $n_3 < 0$ and $n_1 \neq n_2$. We have three positive steady state intensities for this case(Fig.18 (b)).

Case 3. One root is positive. Other two roots are either both negative or complex solutions. We have two positive steady state intensities this time(Fig.18(c)).

Case 4. There is no positive root. We have one positive steady state intensity this time(Fig.18 (d)).

From Eq.(6.15), we can find the relation between roots and the coefficients of equation:

$$n_1 + n_2 + n_3 = -3(2-G)/2, \qquad (6.16)$$

$$n_1n_2 + n_1n_3 + n_2n_3 = 32D^2 + \delta^2 + G^2/2 - 3G + 3, \qquad (6.17)$$

$$n_1n_2n_3 = -[(2-G)(1+\delta^2 - G) - 8D(\delta\tilde{\alpha} - 2D - 2D\delta^2)]/2 . \qquad (6.18)$$

For case 1), equations (6.16), (6.17) and (6.18) give

$G>2$, (6.19)

$$32D^2+\delta^2+G^2/2-3G+3>0\ , \tag{6.20}$$

and

$$(2-G)(1+\delta^2-G)-8D(\delta\tilde{\alpha}-2D-2D\delta^2)<0\ . \tag{6.21}$$

We also find that equation (6.21) holds for case 3, but no information is given from Eqs. (6.16) and (6.17) for case 3).

The same thing happens for case 2 and case 4, Eq. (6.18) gives us

$$(2-G)(1+\delta^2-G)-8D(\delta\tilde{\alpha}-2D-2D\delta^2)>0\ . \tag{6.22}$$

No information is given from Eqs. (6.16) and (6.17) for case 2 and case 4.

In Fig. 19, we plot a 3D picture, G as a function of D and δ, to explore Eqs. (6.21) and (6.22). The surface is given by equation:

$$(2-G)(1+\delta^2-G)-8D(\delta\tilde{\alpha}-2D-2D\delta^2)=0\ . \tag{6.23}$$

If the parameters are inside the surface, there is either case 1 or case 3, i.e. four positive steady state solutions or two positive steady state solutions. Otherwise, there is either case 2 or case 4.

6.2. Linear Stability Analysis

In order to study the stability of the steady state (n_0, ϕ_0) we expand d_n and d_ϕ around n_0 and ϕ_0 to first order in Δn and $\Delta\phi$: $n(t) = n_0 + \Delta n$ and $\phi(t) = \phi_0 + \Delta\phi$, where $\Delta n << n_0$ and $\Delta\phi << \phi_0$. Substituting these into the equations of motion $\frac{dn}{dt} = d_n$ and $\frac{d\phi}{dt} = d_\phi$

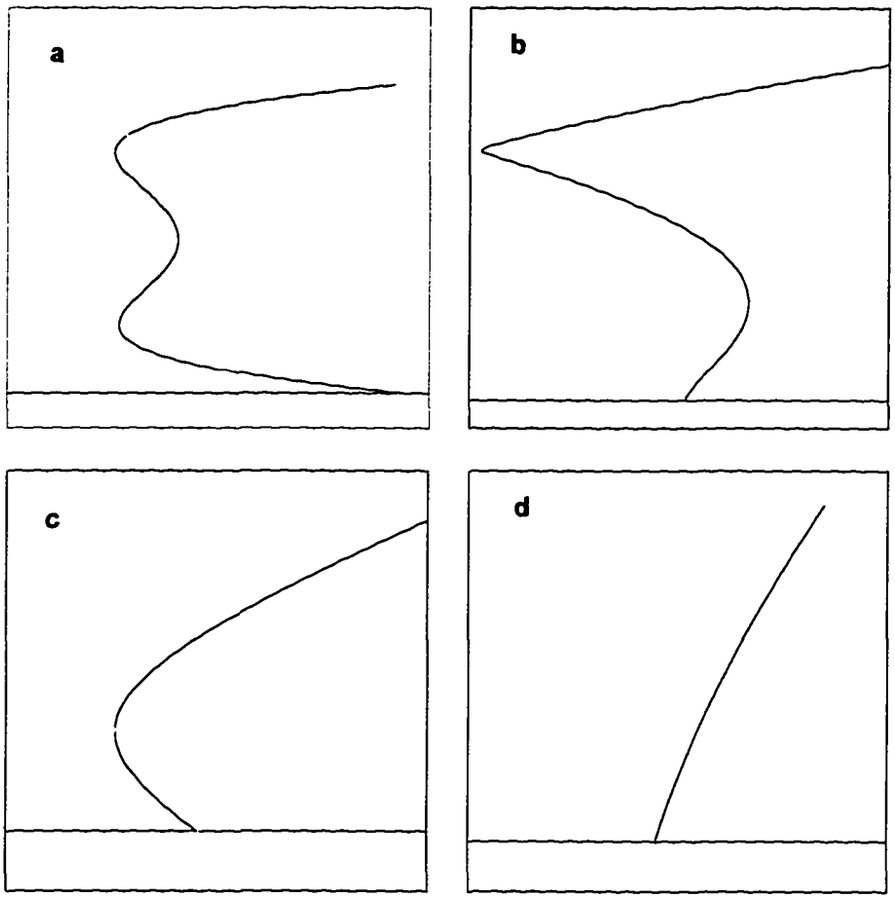

Fig. 18. The steady state as a function of injected atomic coherence, C, for four typical parameter sets. (a) four positive solutions; (b) three positive solutions; (c) two positive solutions; and (d) one positive solution.

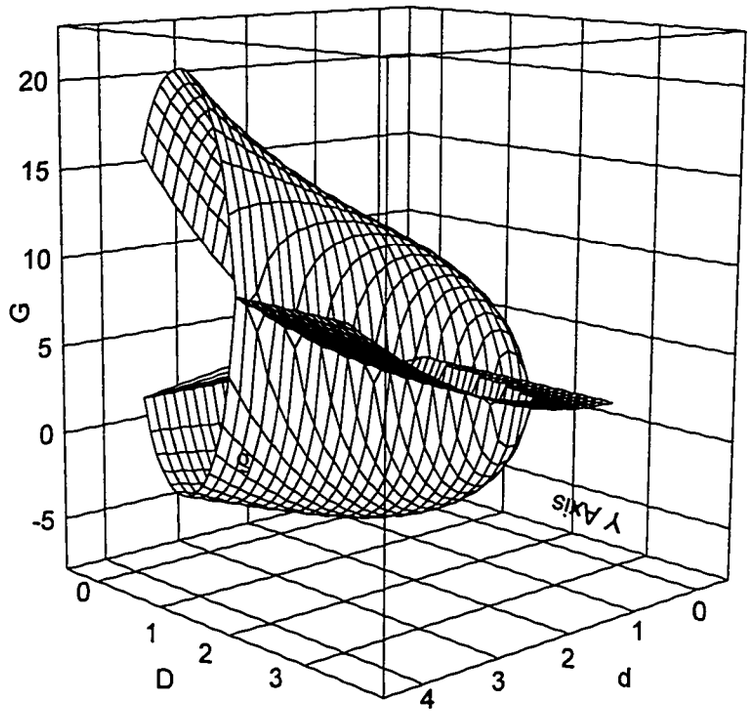

Fig. 19. 3-D figure to show the parameter range for the multivalued steady states.

and neglecting higher order terms in the perturbations, we get the set of linearized equations

$$\frac{\partial \Delta n}{\partial t} = \left(\frac{\partial d_n}{\partial n}\right)_0 \Delta n + \left(\frac{\partial d_n}{\partial \phi}\right)_0 \Delta\phi \ , \tag{6.24}$$

and

$$\frac{\partial \Delta\phi}{\partial t} = \left(\frac{\partial d_\phi}{\partial n}\right)_0 \Delta n + \left(\frac{\partial d_\phi}{\partial \phi}\right)_0 \Delta\phi \ . \tag{6.25}$$

The subscript 0 means that the derivatives have to be evaluated in the steady state. Since this is a system of linear equations we can assume that a simple exponential solution, $\Delta n(t) = \Delta n(0)e^{\lambda t}$ and $\Delta\phi(t) = \Delta\phi(0)e^{\lambda t}$, exists. Substituting this ansatz into the above equations, yields the following characteristic equation for λ,

$$\lambda^2 - \lambda\left(\frac{\partial d_n}{\partial n} + \frac{\partial d_\phi}{\partial \phi}\right) + \left(\frac{\partial d_n}{\partial n}\frac{\partial d_\phi}{\partial \phi} - \frac{\partial d_n}{\partial \phi}\frac{\partial d_\phi}{\partial n}\right) = 0 \ . \tag{6.26}$$

Here for simplicity we dropped the subscript 0 from the derivatives but they are still evaluated in the steady state. Solutions are

$$\lambda_{1,2} = \frac{1}{2}\left\{\left(\frac{\partial d_n}{\partial n} + \frac{\partial d_\phi}{\partial \phi}\right) \pm \sqrt{\left(\frac{\partial d_n}{\partial n} - \frac{\partial d_\phi}{\partial \phi}\right)^2 + 4\frac{\partial d_n}{\partial \phi}\frac{\partial d_\phi}{\partial n}}\right\}$$

$$= \frac{1}{2}\left\{\frac{nG - 2(1+n)n}{(1+n)^2+\delta^2} + \frac{G(1+n) - (1+n)^2 - \delta^2}{1+4n+\delta^2} \pm \right.$$

$$\left.\sqrt{\left(\frac{nG - 2(1+n)n}{(1+n)^2+\delta^2} - \frac{G(1+n) - (1+n)^2 - \delta^2}{1+4n+\delta^2}\right)^2 + \frac{8nD[\delta\tilde{\alpha} - 2D(1+4n+\delta^2)]}{[(1+n)^2+\delta^2](1+4n+\delta^2)}}\right\}. \tag{6.27}$$

The conditions of stability are

$$\mathrm{Re}\left\{\frac{nG-2(1+n)n}{(1+n)^2+\delta^2}+\frac{G(1+n)-(1+n)^2-\delta^2}{1+4n+\delta^2}\pm\right.$$

$$\left.\sqrt{\left(\frac{nG-2(1+n)n}{(1+n)^2+\delta^2}-\frac{G(1+n)-(1+n)^2-\delta^2}{1+4n+\delta^2}\right)^2+\frac{8nD[\delta\tilde{\alpha}-2D(1+4n+\delta^2)]}{[(1+n)^2+\delta^2](1+4n+\delta^2)}}\right\}\le 0. \quad (6.28)$$

From Eqs. (6.27) and (6.28), we can find the stability conditions for the steady states:

$$\left(\frac{\partial d_n}{\partial n}\right)_0+\left(\frac{\partial d_\phi}{\partial \phi}\right)_0\le 0, \quad (6.29)$$

$$\left(\frac{\partial d_n}{\partial n}\right)_0\left(\frac{\partial d_\phi}{\partial \phi}\right)_0-\left(\frac{\partial d_\phi}{\partial n}\right)_0\left(\frac{\partial d_n}{\partial \phi}\right)_0\ge 0. \quad (6.30)$$

The subscript 0 means that the derivatives have to be evaluated in the steady state. We find that for the lower branch, n_0=0, condition (6.29) reads

$$G\le 1+\delta^2, \quad (6.31)$$

and condition (6.30) yields

$$\left(\frac{G-2\delta C\sin 2\phi_0}{1+\delta^2}-1\right)\cdot\frac{2\delta C\sin 2\phi_0}{1+\delta^2}\ge 0. \quad (6.32)$$

We can also find the phase locking condition from Eq.(6.12) (following the standard analysis of Ref.[12]):

$$|2C\delta|\ge|2D(1+\delta^2)-\delta\tilde{\alpha}|, \quad (6.33)$$

and the threshold point from Eq.(6.13a) assuming $n_0=0$

$$(1+\delta^2-G)^2+(\delta\tilde{\alpha}-2D-2D\delta^2)^2-4\delta^2C_{th}^2=0. \quad (6.34)$$

In Fig.20(a), we plot the bistability curve of the intensity, n_0, as a function of the atomic coherence C with G=-2.0, D=1.0, δ=2.0, and $\tilde{\alpha}=10$. The phase, ϕ_0, as a function of C is presented in Fig.20(b) with parameters being the same as in Fig.20(a). The physically

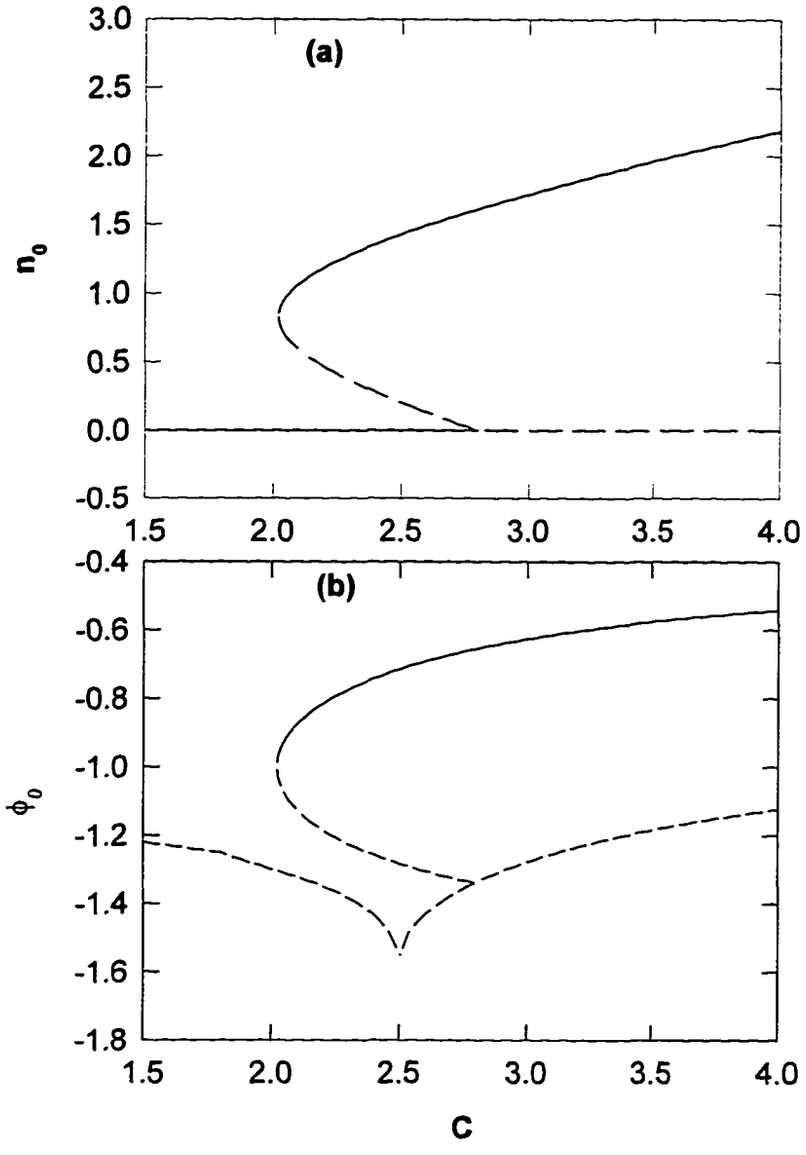

Fig.20. Steady-state scaled intensity n_0 (a) and steady-state phase ϕ_0 (b) as a function of initial atomic coherence C with G=0, D=1, δ=2, and $\tilde{\alpha}$=10. The solid line corresponds to the stable steady state and the dashed line corresponds to the unstable steady state.

accessible region is given by $0 \le C \le \tilde{\alpha}\sqrt{\rho_{aa}\rho_{cc}}$, which, for the given parameters, is $0 \le C \le 5$. For nonzero solutions (steady state satisfies equation (6.13a)), condition (6.30) leads to $\frac{\partial n}{\partial C} \ge 0$. This means that the parts of the curve with negative slope are unstable (in the n-C plane). For the particular set of parameters of Fig.20 we find the phase locking point C_L=2.5, upper turning point C_T=2.0, and threshold point C_{th}=2.8. In the subregion $0 \le C \le 2.0$, there is only one steady state, n_0=0, and it is stable, but the phase ϕ_0 is unlocked. In the subregion $2.0 \le C \le 2.5$, there are three curves: upper branch with positive slope, middle branch with negative slope and lower branch, n_0=0. We know that the part with negative slope is unstable and the other two branches are stable. The time evolution, $n(\bar{t})$, exhibits different behavior for different initial regions, separated by the middle section. Starting from a value below the middle section, $n(\bar{t})$ will reach n_0=0. If the initial value is above the middle section, $n(\bar{t})$ will finally reach the upper branch. The phase, ϕ_0, for the upper branch is locked and the phase, φ_0, for the lower branch, n_0=0, is unlocked. For $2.5 \le C \le 2.8$, intensity vs time behavior is similar to that in previous region, but the phase for n_0=0 is locked to a particular value. Above C_{th}, only the upper branch is stable. This dynamical feature is similar to that in a system of an optical parametric oscillator coupled to N two-level atoms[63,64] and detuned degenerate four-wave mixing.[65]

In Fig.21(a), we present n_0 as a function of C for another situation. In this case, the whole physical region is given by $0 \le C \le 4.68$. Under C=2.4, there is no stable curve. In this unstable region, the time dependent behavior is similar to that in the unstable region of the one-photon correlated-spontaneous-emission laser[Chapter 2]: $n(\bar{t})$ oscillates

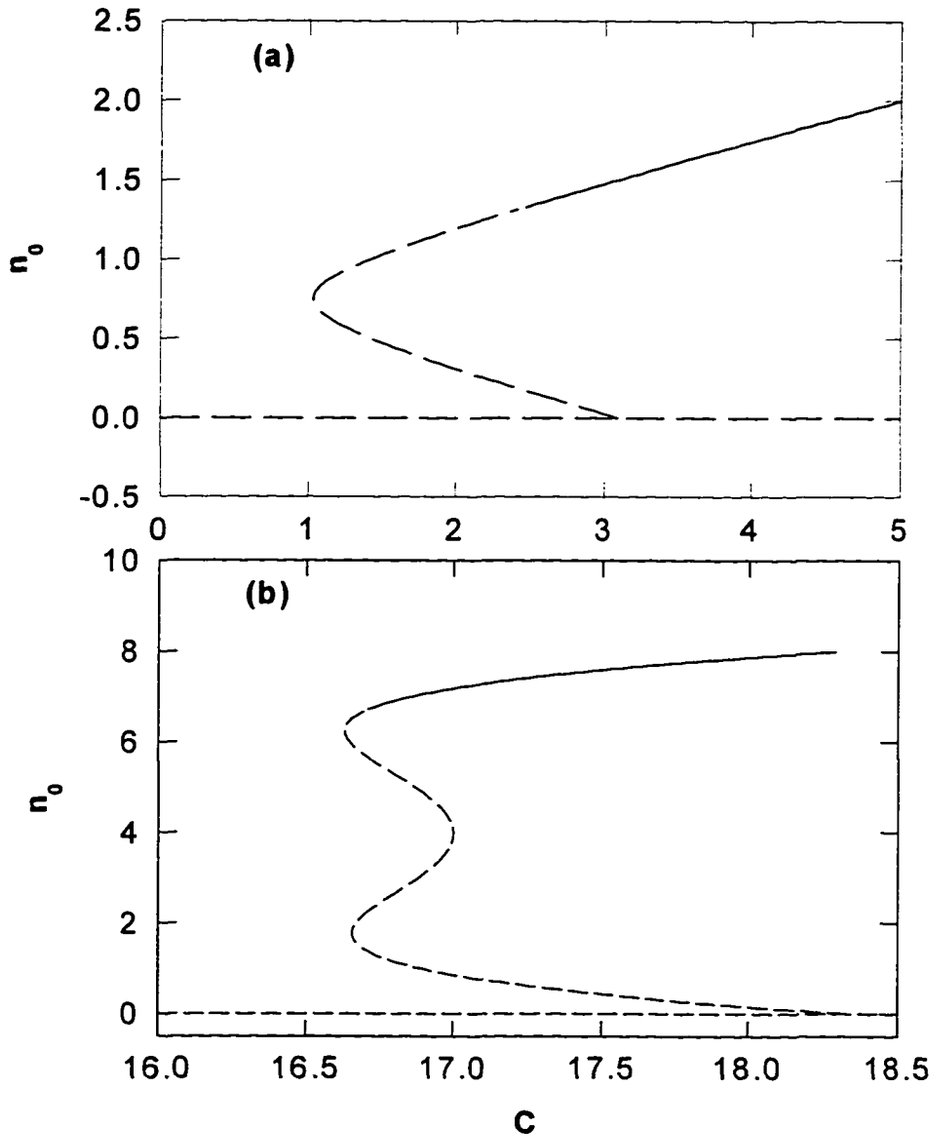

Fig.21. Steady-state scaled intensity n_0 as a function of initial atomic coherence C with (a) G=3.5, D=1, δ=1 and $\tilde{\alpha}$=10; (b) G=10, D=0.78, δ=0.72 and $\tilde{\alpha}$=38. The solid line corresponds to the stable steady state and the dashed line corresponds to the unstable steady state.

around a value which is very close to the critical intensity, n_c=1.3, after the initial transients have decayed. For the phase $\phi(\bar{t})$, superimposed on a straight line which is represented by the average slope of the phase vs. time curve, there is a small oscillation very similar to the oscillation of the average intensity.

Since the equation (6.11) is a quintic equation, one naturally expects to obtain the tristable behavior by properly choosing the parameters. Indeed, Fig.21(b) shows such situation where the physical region is given by $0 \le C \le 18.33$. For $C < 16.65$, there is only one solution n_0=0 which is unstable. In the region $16.70 \le C \le 17.00$, there are five positive solutions, i.e., we have a possibility of tristable operation in this regime. Among them only the top branch is stable. In the region $17.0 \le C \le 18.33$, there are three positive solutions, and still only the top level is stable.

7. Dynamical evolution

So far, we have dealt with the steady states of the system. Let us now consider time dependent scenarios by keeping the full time dependence in the equations. In this section we will investigate time evolution from a given initial condition. We will first study how the system approaches steady state in those regions of the external control parameters where they exist. Then we will investigate the states that evolve from a given initial state in the unstable regions.

For the time dependent case, the equations of motion are

$$\frac{dn}{d\bar{t}} = d_n \,. \tag{7.1}$$

and

$$\frac{d\phi}{d\bar{t}} = d_\phi \ , \tag{7.2}$$

The nonlinear dynamics of the system is completely determined by Eqs. (7.1) and (7.2).

Before studying the transients around stable steady states, let us first get some analytical insight into the relaxation dynamics by studying the trajectories in the n-ϕ plane. By transforming equations (7.1) and (7.2) to the form

$$\frac{dn}{d\phi} = \frac{d_n}{d_\phi} \ , \tag{7.3}$$

we can obtain the governing equation. Since the time $\bar{t}$ does not appear explicitly in this equation, we can exhibit the integral curves in the n-ϕ plane. Each point (n, ϕ) in this plane represents a possible set of initial conditions. A trajectory going through this particular point then determines the time evolution of the system, starting from this initial condition. In Fig.22 we plot the intensity n vs. phase ϕ for several cases. The steady states now correspond to attractive singular points. In Fig.22 (a), we plot n vs. ϕ with G=0, D=1, δ=2, $\tilde{\alpha}$ =10 and C=2.6. Points a and b correspond to the stable upper branch and stable lower branch (n_0=0), respectively. Depending on the initial conditions, the point $(n(\bar{t}),\phi(\bar{t}))$ moves, with the increase of the time $\bar{t}$, along the integral curve and converges to the stable point a or b.

Now we discuss time evolution from a given initial condition in those regions of the external control parameters where the steady state becomes unstable, i.e., beyond the critical point. We find that $n(\bar{t})$ oscillates around a value which is very close to the critical intensity, n_c, after the initial transients have decayed. The period of oscillations, T, can be found from

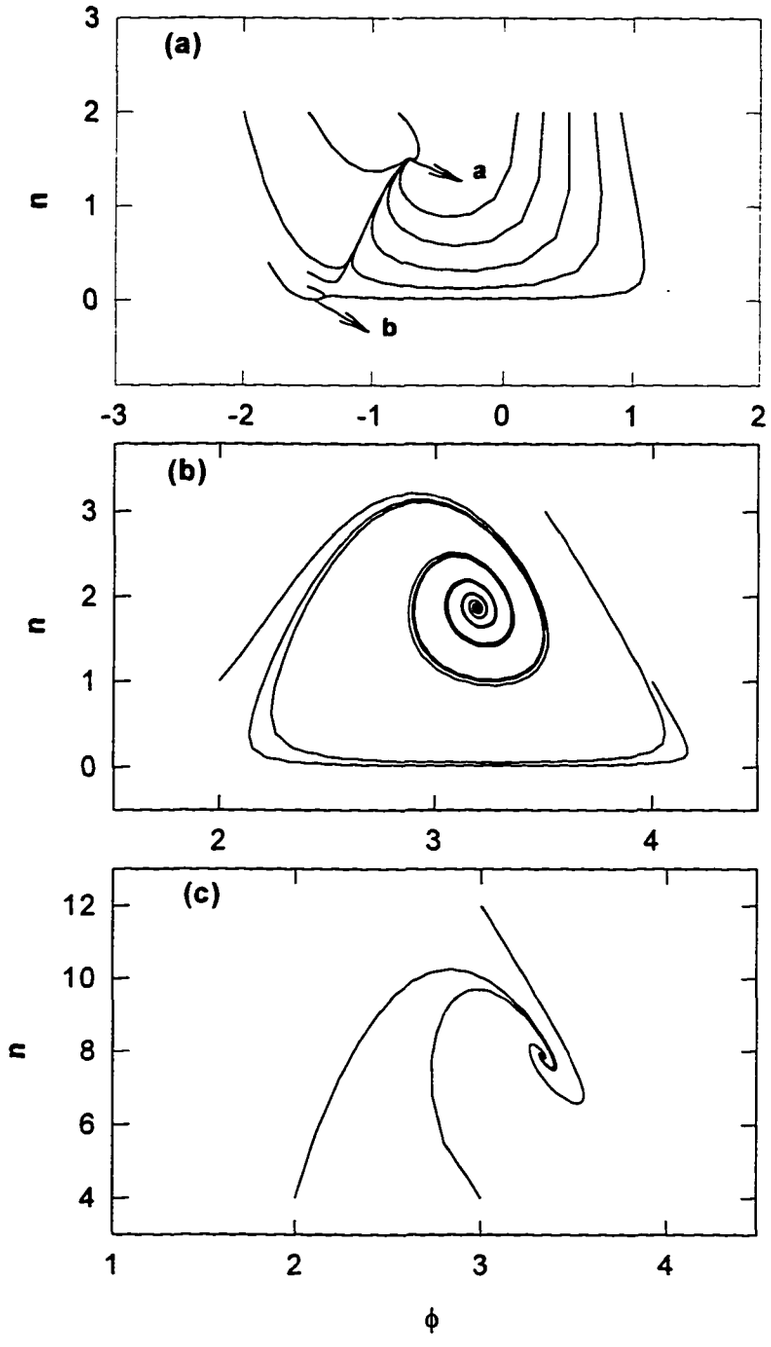

Fig.22. n-ϕ trajectories for (a) G=0, D=1.0, δ=2, $\tilde{\alpha}$=10 and C=2.6; (b) G=3.5, D=1.0, δ=1, $\tilde{\alpha}$=10 and C=4.5; (c) G=10, D=0.78, δ=0.72, $\tilde{\alpha}$=38 and C=18;

$$T = \int_0^{2\pi} \frac{d\varphi}{a - b\cos\phi} = \frac{2\pi}{\sqrt{a^2 - b^2}}, \tag{7.4}$$

where $a = D - \frac{\delta\tilde{\alpha}}{2(1 + n_c + \delta^2)}$, and $b = \frac{\delta C}{1 + n_c + \delta^2}$.

The intensity $n(\bar{t})$ and phase $\phi(\bar{t})$ vs. $\bar{t}$ are depicted in Fig.23 with G=3.5, D=1, δ=1, $\tilde{\alpha}$=10 and C=2.5. The time dependence for phase has two ingredients. First, there is a constant shift of the operating frequency which results in a steady increase of the phase, strictly proportional with time. This is represented by the average slope of the phase vs. time curve. Second, superimposed on this straight line evolution, there is a small oscillation very similar to the oscillation of the average intensity. In particular, the frequency of these phase oscillations is the same as that of the intensity oscillations, given by Eq.(7.4).

We next display this oscillatory behavior from another point of view. Namely, we again discuss the integral curves, resulting from Eq. (7.3). This time, however, instead of displaying the trajectories in the n-ϕ plane, we will plot them in the X-Y phase plane of quadratures, where $X = \sqrt{n_0}\cos\phi_0$ and $Y = \sqrt{n_0}\sin\phi_0$ are the usual quadrature component variables. Fig.24 shows the trajectories in the X-Y plane with G=3.5, D=1, δ=1, $\tilde{\alpha}$=10, and C=2.0. Each trajectory approaches a stable limit cycle. The point $(X(\bar{t}), Y(\bar{t}))$, starting from any initial condition, after the initial transients, i.e., after the approach to the limit cycle, moves along the limit cycle as $\bar{t}$ increases. The period required for the point to complete one cycle is given by (7.4).

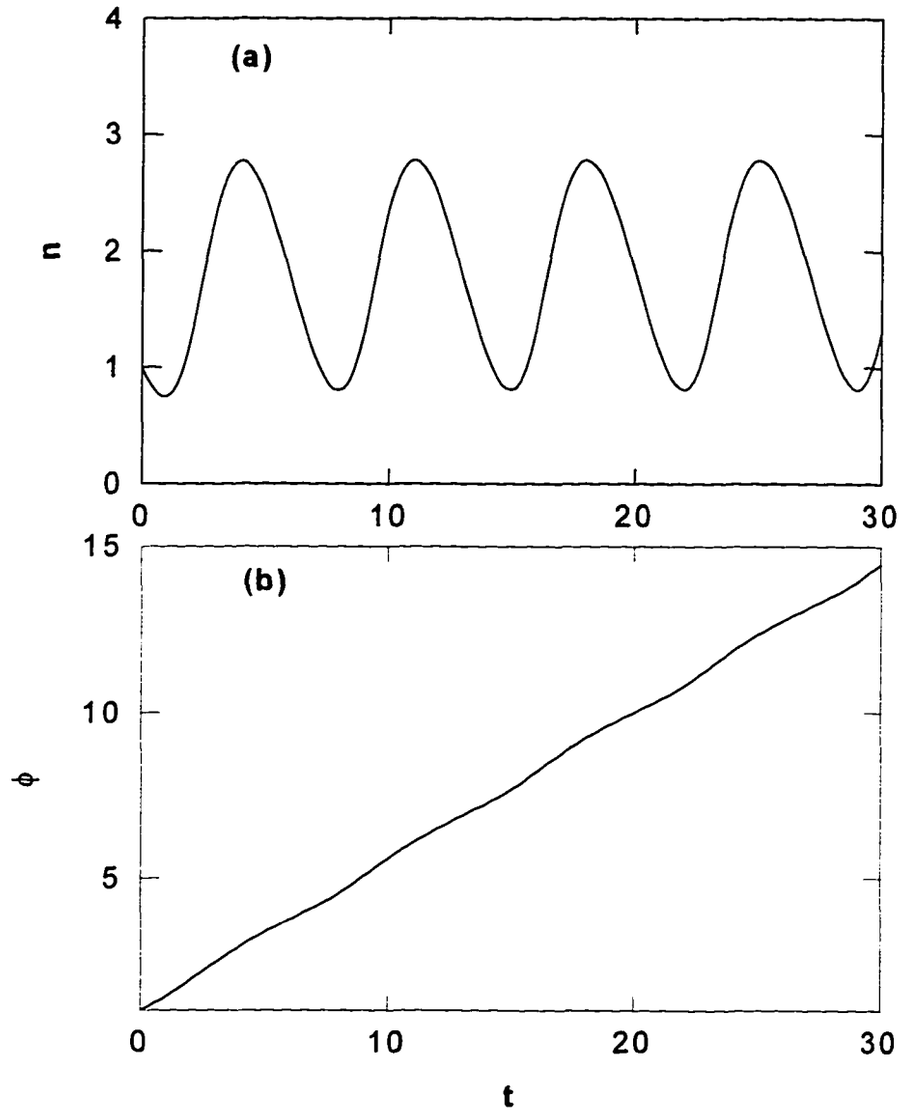

Fig.23. Time evolution of the intensity n (a) and phase (b) with G=3.5, D=1.0, δ=1.0, $\tilde{\alpha}$=1.0, and C=2.5.

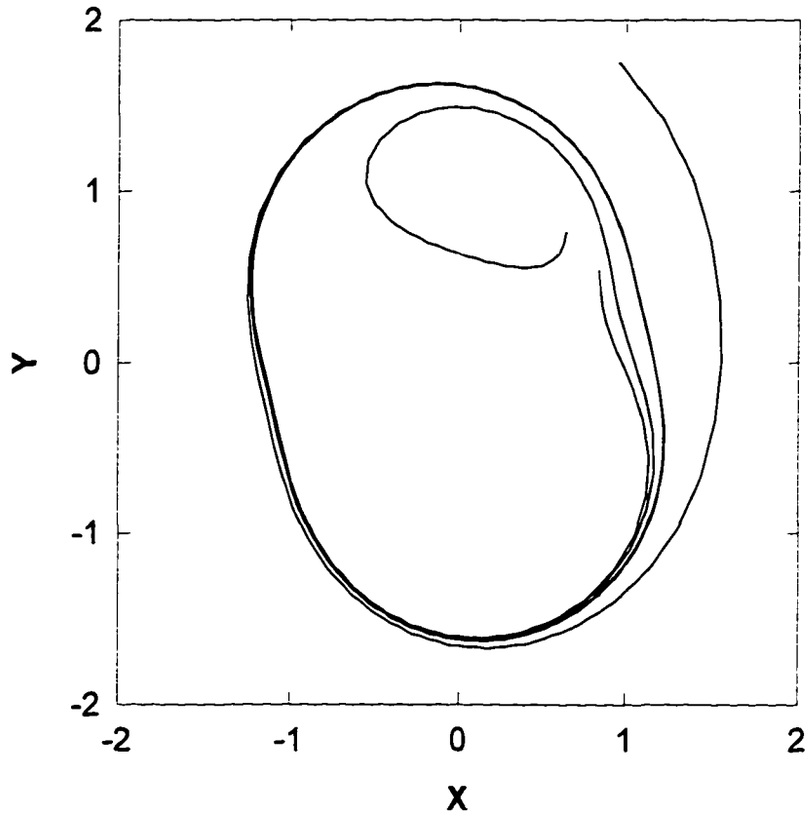

Fig.24. Integral Curves in the phase plane of quadratures, X and Y, with G=3.5, D=1.0, δ =1.0, $\tilde{\alpha}$=10, and C=2.0

Finally, we present a more detailed numerical analysis around the Hopf-bifurcation point. We show our numerical results for the intensity vs. coherence in Fig.25. Parameters are the same as in Fig.21 (b). The dashed line corresponds to the unstable steady state, the solid line to stable steady state, and the triangle to the average value of the stable periodic solution. The circles and dotted line show the boundary of the stable range. The intensity with initial value n(0), which is inside the range between the circles, will reach the stable steady state. The intensity with initial value n(0), which is outside the range, will oscillate around the value given by the triangle. Since the final state depends on initial values, n(0) and $\phi(0)$, we show the n(0)-$\phi(0)$ contour in Fig.26. Starting from the center point, the values of coherence, C, are 16.7, 16.75, 16.8, 16.85, 16.9 16.95, 16.98, respectively. For a specific C value, if n(0) and $\phi(0)$ are inside the corresponding contour, the final state is stable steady state. Otherwise, the final state is stable periodic solution.

8. Noise Squeezing in the Locked Region

In this section, we will use the Fokker-Planck equations (6.5)-(6.10) to study intensity noise $<(\Delta n)^2>$ and phase noise $<(\Delta\phi)^2>$ in the phase locked region. From the Fokker-Planck equation, we can get an infinite set of coupled ordinary differential equations for the moments of the distribution. If we assume the noise to be weak, $\eta <<$, we can truncate these equations into a finite set of nonlinear equations. In this paper we assume that only the first and second - order moments are nonzero. These nonzero moments obey the following equations:

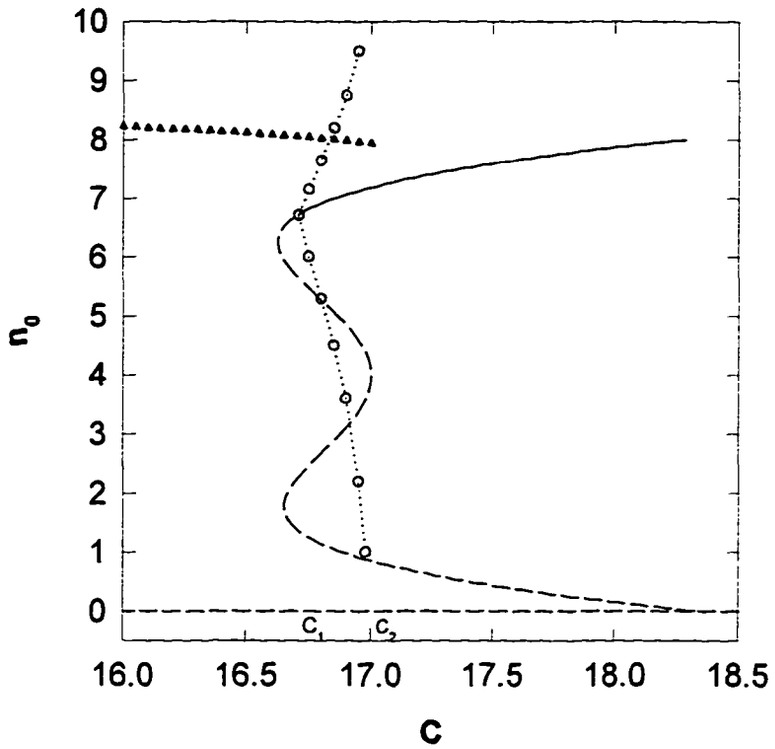

Fig.25. Intensity n_0 vs. atomic coherence C with G=10, D=0.78, δ=0.72, and $\tilde{\alpha}$=38. Solid line corresponds to stable steady state, dashed line to unstable steady state, triangle to the average value of the periodic solution, and circles and dotted line show the boundary between region of the initial values leading to stable steady state and oscillatory behavior, respectively.

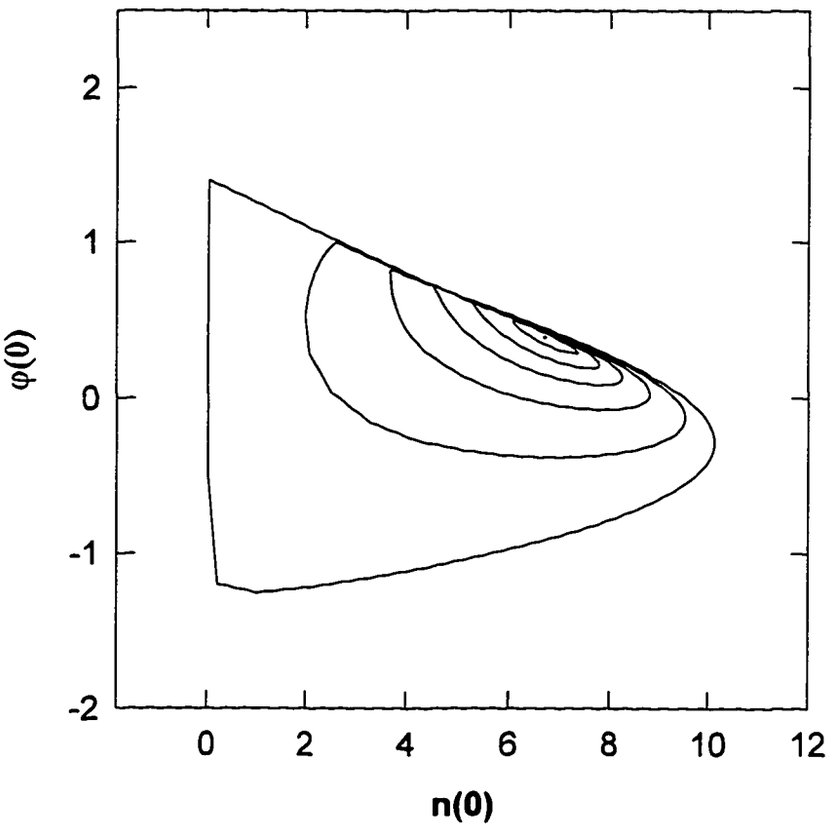

Fig.26. The initial value n_0-ϕ_0 contour with G=10, D=0.78, δ=0.72, and $\tilde{\alpha}$=38. The C value, starting from center point, is 16.7, 16.75, 16.8, 16.85, 16.9, 16.95, 16.98, respectively.

$$\frac{d}{d\bar{t}} < n > = < d_n > , \tag{8.1}$$

$$\frac{d}{d\bar{t}} < \phi > = < d_\phi > , \tag{8.2}$$

$$\frac{d}{d\bar{t}} < (\delta n)^2 > = 2 < d_n \delta n > + 2\eta < D_{nn} > , \tag{8.3}$$

$$\frac{d}{d\bar{t}} < (\delta \phi)^2 > = 2 < d_\phi \delta \phi > + 2\eta < D_{\phi\phi} > , \tag{8.4}$$

$$\frac{d}{d\bar{t}} < (\delta n)(\delta \phi) > = < d_n \delta \phi > + < d_\phi \delta n > + 2\eta < D_{n\phi} > . \tag{8.5}$$

Here we introduced the notations $\delta n = n - \langle n \rangle$, $\delta \phi = \phi - \langle \phi \rangle$. In the following we discuss the steady-state variances of the intensity and phase. In the Q representation, the intensity variance is

$$< (\Delta I)^2 > = < (\delta I)^2 > - < I > , \tag{8.6}$$

and the phase variance is

$$< (\Delta \phi)^2 > = < (\delta \phi)^2 > - \frac{1}{4 < I >} , \tag{8.7}$$

where $(\delta...)$ corresponds to the antinormally ordered part of $(\Delta...)$.

Expanding d_n, d_ϕ, D_{nn}, $D_{n\phi}$, and $D_{\phi\phi}$ around the steady state, n_0 and ϕ_0, up to the first order in δn and $\delta \phi$, we get

$$\frac{d}{dt}<(\delta n)^2>=2\left(\frac{d}{dn}d_n\right)_0<(\delta n)^2>+2\left(\frac{d}{d\phi}d_n\right)_0<(\delta n)(\delta\phi)>+2\eta<D_{nn}>_0\ , \tag{8.8}$$

$$\frac{d}{dt}<(\delta\phi)^2>=2\left(\frac{d}{d\phi}d_\phi\right)_0<(\delta\phi)^2>+2\left(\frac{d}{dn}d_\phi\right)_0<(\delta n)(\delta\phi)>+2\eta<D_{\phi\phi}>_0\ , \tag{8.9}$$

$$\frac{d}{dt}<(\delta n)(\delta\phi)>=\left[\left(\frac{d}{dn}d_n\right)_0+\left(\frac{d}{d\phi}d_\phi\right)_0\right]<(\delta n)(\delta\phi)>+\left(\frac{d}{dn}d_\varphi\right)_0<(\delta n)^2>$$

$$+\left(\frac{d}{d\phi}d_n\right)_0<(\delta\phi)^2>+2\eta<D_{n\varphi}>_0. \tag{8.10}$$

For the lower branch the steady state is $n_0=0$, and we obtain the following expressions for the diffusion coefficients from Eqs(8.8)-(8.10):

$$D_{nn}(n_0=0)=n_0\frac{0.5\tilde{\alpha}(1-G)-C\cos 2\phi+\delta C\sin 2\phi}{1+\delta^2}+n_0\ , \tag{8.11}$$

$$D_{\phi\phi}(n_0=0)=\frac{1}{4n}\left[\frac{-G+2C\cos 2\phi-2\delta C\sin 2\phi+\tilde{\alpha}}{2(1+\delta^2)}+1\right], \tag{8.12}$$

$$D_{n\phi}(n_0=0)=\frac{\delta C\cos 2\phi+C\sin 2\phi}{2(1+\delta^2)}\ . \tag{8.13}$$

At threshold, $C=C_{th}$, the phase diffusion coefficient becomes

$$D_{\varphi\varphi}(n_0=0)=\frac{1}{4n_0}\left(\frac{-G}{1+\delta^2}+\frac{3}{2}+\frac{D}{\delta}\right), \tag{8.14}$$

where we have used the threshold condition (6.19). In view of Eq.(8.14), it is obvious that the field-cavity detuning D will increase phase noise. Recall that in the phase locking equation (6.18), D can play the role of a locking term in some cases. For example, if we

choose G=-2, δ=2, $\tilde{\alpha}$=1, and increase D, fromEq. (8.14) we find $D_{\phi\phi}$ increasing, but at the same time, from Eq.(6.18), the phase locked region increases.

By setting d/dt=0 in equations (8.8), (8.9), and (8.10) and solving for $<(\delta n)^2>$ and $<(\delta\phi)^2>$, then inserting these into (8.6) and (8.7), we can get

$$\frac{<(\Delta I)^2>}{I} = \frac{D_2(D_2D_{22} - D_4D_{11} - 2D_3D_{12}) + D_3(D_1 + D_3)D_{11}}{n(D_1 + D_3)(D_2D_4 - D_1D_3)} - 1 , \tag{8.15}$$

and

$$<(\Delta\phi)^2> I = n\frac{D_4(D_4D_{11} - D_2D_{22} - 2D_1D_{12}) + D_1(D_1 + D_3)D_{22}}{(D_1 + D_3)(D_2D_4 - D_1D_3)} - \frac{1}{4} . \tag{8.16}$$

Here we introduced the notation $D_1 = \left(\frac{\partial d_n}{\partial n}\right)_0$, $D_2 = \left(\frac{\partial d_n}{\partial \phi}\right)_0$, $D_3 = \left(\frac{\partial d_\phi}{\partial \phi}\right)_0$, $D_4 = \left(\frac{\partial d_\phi}{\partial n}\right)_0$

and $D_{11} = (D_{nn})_0$, $D_{12} = (D_{n\phi})_0$, $D_{22} = (D_{\phi\phi})_0$ (all quantities are supposed to be taken at steady state).

We choose three typical sets of parameters to explore the phase squeezing of quantum noise in the two-photon CEL. The steady state operation and the corresponding phase noise with these two sets of parameters are plotted in Figs.27-29.

A particular bistable curve related to steady state equation (6.13) with G=-1.0, D=0.2, δ = 4.0 and $\tilde{\alpha}$=12.0 is given in Fig.27(a). Below the threshold point, C_{th}=5.62, the lower branch(I) n_0=0 is stable and phase locking occurs at C_L=5.15. The middle branch(II) is unstable. The whole upper branch(III) is stable and phase is locked. We plot the scaled phase noise $<(\Delta\phi)^2>I$ for the lower branch(I) and upper branch (III) of Fig.27(a) vs. initial atomic coherence, C, in Fig.27(b). First, we see that there is 40% phase squeezing in the lower branch. More importantly, we find nearly 15% phase

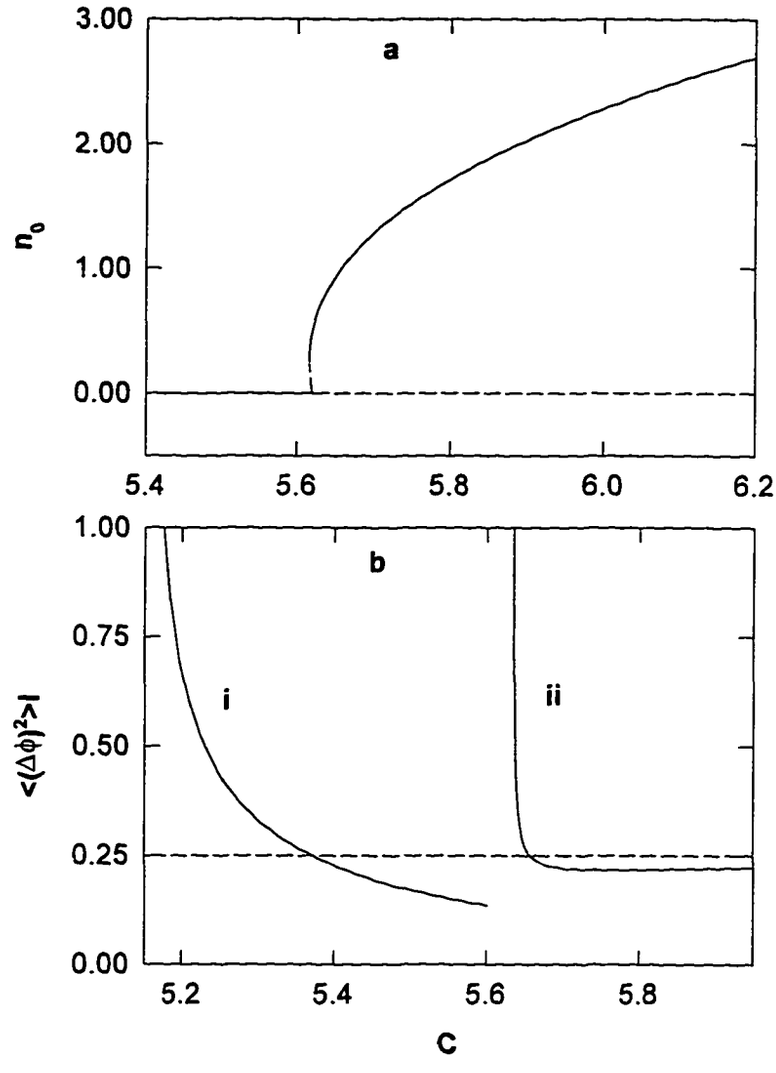

Fig. 27. (a) Steady State intensity n_0 as a function of C with G=-1, D=0.2, δ=4 and $\tilde{\alpha}$=12. The solid line corresponds to the stable steady state, and the dashed line corresponds to the unstable steady state. (b) Steady state phase noise as a function of C for the lower branch in (a) (line i) and the upper branch in (a) (line ii). The dashed line corresponds to the shot-noise limit.

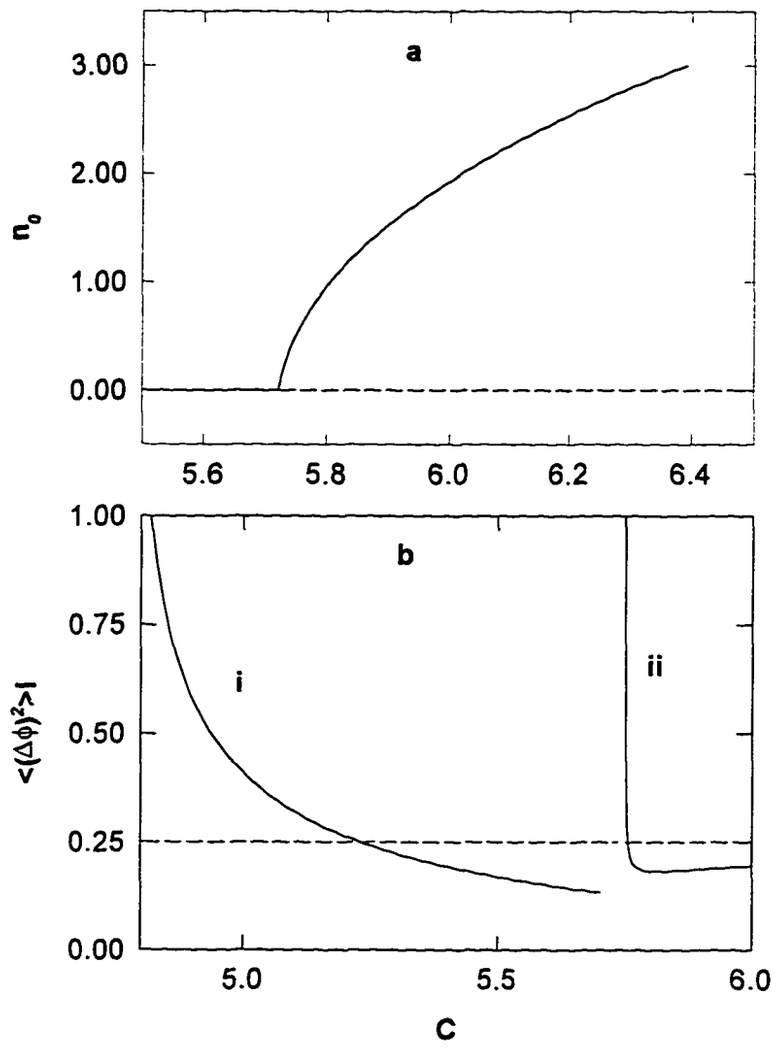

Fig. 28. (a) Steady State intensity n_0 as a function of C with G=-1, D=0.2, δ=6 and $\tilde{\alpha}$=12. The solid line corresponds to the stable steady state, and the dashed line corresponds to the unstable steady state. (b) Steady state phase noise as a function of C for the lower branch in (a) (line i) and the upper branch in (a) (line ii). The dashed line corresponds to the shot-noise limit.

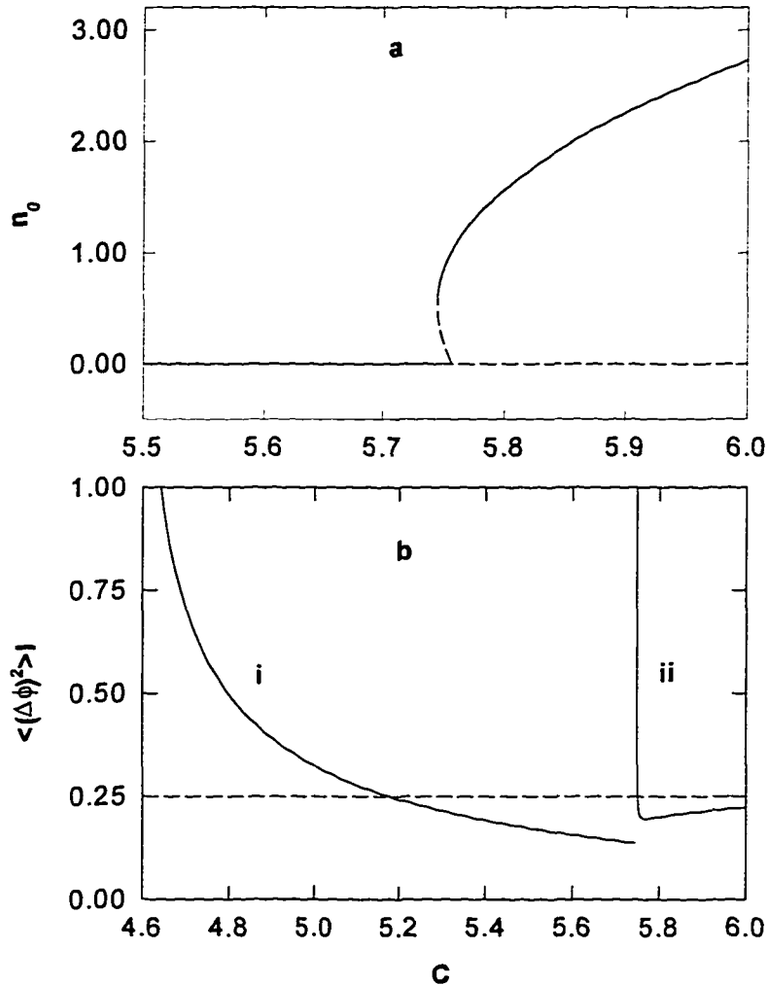

Fig. 29. (a) Steady State intensity n_0 as a function of C with G=1, D=0.2, δ=7 and $\tilde{\alpha}$=12. The solid line corresponds to the stable steady state, and the dashed line corresponds to the unstable steady state. (b) Steady state phase noise as a function of C for the lower branch in (a) (line i) and the upper branch in (a) (line ii). The dashed line corresponds to the shot-noise limit.

squeezing for almost the whole physical region of the upper branch except the large noise at the threshold point. Since this squeezing occurs at the upper branch with finite intensity, we therefore have obtained a bright squeezing.

In Fig.28(a), we display the intensity n_0 as a function of C with G=-1.0, D=0.2, δ =6.0 and $\tilde{\alpha}$ =12. In this case, there are still two stable branches under stationary operating conditions even though the S-shaped bistable hysteresis no longer exists. The stable and phase locked region for the lower branch starts from C_L = 4.77 to C_{th} = 5.72. The plots of the phase noise as a function of C for the lower branch and the upper branch are plotted in Fig.28(b). We see that up to 30% phase squeezing can be obtained in some regions of the upper branch. It again corresponds to bright squeezing.

In Fig.29(a), another kind of bistable behavior is exhibited with G=1.0, D=0.2, δ =7.0 and $\tilde{\alpha}$=12. The stable and phase locked region for the lower branch starts from C_L=4.57 to C_{th}=5.32. Unlike the previous two cases, now there is population inversion. In Fig.29(b), the corresponding phase noise are plotted for the lower and upper branch, respectively. As we can see, close to 25% phase squeezing has been obtained in the upper branch with the population inversion. This is in contrast to Ref. [43] where the bright squeezing with the population inversion is achieved by introducing an additional lower level and to Ref.[44] where one makes use of a fast intermediate relay level. Here we only need to adjust the cavity detuning, atomic detuning, and other parameters to meet the requirement.

Chapter IV

Two-Photon Micromaser with the injected Atomic Coherence

9. Master Equation

We consider a two-photon micromaser consisting of a single mode cavity into which three-level atoms are injected at a low rate, so that, on the average, there is at most one atom inside the cavity at a given time. The atomic decay is negligible. The cavity damping is considered so weak as to be negligible during the interaction time. We will assume that the atoms are injected in a coherent superposition of the upper level $|a\rangle$ and the lower level $|c\rangle$, with no initial population in the middle level $|b\rangle$.

The Hamiltonian for the system, in the rotating wave approximation, is given by

$$H = H_{at} + H_F + H_{int} \ , \tag{9.1}$$

where H_{at}, H_F, and H_{int} are, respectively, the atom, field, and interaction terms with

$$H_{at} = \sum_{j=a,b,c} \hbar\omega_j |j\rangle\langle j| \ , \tag{9.2}$$

$$H_F = \hbar\Omega(a^+a + \tfrac{1}{2}) \ , \tag{9.3}$$

$$H_{int} = \hbar g_{ab}(a|a\rangle\langle b| + a^+|b\rangle\langle a|) + \hbar g_{bc}(a|b\rangle\langle c| + a^+|c\rangle\langle b|) \ . \tag{9.4}$$

Here a and a^+ are the field annihilation and creation operators, respectively; Ω is the cavity-mode frequency; $\hbar\omega$ is the energy of level i and $|i\rangle$ are the atomic states(i=a,b,c); g_{ab} and g_{bc} are the coupling constants for the transitions $|a\rangle\rightarrow|b\rangle$, and $|b\rangle\rightarrow|c\rangle$, respectively (for simplicity from now on we consider $g_{ab}=g_{bc}=g$). We have assumed that

only the $|a\rangle \rightarrow |b\rangle$, and $|b\rangle \rightarrow |c\rangle$ transitions are allowed. We consider the case that the atoms are injected into the laser cavity with initial populations $\rho^j_{aa}(t_j) = \rho_{aa}$ and $\rho^j_{cc}(t_j) = \rho_{cc}$ (=1-ρ_{aa}) and initial coherence between the top and bottom levels $\rho^j_{ac}(t_j) = \rho^j_{ca}(t_j)^* = \overline{\rho}_{ac} \exp(-2ivt_j)$. The middle level b is unpopulated. The atomic injection rate is r_a.

The interaction Hamiltonian in the interaction picture can be found to be

$$V_I = \begin{pmatrix} 0 & \hbar g a e^{-i\Delta t} & 0 \\ \hbar g a^+ e^{i\Delta t} & 0 & \hbar g a e^{i\Delta t} \\ 0 & \hbar g a^+ e^{-i\Delta t} & 0 \end{pmatrix}, \tag{9.5}$$

where $\Delta=\Delta_1=\omega_{ab}-\nu=\Delta_2=\omega_{bc}-\nu$ are the one-photon detunings for the upper and lower transitions, respectively. If $|a, n\rangle$, $|b, n+1\rangle$, and $|c, n+2\rangle$ represent the atomic states $|a\rangle$, $|b\rangle$, and $|c\rangle$ with n, n+1, and n+2 photons, respectively, in the cavity, we can find the state of the system at time t

$$|\Psi_n(t)\rangle = C_{a,n}(t)|a,n\rangle + C_{b,n+1}(t)|b,n+1\rangle + C_{c,n+2}(t)|c,n+2\rangle , \tag{9.6}$$

with the initial state

$$|\Psi_n(t_0)\rangle = \alpha|a,n\rangle + \beta|c,n+2\rangle . \tag{9.7}$$

Substituting Eq.(9.6) into Schrödinger equation and by using Eq.(9.7), one finds

$$C_{a,n} = \frac{\alpha(n+2)-\beta E_n}{2n+3} + \frac{\alpha(n+1)+\beta E_n}{2n+3}\left(\mathrm{Cos}(B_n g\tau) + \frac{i\Delta}{2B_n}\mathrm{Sin}(B_n g\tau)\right)\exp\left(\frac{-i\Delta\tau}{2}\right), \tag{9.8}$$

$$C_{b,n+1} = -i\frac{\alpha\sqrt{n+1}+\beta\sqrt{n+2}}{B_n}\exp(i\Delta t_0 + i\Delta\tau/2)\mathrm{Sin}(B_n g\tau) , \tag{9.9}$$

$$C_{c,n+2} = \frac{\beta(n+1)-\alpha E_n}{2n+3} + \frac{\beta(n+2)+\alpha E_n}{2n+3}\left(\mathrm{Cos}(B_n g\tau) + \frac{i\Delta}{2B_n}\mathrm{Sin}(B_n g\tau)\right)\exp\left(\frac{-i\Delta\tau}{2}\right), \tag{9.10}$$

where

$$B_n = \sqrt{\Delta^2 / 4g^2 + (2n+3)}\ , \tag{9.11a}$$

$$E_n = \sqrt{(n+1)(n+2)}\ , \tag{9.11b}$$

and τ=t-t_0 is the interaction time.

In the interaction picture, the reduced density matrix of the cavity field, $\rho(t)$, satisfies the equation of motion

$$\dot{\rho} = r_a \delta\rho + L\rho\,, \tag{9.12}$$

where $\delta\rho$ is the change in ρ due to an atom interacting with the field for the time τ

$$\delta\rho = \rho(t_0 + \tau) - \rho(t_0). \tag{9.13}$$

$L\rho$ is the Liouvillian operator which describes losses due to the coupling of the cavity mode to a thermal bath given by

$$L\rho = \gamma(n_b + 1)(2a\rho a^+ - a^+ a\rho - \rho a^+ a) + \gamma n_b (2a^+ \rho a - aa^+ \rho - \rho aa^+). \tag{9.14}$$

Here γ is the cavity damping rate, and n_b is the thermal equilibrium mean photon number. The reduced density matrix for the field alone is obtained by tracing over the atomic states

$$\rho_{nm}(t) = \sum_{\alpha} \rho_{\alpha n;\alpha m} \quad (\alpha = a, b, c), \tag{9.15}$$

where

$$\rho_{nm} = < n|\rho|m > \ n, m = 0, 1, \ldots \tag{9.16}$$

one can write

$$\delta\rho_{nm} = \rho_{an,am}(t_0 + \tau) + \rho_{bn,bm}(t_0 + \tau) + \rho_{cn,cm}(t_0 + \tau) - \rho_{an,am}(t_0) - \rho_{cn,cm}(t_0). \tag{9.17}$$

By using Eqs.(9.8) - (9.17), the master equation can be expressed in terms of the initial reduced density matrix elements ρ_{aa}, ρ_{cc}, ρ_{ac}, and ρ_{ca}.

$$\rho(t_0)=\begin{pmatrix}\rho_{aa} & 0 & \rho_{ac}\\ 0 & 0 & 0\\ \rho_{ca} & 0 & \rho_{cc}\end{pmatrix}, \tag{9.18}$$

where ρ_{aa}, ρ_{cc}, and $\rho_{ac}=\rho_{ca}^{*}$ are the same for all atoms. Its explicit expression is given in the following,

$$\begin{aligned}\dot{\rho}_{nm} = N_{ex}\Bigg\{&\rho_{aa}\Bigg\{\rho_{nm}\left[\frac{n+2}{2n+3}+\frac{n+1}{2n+3}[]_n\exp\left(\frac{i\Delta\tau}{2}\right)\right]\left[\frac{m+2}{2m+3}+\frac{m+1}{2m+3}[]_m^{*}\exp\left(-\frac{i\Delta\tau}{2}\right)\right]\\ &+\rho_{n-1,m-1}\left[\frac{\sqrt{nm}}{B_{n-1}B_{m-1}}\mathrm{Sin}(B_{n-1}g\tau)\mathrm{Sin}(B_{m-1}g\tau)\right]\\ &+\rho_{n-2,m-2}\frac{\sqrt{n(n-1)}}{2n-1}\frac{\sqrt{m(m-1)}}{2m-1}\left[-1+[]_{n-2}\exp\left(\frac{i\Delta\tau}{2}\right)\right]\left[-1+[]_{m-2}^{*}\exp\left(-\frac{i\Delta\tau}{2}\right)\right]\Bigg\}\\ +\rho_{cc}\Bigg\{&\rho_{n+2,m+2}\frac{\sqrt{(n+1)(n+2)(m+1)(m+2)}}{(2n+3)(2m+3)}\left[-1+[]_n\exp\left(\frac{i\Delta\tau}{2}\right)\right]\left[-1+[]_m^{*}\exp\left(-\frac{i\Delta\tau}{2}\right)\right]\\ &+\rho_{n+1,m+1}\left[\frac{\sqrt{(n+1)(m+1)}}{B_{n-1}B_{m-1}}\mathrm{Sin}(B_{n-1}g\tau)\mathrm{Sin}(B_{m-1}g\tau)\right]\\ &+\rho_{nm}\left[\frac{n-1}{2n+3}+\frac{n}{2n+3}[]_n\exp\left(\frac{i\Delta\tau}{2}\right)\right]\left[\frac{m-1}{2m+3}+\frac{m}{2m+3}[]_m^{*}\exp\left(-\frac{i\Delta\tau}{2}\right)\right]\Bigg\}\\ +\rho_{ac}\Bigg\{&\rho_{n,m+2}\left[\frac{n+2}{2n+3}+\frac{n+1}{2n+3}[]_n\exp\left(\frac{i\Delta\tau}{2}\right)\right]\frac{\sqrt{(m+1)(m+2)}}{2m+3}\left[-1+[]_m^{*}\exp\left(-\frac{i\Delta\tau}{2}\right)\right]\\ &+\rho_{n-1,m+1}\left[\frac{\sqrt{n(m+1)}}{B_{n-1}B_{m-1}}\mathrm{Sin}(B_{n-1}g\tau)\mathrm{Sin}(B_{m-1}g\tau)\right]\end{aligned}$$

$$+\rho_{n-2,m}\frac{\sqrt{n(n-1)}}{2n-1}\left[-1+\square_{n-2}\exp\left(\frac{i\Delta\tau}{2}\right)\right]\left[\frac{m-1}{2m-1}+\frac{m}{2m-1}\square^{*}_{m-2}\exp\left(-\frac{i\Delta\tau}{2}\right)\right]\Bigg\}$$

$$+\rho_{ca}\Bigg\{\rho_{n+2,m}\frac{\sqrt{(n+1)(n+2)}}{2n+3}\left[-1+\square_{n}\exp\left(\frac{i\Delta\tau}{2}\right)\right]\left[\frac{m+2}{2m+3}+\frac{m+1}{2m+3}\square^{*}_{m}\exp\left(-\frac{i\Delta\tau}{2}\right)\right]$$

$$+\rho_{n+1,m-1}\left[\frac{\sqrt{m(n+1)}}{B_{n-1}B_{m-1}}\mathrm{Sin}(B_{n-1}g\tau)\mathrm{Sin}(B_{m-1}g\tau)\right]$$

$$+\rho_{n,m-2}\left[\frac{n-1}{2n-1}+\frac{n}{2n-1}\square_{n-2}\exp\left(\frac{i\Delta\tau}{2}\right)\right]\frac{\sqrt{m(m-1)}}{2m-1}\left[-1+\square^{*}_{m-2}\exp\left(-\frac{i\Delta\tau}{2}\right)\right]\Bigg\}\Bigg\}$$

$$-N_{ex}+n_b\sqrt{nm}\rho_{n-1,m-1}+(n_b+1)\sqrt{(n+1)(m+1)}\rho_{n+1,m+1}$$

$$-[n+m+2n_b(n+m+1)]\rho_{nm}\ , \qquad (9.19)$$

where $N_{ex}=r_a/\gamma$ represents the average number of atoms that pass through the cavity during the lifetime of the field, and

$$\square_n=[\cos(B_n g\tau)+\frac{i\Delta}{2B_n}\sin(B_n g\tau)], \qquad (9.20)$$

and B_n is given by Eq.(9.11a). We introduce several parameters here, gain, $G=\rho_{aa}-\rho_{bb}$, and coherence, $C=\pm|\rho_{ac}|$. In the following sections we will using this master equation to study the steady state photon statistics and line-width.

10. Steady State Photon Statistics

By setting n = m, the equation of motion for the diagonal elements $p(n)=\rho_{nn}$, which represent the probability of n photons in the field, can be obtained from Eq.(9.19).

At steady state, the equation for the probability $p(n) = \rho_{nn}$ can be found by setting the derivative $\frac{d\rho_{nm}}{dt} = 0$ in Eq.(9.19).

Due to the presence of the off-diagonal density-matrix elements $\rho_{n,n+2}$ and $\rho_{n+2,n}$, it is very difficult to solve for ρ_{nn}. Here we consider a very simple case. We assume that the coherence between level a and level c is zero, C = 0. The equation for P(n) can be written as

$$a_{n-2}P(n-2)+b_{n-1}P(n-1)+c_nP(n)+d_{n+1}P(n+1)+e_{n+2}P(n+2)=0, \tag{10.1}$$

where

$$a_n = N_{ex}\rho_{aa}\frac{(n+1)(n+2)}{(2n+3)(2n+3)}\left[1+\square_n\square_n^{*}-\square_n^{*}\exp\left(\frac{i\Delta\tau}{2}\right)-\square_n\exp\left(-\frac{i\Delta\tau}{2}\right)\right], \tag{10.2a}$$

$$b_n = N_{ex}\rho_{aa}\frac{n+1}{B_n^2}\mathrm{Sin}^2(B_n g\tau)+n_b(n+1), \tag{10.2b}$$

$$\begin{aligned} c_n = {} & N_{ex}\rho_{aa}\left[\frac{n+2}{2n+3}+\frac{n+1}{2n+3}\square_n\exp\left(\frac{i\Delta\tau}{2}\right)\right]\left[\frac{n+2}{2n+3}+\frac{n+1}{2n+3}\square_n^{*}\exp\left(-\frac{i\Delta\tau}{2}\right)\right] \\ & +N_{ex}\rho_{cc}\left[\frac{n-1}{2n-1}+\frac{n}{2n-1}\square_{n-2}\exp\left(\frac{i\Delta\tau}{2}\right)\right]\left[\frac{n-1}{2n-1}+\frac{n}{2n-1}\square_{n-2}^{*}\exp\left(-\frac{i\Delta\tau}{2}\right)\right] \\ & -N_{ex}-[n_b(2n+1)+n], \end{aligned} \tag{10.2c}$$

$$d_{n+1} = N_{ex}\rho_{cc}\frac{n+1}{B_{n-1}^2}\mathrm{Sin}^2(B_{n-1}g\tau)+(n_b+1)(n+1), \tag{10.2d}$$

$$e_{n+2} = N_{ex}\rho_{cc}\frac{(n+1)(n+2)}{(2n+3)(2n+3)}\left[1+\square_n\square_n^{*}-\square_n^{*}\exp\left(\frac{i\Delta\tau}{2}\right)-\square_n\exp\left(-\frac{i\Delta\tau}{2}\right)\right], \tag{10.2e}$$

with B_n given in Eq.(9.11a), and $\square_n$ given in Eq.(9.20). We can solve Eq.(10.1) numerically. First, we introduce two set of parameters α_i and β_i:

$$\alpha_1 = \frac{-c_0}{d_1},\ \beta_1 = \frac{-e_2}{d_1};\quad \alpha_2 = \frac{-b_0 - c_1\alpha_1}{d_2 + c_1\beta_1},\ \beta_2 = \frac{-e_3}{d_2 + c_1\beta_1}$$

$$\alpha_3 = \frac{-a_0 - b_1\alpha_1 - b_1\beta_1\alpha_2 - c_2\alpha_2}{d_3 + b_1\beta_1\beta_2 + c_2\beta_2},\quad \beta_3 = \frac{-e_4}{d_3 + b_1\beta_1\beta_2 + c_2\beta_2},$$

and

$$\alpha_k = \frac{-a_{k-3}(\alpha_{k-3} - \beta_{k-3}\alpha_{k-2} - \beta_{k-3}\beta_{k-2}\alpha_{k-1}) - b_{k-2}(\alpha_{k-2} - \beta_{k-2}\alpha_{k-1}) - c_{k-1}\alpha_{k-1}}{d_k + a_{k-3}\beta_{k-3}\beta_{k-2}\beta_{k-1} + b_{k-2}\beta_{k-2}\beta_{k-1} + c_{k-1}\beta_{k-1}}$$

$$\beta_k = \frac{-e_{k+1}}{d_k + a_{k-3}\beta_{k-3}\beta_{k-2}\beta_{k-1} + b_{k-2}\beta_{k-2}\beta_{k-1} + c_{k-1}\beta_{k-1}}. \qquad (10.3)$$

The solution of p(n) can be found

$$p(N) = \alpha_N p(0),\quad \text{and } p(n) = (\alpha_n + \beta_n\alpha_{n+1})p(0) \qquad n=N-1, N-2, \ldots, 2, 1\ . \qquad (10.4)$$

Here we truncate p(n) at n=N, and p(0) is determined from the normalization relation

$$\sum_{n=0}^{\infty} p(n) = 1\ . \qquad (10.5)$$

In the following subsections, we will study the photon statistics predicted by Eq.(10.4).

10.1. Resonant Two-Photon Micromaser

When the three atomic levels a, b, and c are equally spaced, $\omega_{ab} = \omega_{bc}$, we have one-photon resonance, $\Delta = 0$. In this case, both the one-photon and two-photon transitions are possible. First we investigate the mean photon number, it is given by

$$< n >= \sum_{n=0}^{\infty} np(n). \qquad (10.6)$$

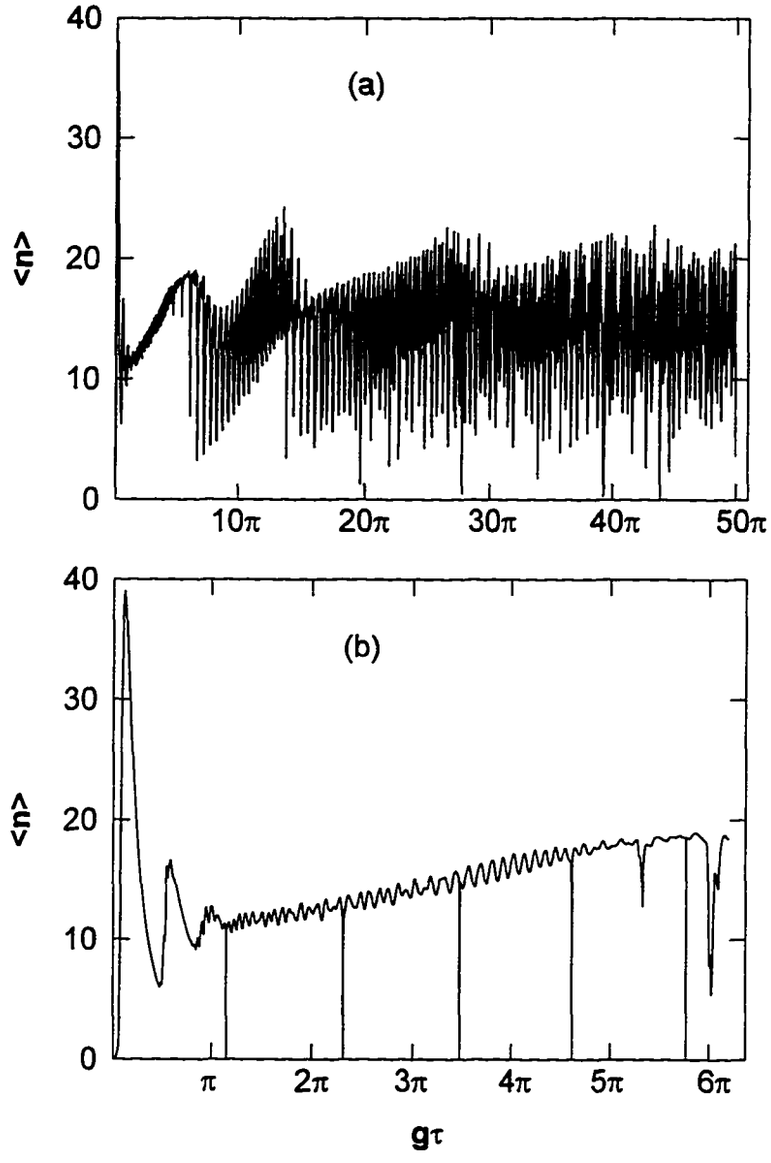

Fig. 30. Steady state mean photon number <n> as a function of interaction time gτ for N_{ex}=20, n_b=0, Δ=0, G=1,C=0. (b) Expanded view of (a) for short interaction time showing trapping states.

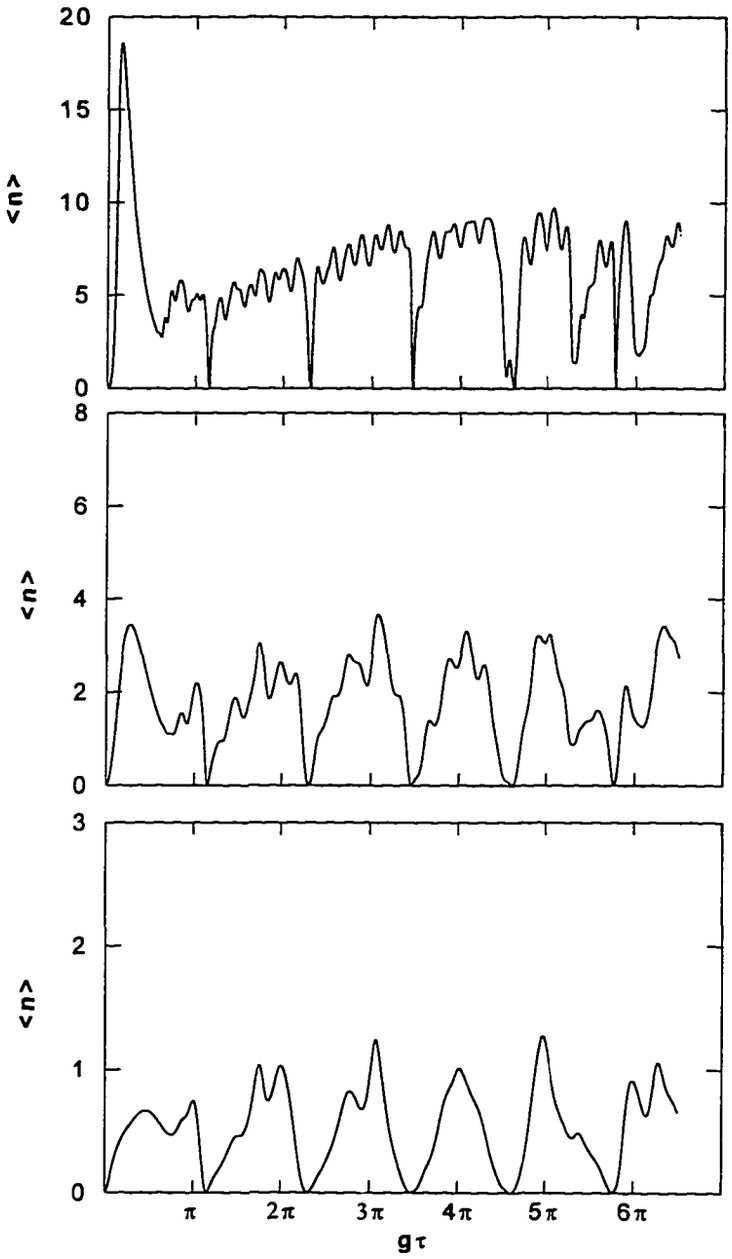

Fig. 31. Steady state mean photon number <n> as a function of interaction time gτ for (a) N_{ex}=20, n_b=0, Δ=0, G=0.5,C=0. (b) N_{ex}=20, n_b=0, Δ=0, G=0.,C=0. (c) N_{ex}=20, n_b=0, Δ=0, G=-0.5,C=0.

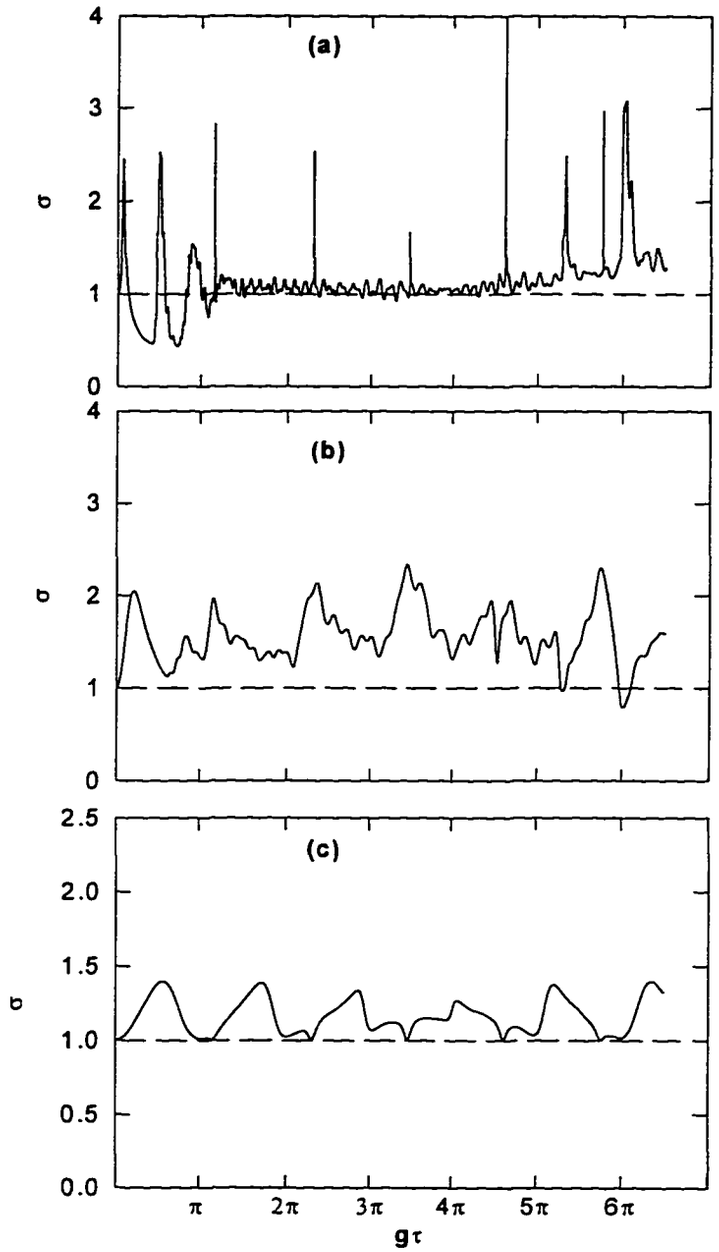

Fig. 32. Steady state mean photon number deviation σ as a function of interaction time gτ for (a) N_{ex}=20, n_b=0, Δ=0, G=1.0,C=0. (b) N_{ex}=20, n_b=0, Δ=0, G=0.,C=0. (c) N_{ex}=20, n_b=0, Δ=0, G=-0.999, C=0.

In Figs. 30-31, we display the mean photon number <n> as a function of the interaction time $g\tau$. Fig. 30 displays the regular two-photon micromaser with parameters $\Delta=0$, $N_{ex}=0$, $n_b=0$, G=1, and C=0. Fig.30b shows the short interaction times region to exhibit the trapping states clearly. In this two-photon resonant case, there is only one sequence of trapping states, |0>. These trapping states occur at[56]

$$g\tau = 0, \frac{2\pi}{\sqrt{3}}, \frac{4\pi}{\sqrt{3}}, \frac{6\pi}{\sqrt{3}}, \ldots . \tag{10.7}$$

In Fig.31, we plot <n> as a function of $g\tau$ for the atoms prepared in a coherent superposition with different values of gain G. We note that as G decreases, the mean photon number decreases, and the structure becomes more smooth. Next, we examine the photon number standard deviation

$$\sigma = \sqrt{\frac{<n^2> - <n>^2}{<n>}} . \tag{10.8}$$

It is plotted as a function of $g\tau$ in Fig.32 for different values of gain G. The results show that, in general, σ oscillates. The field can have sub-Poissonian statistics ($\sigma < 1$) or super-Poissonian ($\sigma > 1$). By decreasing G from the initially purely excited (G=1) two-photon micromaser to the deexcited ($G \approx -1$) two-photon micromaser, one can change the cavity field from being sub-Poissonian to super-Poissonian. Fig.32(c) shows that the field exhibits super-Poissonian statistics during the whole time.

10.2. True Two-Photon Micromaser

In this subsection we examine the off-resonant case $\Delta \neq 0$ for the two-photon micromaser. We study the behavior of the first two moments of the steady state photon

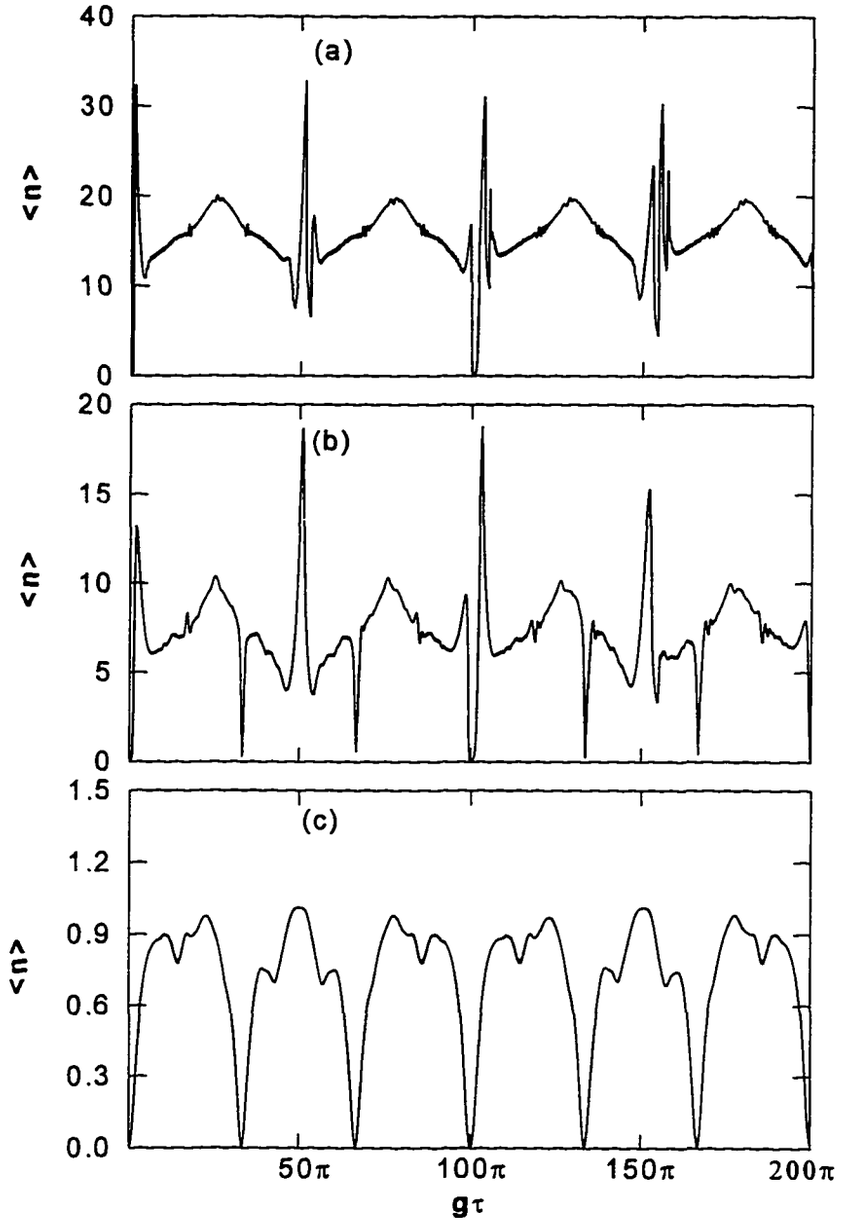

Fig. 33. Steady state mean photon number <n> as a function of interaction time gτ for (a) N_{ex}=20, n_b=0, Δ=50g, G=1,C=0. (b) N_{ex}=20, n_b=0, Δ=50g, G=0.5,C=0. (c) N_{ex}=20, n_b=0, Δ=50g, G=-0.5,C=0.

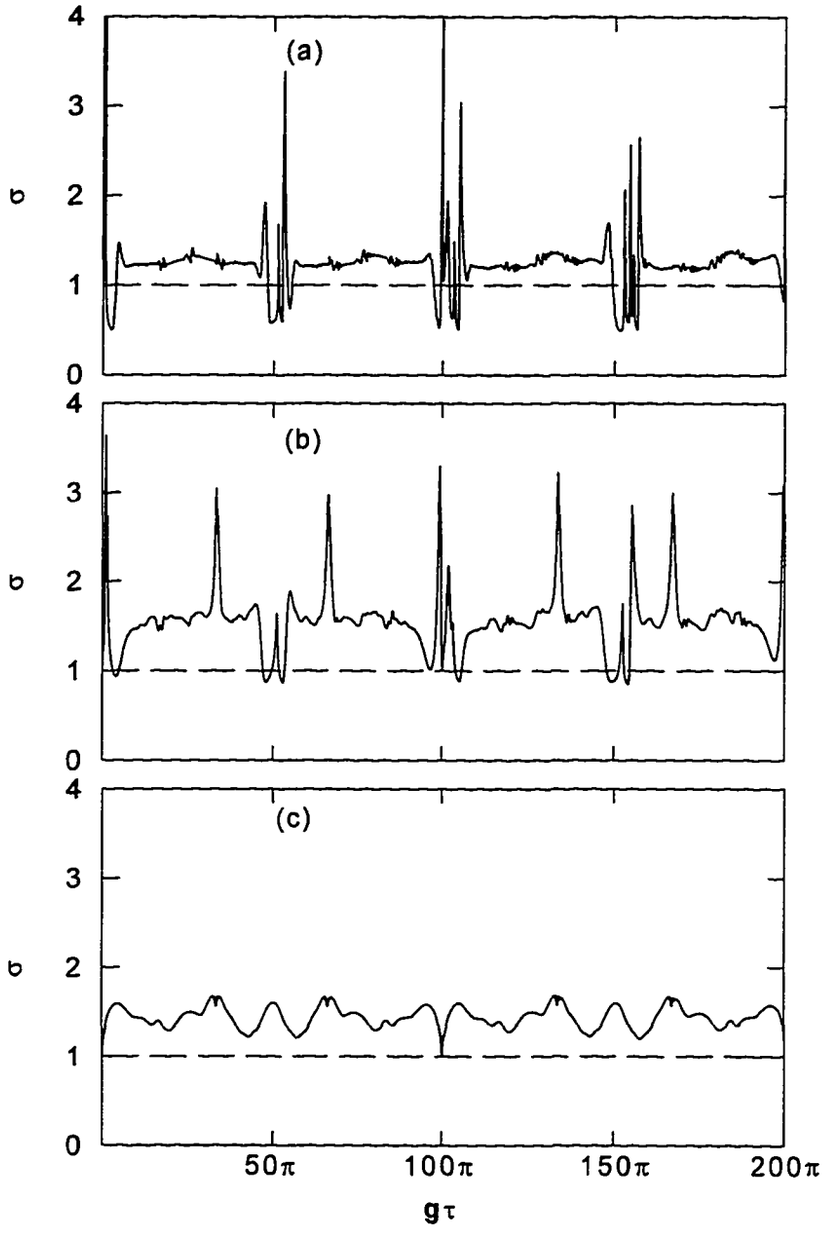

Fig. 34. Steady state mean photon number deviation σ as a function of interaction time gτ for(a) N_{ex}=20, n_b=0, Δ=50g, G=1,C=0. (b) N_{ex}=20, n_b=0, Δ=50g, G=0.5,C=0. (c) N_{ex}=20, n_b=0, Δ=50g, G=-0.5,C=0.

distribution function, mean photon number <n>, and photon number deviation σ. In Figs. 33, and 34 we depict <n> and σ as a function of the interaction time gτ for large detuning Δ = 50 and different values of gain G. In the case of G = 1, Fig.33(a), the system already exhibits the regular, periodic features expected from a true two-photon transition and there are dips at gτ = 100π, 200π, ... These are not trapping states. The major difference between the true two-photon micromaser and the one-photon micromaser is that there is no trapping state, even no vacuum trapping states in the present system.[56] Fig.33(b) and (c) show that the periodic behavior becomes more regular as G decreases. The σ plots in Fig.34 show that by changing G, one can change the photon distribution.

11. Spectrum

In this section, we turn to the discussion of the spectrum of the two-photon micromaser. The calculation of the spectrum is given by

$$S(\omega-\omega_c) = \mathrm{Re}\int_0^\infty < a^+(t)a(0) > e^{-i(\omega-\omega_c)t}dt\,. \tag{11.1}$$

We can express the correlation function $<a^+(t)a(0)>$ by the Green's function of the master equation for the field density operator,[60]

$$< a^+(t)a(0) >= \sum_{l,m} G_{l,m}(t)\sqrt{(l+1)(m+1)}P_{m+l}\,, \tag{11.2}$$

where

$$G_{l,m}(t) = \mathrm{Tr}_r[U_{l,m}(t)\rho_r^{(s)}U^+_{m+l,l+l}(t)], \tag{11.3}$$

and the time-evolution operator U(t)

$$U_{j,k}(t) =< j|U(t)|k >, \qquad U^+_{j,k}(t) =< j|U^+(t)|k >, \tag{11.4}$$

where the subscript r stands for the reservoir, and (s) for the steady state.

The initial condition for $G_{l,m}(t)$ reads

$$G_{l,m}(t=0)=\delta_{l,m}. \tag{11.5}$$

In order to obtain the time dependence of the Green's function $G_{l,m}$ we interpret the $G_{l,m}$ as the off-diagonal element $<l|G^{(m)}|l+1>$ of the operator

$$G^{(m)}(t)=Tr_r[U(t)(|m><m+1|)\rho_r^{(s)}U^{+}(t)]. \tag{11.6}$$

Since the time-evolution operator U(t) enters into $G^{(m)}(t)$ in the same way as into the field-density operator,

$$\rho_f(t)=Tr_r[U(t)\rho_{f,r}(0)U^{+}(t)], \tag{11.7}$$

the operator $G^{(m)}(t)$ must obey the same master equation as the field-density operator. In this section, we apply the Green's function $G_{l,m}=<l|G^{(m)}|l+1>$ to the two-photon micromaser system. Here we only consider the normal two-photon micromaser, i.e., we set $\rho_{aa}=1$, $\rho_{cc}=0$, and $\rho_{ac}=\rho_{ca}=0$ in Eq.(9.19). As we mentioned before, the Green's function $G_{l,m}=<l|G^{(m)}|l+1>$ obeys the same master equation as the field density operator $\rho_{l,l+1}$. We can find the equation for $G_{l,m}$ by replacing $\rho_{l,l+1}$ with $G_{l,m}$ in Eq.(9.19). By using Laplace transform of $G_{l,m}(t)$

$$\tilde{G}_{l,m}(s)=\int_0^{\infty}e^{-st}G_{l,m}(t)dt, \tag{11.8}$$

we obtain the following recurrence relation

$$a_{l-2,l-1}\tilde{G}_{l-2,m}+b_{l-1,l}\tilde{G}_{l-1,m}+(c_{l,l+1}-s)\tilde{G}_{l,m}+d_{l+1,l+2}\tilde{G}_{l+1,m}=-\delta_{lm}. \tag{11.9}$$

The solution for $\tilde{G}_{l,m}(s)$ can be found by again introducing two set of parameters, $\{\alpha_j\}$ and $\{\beta_j\}$:

$$\alpha_0 = \frac{\delta_{0m}}{c_{01} - s},\ \beta_0 = \frac{d_{12}}{c_{01} - s};\quad \alpha_1 = \frac{\delta_{1m} - b_0\alpha_0}{c_{12} - s - b_0\beta_0},\ \beta_1 = \frac{d_{23}}{c_{12} - s - b_0\beta_0}$$

and

$$\alpha_k = \frac{\delta_{km} - a_{k-2,k-1}\alpha_{k-2} + a_{k-2,k-1}\beta_{k-2}\alpha_{k-1} - b_{k-1,k}\alpha_{k-1}}{c_{k,k+1} - s - b_{k-1}\beta_{k-1} + a_{k-2,k-1}\beta_{k-2}\beta_{k-1}}, \qquad k=2, 3, \ldots L \qquad (11.10a)$$

$$\beta_k = \frac{d_{k+1,k+2}}{c_{k,k+1} - s - b_{k-1}\beta_{k-1} + a_{k-2,k-1}\beta_{k-2}\beta_{k-1}}. \qquad (11.10b)$$

$\tilde{G}_{l,m}$ can be expressed in terms of $\{\alpha\}$ and $\{\beta\}$:

$$\tilde{G}_{L,m}(s) = \alpha_L, \qquad (11.11a)$$

and

$$\tilde{G}_{i,m}(s) = \alpha_i - \beta_i\tilde{G}_{i+1,m}, \qquad i=L-1, L-2, \ldots.2, 1, 0. \qquad (11.11b)$$

Here we assume $\tilde{G}_{n,m} = 0$ for $n > L$.

Finally we obtain the spectrum of the micromaser

$$S(\omega - \omega_c) = \mathrm{Re}\sum_{l,m}\tilde{G}_{l,m}[i(\omega - \omega_c)]\sqrt{(l+1)(m+1)}P_{m+1}. \qquad (11.12)$$

In the following we plot the normalized spectrum $S(\omega - \omega_c)/S(0)$ for various values of parameters. In Fig. 35 we plot normalized spectrum $S(\omega - \omega_c)/S(0)$ for resonant two-photon micromaser with $\Delta = 0$, and $N_{ex} = 20$, $g\tau = 6$, and various values of thermal photon number n_b. The micromaser spectrum $S(\omega - \omega_c)/S(0)$ is Lorentzian. In one-photon micromaser, the linewidth decreases as the thermal mean photon number n_b increases. This feature is quite different from a standard laser case.[60] Fig. 35 shows the same feature for the resonant two-photon micromaser. In Fig. 36 we show the normalized spectrum

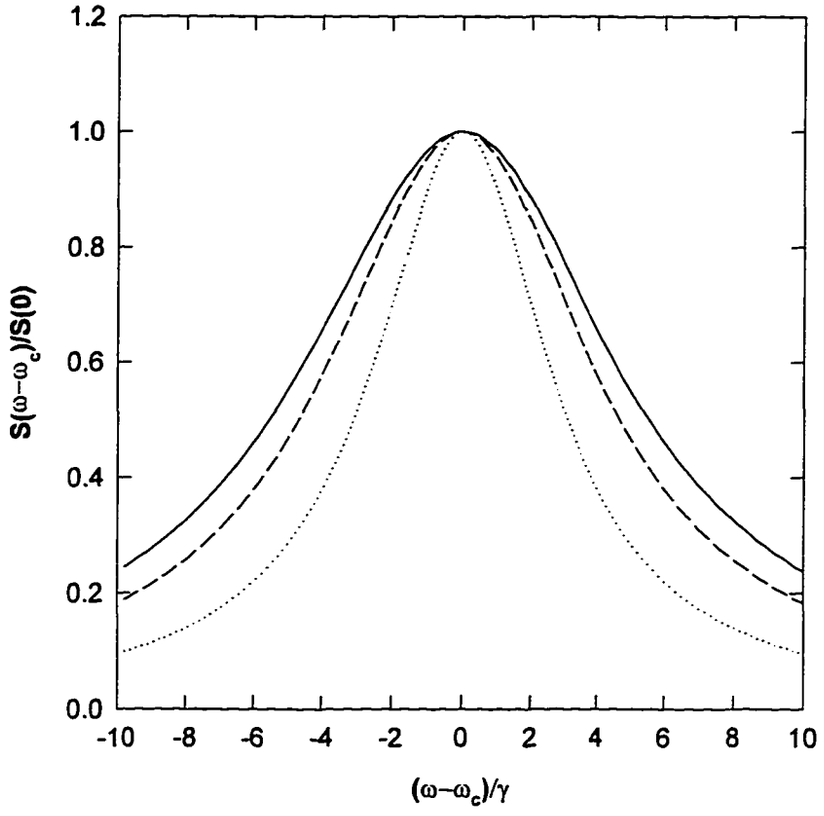

Fig. 35. Normalized spectrum $S(\omega - \omega_c)/S(0)$ as a function of the parameter $(\omega - \omega_c)/\gamma$ for $N = 20$, $\Delta = 0$, $g\tau = 6$ and for $n_b = 0.0001$ (solid line), $n_b = 1$ (dashed line), and $n_b = 5$ (dotted line).

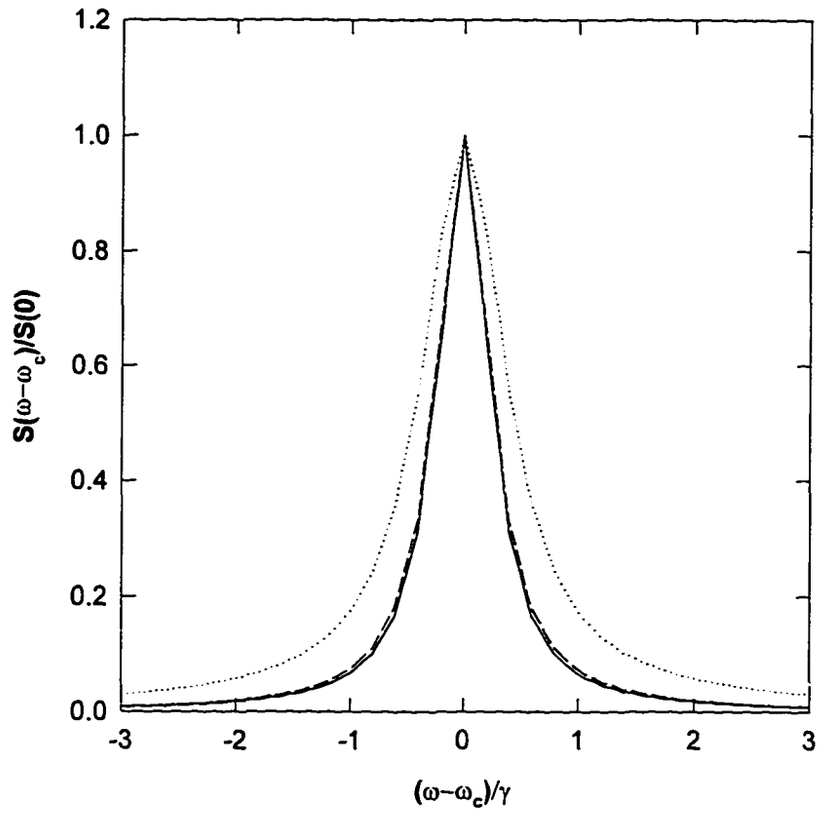

Fig. 36. Normalized spectrum $S(\omega - \omega_c)/S(0)$ as a function of the parameter $(\omega - \omega_c)/\gamma$ for $N_{ex} = 20$, $\Delta = 50g$, $g\tau = 6$ and for $n_b = 0.0001$ (solid line), $n_b = 1$ (dashed line), and $n_b = 5$ (dotted line).

$S(\omega - \omega_c) / S(0)$ versus $(\omega - \omega_c)/\gamma$ for truly two-photon micromaser with $\Delta = 0$, and $N_{ex} = 20$, $g\tau = 6$, and three different values of thermal photon number n_b. We found that the shape of the micromaser spectrum is not very sensitive to the thermal mean photon number n_b. The linewidth increases as the thermal photon number increases. This feature is different from the one-photon micromaser case showed in Fig. 35.

Chapter V

Summary

In Chapter II, we have analyzed the influence of the injected atomic coherence on laser operation. The numerical results for the intensity and phase of the laser have been obtained from the semiclassical equations of motion. We have discussed the steady-state laser operation first. It has been shown that lasing without population inversion occurs in the system. We have also found that, in the usual laser regime, i.e., above threshold, the plot of intensity vs. amplitude of atomic coherence, $n_0(C)$, becomes S - shaped (Fig.2), similarly to optical bistability. With the help of linear stability analysis we have shown that both below and above threshold the $n_0(C)$ curve contains unstable parts. The size of the unstable region increases with increasing cavity - field detuning. In the unstable region both the intensity and phase exhibit periodic oscillations. We gave an analytic expression for the oscillation frequency.

In the stable region the operating frequency of the laser is locked to the atomic frequency. This requires that $C>C_c$ where, in turn, the critical coherence is a function of the detuning D and gain G in such a way that with increasing detuning the instability region also increases. In the unstable region, in addition to the oscillatory behavior of the intensity and phase, there is also a shift in the operating frequency of the laser. This shift is such that our expression reduces to the frequency pulling expression of an incoherently pumped laser when the amplitude of the injected coherence is zero and rises

monotonically with increasing C to match the atomic frequency at the critical point. We can, thus, interpret the unstable region as a competition between the atomic frequency and the pulled frequency of a detuned laser. The coherence in this region is not sufficient to maintain stable locking to the atomic frequency but, via the driving terms in the nonlinear equations of motion, it makes the laser feel its presence in the dynamics and leads to the constant interplay between these two frequencies. A study of the trajectories of the laser reveals that in this case there is a stable limit cycle in the phase plane of the quadratures.

We have investigated the influence of the pumping statistics on the laser with injected atomic coherence. We have found that with random pumping statistics(p=0) there is quantum noise reduction for both intensity and phase, but there is no squeezing for any of them, because the diffusion coefficients D_{II} and $D_{\phi\phi}$, although reduced by ρ_{ab}, remain always larger than zero($D_{II} \geq 0$ and $D_{\phi\phi}>0$). In the present paper we have focused our attention on the regular pumping statistics(p=1). In steady state the regular distribution leads to the squeezing of the intensity noise. For short times the phase noise is squeezed (transient squeezing) and the solutions crucially depend on the initial intensity.

In Chapter III, we have studied the nonlinear theory of the two-photon laser with initial atomic coherence from a set of nonlinear equations for the moments derived from the Fokker-Planck equation. First, we analyzed the steady state operation and bistable behavior of the system. Similar to the one-photon laser with initial atomic coherence, our

results showed that, below threshold, the system can exhibit the following features: bistability (hysteresis cycle) and lasing without population inversion occurs and phase can be locked to a particular value. We also showed that in certain cases, a Hopf bifurcation takes place. Below the Hopf bifurcation point, the system is unstable. The time-dependent behavior of the intensity and phase in the unstable region consists of periodic oscillations. Furthermore, we have shown that, for certain parameters, even the tristability can be found. We have also studied the field dynamics. We find that the time-dependent behavior of laser intensity in the unstable regimes is oscillatory(quasiperiodic), and show that there is a stable limit cycle in the phase plane of the quadratures.

Next, we investigated the noise quenching and squeezing in the bistability region. Besides showing that phase noise can be squeezed on the lower branch, we find that the phase squeezing persists for the upper branch even with the population inversion. We thus obtain a bright squeezing source which is compatible with population inversion in a simple two-photon CEL. This is, perhaps, the most interesting finding of the paper. Processes that are commonly used to generate squeezed states usually permit the generation of the squeezed vacuum state, i.e., the mean of the amplitude is zero. Here we have a process which, in principle, can lead to the generation of a squeezed coherent state, i.e., a state with nonvanishing mean for the amplitude. It should be emphasized that this feature persists on a finite portion of the upper branch above threshold with the magnitude of phase squeezing up to 30%.

In Chapter IV, we have investigated the photon statistics and the spectrum of the two-photon micromaser. We have derived a master equation for the two-photon micromaser with the injected atomic coherence. Due to the off-diagonal coipling it is difficult to solve this master equation, therefore we have examined a special case, assuming zero coherence. We studied the photon statistics for the fully excited, partially excited and deexcited two-photon micromaser. Finally, we investigated the spectrum by using Green's function to calculate the two-time correlation function of the micromaser field. We have shown the influence of the thermal mean photon number on the spectrum of the two-photon micromaser.

References

[1] M.O.Scully and W.E.Lamb, Jr., Phys. Rev. **159**, 208(1967).

[2] H. Haken, *Laser Theory*, Vol. **25**, Part 2c of Handbuch der Physik, edited by L. Genzel (Springer, Berlin-New York, 1970).

[3] W. H. Louisell, *Quantum Statistical Theory of Radiation* (Wiley, New York, 1973).

[4] J. A. Bergou, L. Davidovich, M. Orszag, C. Benkert, M. Hillery and M. O. Scully, Phys. Rev. A **40**, 5073 (1989).

[5] C. Benkert, M. O. Scully, J. A. Bergou, L. Davidovich, M. Hillery and M. Orszag, Phys. Rev. A **41**, 2756 (1990).

[6] M. A. M. Marte and D. F. Walls, Phys. Rev. A **37**,1235 (1987).

[7] M. A. M. Marte , H. Ritsch and D. F. Walls, Phys. Rev. Lett. **61**, 1093 (1988); Phys. Rev. A **38**, 3577 (1988).

[8] M. C. Teich and B. E. A.Saleh, JOSA **B2**, 275 (1985).

[9] S. Machida, Y. Yamamoto and Y. Itaya, Phys. Rev. Lett. **58**, 1000 (1987).

[10] S. Machida and Y. Yamamoto, Phys. Rev. Lett. **60**, 792 (1988).

[11] Y. M. Golubev and I. V. Sokolov, Sov. Phys. JETP **60**, 234 (1984).

[12] Y. Yamamoto, S. Machida and O. Nilsson, Phys. Rev. A **34**, 4025 (1986); A **35**, 5114 (1987).

[13] M. A. M. Marte and P. Zoller, Phys. Rev. A **40**, 5774 (1989).

[14] T. A. B. Kennedy and D. F. Walls, Phys. Rev. A **40**, 6366 (1989).

[15] F. Haake, S. M. Tan and D. F. Walls, *ibid.* **40**, 7121 (1989); **41**, 2808 (1990).

[16] M. O. Scully, Phys. Rev. Lett. **55**, 2802(1985).

[17] M. O. Scully, K. Wódkiewicz, M. S. Zubairy, J. Bergou, N. Lu, and J. Meyer terVehn, Phys. Rev. Lett. **60**, 1832(1988).

[18] N. Lu, J. Bergou, Phys. Rev. A **40**, 237(1989).

[19] J. A. Bergou, M. Orszag and M. O. Scully, Phys. Rev. A **38**, 754 (1988); ibid 763; and ibid 768.

[20] M. O. Scully and M. S. Zubairy, Phys. Rev. A **35**, 752 (1987).

[21] W. Schleich and M. O. Scully, Phys. Rev. A **37**, 1261 (1988).

[22] J. A. Bergou, J. Zhang and A. Hourri, Phys. Rev. A **50**, 4188(1994).

[23] J. Gea - Banacloche, Phys. Rev. Lett. **59**, 543 (1987).

[24] N. Lu and J. A. Bergou, Phys. Rev. A **40**, 250 (1989).

[25] J. A. Bergou, N. Lu and M. O. Scully, Opt. Commun. **73**, 57 (1989).

[26] M. B. Spencer and W. E. Lamb, Jr., Phys. Rev. A **5**, 884(1972).

[27] W. W. Chow, M. O. Scully, and E. W. van Stryland, Opt. Commun. **15**, 258(1975).

[28] H. Zeghlache and V. Zehnlé, Phys. Rev. A **46**, 6015(1992).

[29] T. Carty, M. Sargent III, Phys. Rev. A **42**, 1544(1990).

[30] C. Benkert, M. O. Scully, and M. Orszag, Phys. Rev. A **42**, 1487(1990).

[31] S. E. Harris, Phys. Rev. Lett. **62**, 1033(1989).

[32] M. O. Scully, S.-Y. Zhu, and A. Gavrielides, Phys. Rev. Lett. **62**, 2813(1989).

[33] J. A. Bergou and P. Bogar, Phys. Rev. A **43**, 4889(1991).

[34] M. Sargent III, M. O. Scully and W. E. Lamb, Jr., *Laser Physics* (Addison-Wesley, Reading, MA, 1974).

[35] C.Benkert and M. O. Scully, J. Bergou, and M. Orszag, Phys. Rev. A **41**, 4069 (1990).

[36] C.Benkert and M. O. Scully, ibid **42**, 2817 (1990).

[37] G.S.Agarwal, J.Bergou, C.Benkert and M.O.Scully, Phys. Rev. A **43**, 6451 (1991).

[38] H.P.Yuen, Phys. Rev. A **13**, 226(1976).

[39] L.A.Lugiato and G.Strini, Opt. Commun. **41**, 447(1982).

[40] M.D.Reid and D.F.Walls, Phys. Rev. A **28**, 332(1983).

[41] M.Brune, J.M.Raimond, and S.Haroche, Phys. Rev. A **35**, 154(1987).

[42] L.Davidovich, J.M.Raimond, M.Brune, and S.Haroche, *ibid.* **36**, 377(1987).

[43] J.Bergou, C.Benkert, L.Davidovich, M.O.Scully, S.Y.Zhu, and M.S.Zubairy, Phys. Rev. A **42**, 5544(1990).

[44] S.M.Dutra and L.Davidovich, Phys. Rev. A **49**, 2986(1994).

[45] N.Lu, F-X.Zhao, and J.Bergou, Phys. Rev. A **39**, 5189(1989).

[46] N.Lu and S.Y.Zhu, Phys. Rev. A **40**, 5735(1989).

[47] J.Bergou, J.Zhang and C.Su, Phys. Rev. A **52**, 3183(1995).

[48] D.Meschede, H.Walther, and G.Müller, Phys. Rev. Lett. **54**, 551(1985).

[49] L.A.Lugiato, M.O.Scully, and H.Walther, Phys. Rev. A **36**, 740 (1987).

[50] P.Filipowicz, J.Javanainen, and P.Meystre, Phys. Rev. A **34**, 3077 (1986).

[51] G.Rempe, H.Walther, and N,Klein, Phys. Rev. Lett. **58**, 353 (1987).

[52] P.Meystre, G.Rempe, and H.Walther, Opt. Lett. **13**, 1078 (1988).

[53] J.J.Slosser, and P.Meystre, Phys. Rev. A **41**, 3967 (1990).

[54] S.Qamar, K.Zaheer, and M.S.Zubairy, Opt. Commun. **78**, 341 (1990).

[55] M.Brune, J.M.Raimond, P. Goy, L.Davidivich, and S.Haroche, Phys. Rev. Lett. **59**, 1899 (1987).

[56] I.Ashraf, J.Gea-Banacloche, and M.S.Zubairy, Phys. Rev. A **42**, 6704 (1990).

[57] M.O.Scully, H.Walther, G.S.Agarwal, T.Quang, and W.Schleich, Phys. Rev. A **44**, 5992 (1991).

[58] S.Qammar and M.S.Zubairy, Phys. Rev. A **44**, 7804 (1991).

[59] N. Lu, Phys. Rev. A **47**, 1347 (1993).

[60] T. Quang, G.S.Agarwal, J.Bergou, M.O.Scully, H.Walther, K.Vogel, and W.P. Schleich, Phys. Rev. A **48**, 803 (1993)

[61] J. Bergou, M. Orszag, M. O. Scully, K. Wódkiewicz, Phys. Rev. A **39**, 5136(1989).

[62]. J. Bergou and M. Hillery, Phys. Rev. A **49**, 1214(1994).

[63] M. Xiao and S.Jin, Phys. Rev. A **45**, 483(1992).

[64] S.Jin and M.Xiao, Phys. Rev. A **49**, 499(1994).

[65] K.Wang and Y.Wang, J. Opt. Soc. Am B**10**, 2130(1993).